D I S S E R T A T I O N

Membrane fusion mediated by the influenza virus hemagglutinin –

The pH dependence of conformational change and its relevance for host adaptation

zur Erlangung des akademischen Grades

d o c t o r r e r u m n a t u r a l i u m

eingereicht an der Lebenswissenschaftlichen Fakultät
der Humboldt Universität zu Berlin von

MSc. Caroline Mair

Präsident der Humboldt Universität zu Berlin:
Prof. Dr. Jan-Hendrik Olbertz

Dekan der Lebenswissenschaftlichen Fakultät:
Prof. Dr. Richard Lucius

Gutachter/in:
1. Prof. Dr. Andreas Herrmann
2. PD Dr. Michael Veit
3. Prof. Dr. Yves Gaudin

Tag der Einreichung: 16.12.2014
Tag der mündlichen Prüfung: 15.04.2015

"Imagination is more important than knowledge. For knowledge is limited, whereas imagination embraces the entire world, stimulating progress, giving birth to evolution [...]."

Albert Einstein

Zusammenfassung

Der Eintritt von Influenza A Viren in Wirtszellen erfolgt anhand des Hämagglutinin (HA) Proteins. Neueste Entwicklungen zielen darauf ab, die fusionsinduzierende Konformationsänderung des HA und damit die Freisetzung des viralen Genoms in die Wirtszelle zu inhibieren. Der Fusionsprozess ist pH-abhängig da nur bei einem niedrigen pH-Wert (~5.0-6.0) die Protonierung bestimmter Reste innerhalb des HA eine Konformationsänderung, und somit die Membranfusion, auslöst. Die Identifizierung von konservierten, titrierbaren Resten und die Aufklärung der Strukturveränderungen im HA ermöglichen eine gezielte Entwicklung neuer antiviraler Medikamente.

In dieser Arbeit wurden bestimmte Histidine im HA mittels umfassender experimenteller und theoretischer Methoden als potentielle pH-Sensoren untersucht. Dabei konnte das Histidin an Position 184 als wichtiger Schalter der pH-induzierten Konformationsänderung identifiziert werden. Außerdem bewirkte der Austausch des geladenen Rests an Position 216 in der Nähe des His184 eine Veränderung der pH-Abhängigkeit des H5 HA aufgrund der Beeinflussung des pK_a-Werts des His184. Da die Mutation R216E im HA des hochpathogenen H5N1 Virus in allen Isolaten während der Vogelvirenseuche im Jahr 2003/04 detektiert wurde, deutet das Ergebnis daraufhin, dass diese Mutation zur Entstehung des hochvirulenten Vogelvirus und dessen Adaptierung an den Menschen beigetragen hat.

In diesem Zusammenhang wurde auch der Einfluss der pH-Abhängigkeit des HA auf die Fusion und Infektiosität von Viren in lebenden Zellen getestet. Eine destabilisierende Mutation im HA eines rekombinanten WSN-H3 Virus reduzierte dessen Infektions- und Replikationseffizienz in MDCK-Zellen, was auf den endosomalen pH-Wert dieser Zellen zurückgeführt werden konnte. Die Messung der Virus-Endosom-Fusionskinetik in lebenden Zellen machte außerdem die Bedeutung der pH-Abhängigkeit des HA für den Zeitpunkt der Membranfusion und dessen Einfluss auf die Effizienz der Virusinfektion deutlich.

Abstract

The entry of influenza A virus into host cells is established by the hemagglutinin (HA) protein. New antiviral strategies aim to inhibit the fusion inducing conformational change of HA and thereby liberation of the viral genome into the cell. This process is strictly pH dependent since the conformational change of HA initiating the fusion of membranes only occurs upon protonation of yet unknown residues within HA at low pH (~5.0-6.0). The identification of conserved titrable residues and better understanding of the sequential structural rearrangements within HA may facilitate the development of new broad-spectrum antivirals.

In the present work His184 and His110 were characterized as potential pH sensors by a comprehensive mutational and computational analysis. The results suggest that His184, but not His110, is an important regulator of HA conformational change at low pH. Furthermore, an exchange of charge at position 216 in vicinity to His184 was shown to alter the pH dependence of conformational change and of fusion in correlation to the known pK_a dependence of histidines on neighboring residues. The result advocates that the mutation R216E, which emerged in the highly pathogenic H5 HA in 2003-2004, contributed to an altered acid stability of H5 HA via its effect on His184 and thus to the adaptation of avian H5N1 viruses to the human host.

Therefore, the role of an altered acid stability of HA for viral fusion and infectivity in living cells was assessed. Recombinant viruses containing a destabilizing mutation in the HA protein were found to have a reduced infectivity and replication efficiency in MDCK cells compared to the respective wild type. Studying virus-endosome fusion kinetics in these cells we could resolve a significant difference in the timing of fusion induction suggesting that the time-point of fusion is a critical determinant of viral infection efficiency which depends on the endosomal acidification as well as on the acid stability of HA.

Contents

1 Introduction

1.1 Influenza A viruses

1.1.1 Epidemiology and history of influenza viruses

Infection with seasonal human influenza virus varies from year to year resulting in 3 to 5 million cases of severe illness and 250 000 to 500 000 deaths annually (World Health Organization, WHO). In addition to these yearly epidemic outbreaks recurring influenza pandemics cause millions of human deaths worldwide. Historical reports suggest that influenza epidemics have already appeared since the Middle Ages or even since ancient times and at least 14 influenza pandemics were speculated to have occurred since 1500. However, it was not until 1931 that influenza viruses could be isolated by Richard Shope [1] coining the starting point of research in the field of virology. Now, we know that influenza viruses are enveloped negative stranded RNA viruses with a segmented genome assigned to the family of *orthomyxoviridae*. They are classified into influenza A, B and C viruses according to their host range and pathogenicity. Whereas B and C type viruses are exclusively isolated from humans, the natural reservoir of influenza A viruses are aquatic birds where they circulate mostly without causing any symptoms. Only when transmitted to poultry, low mammals and humans they cause respiratory disease. Based on the antigenic properties of the spike proteins hemagglutinin (HA) and neuraminidase (NA) influenza A viruses can be further classified into 18 HA and 10 NA subtypes.

Influenza A and B type viruses are the causative agents of the seasonal flu outbreaks and are therefore included into the vaccine formulations every year, whereas influenza C viruses only cause mild infections and localized outbreaks. Avian derived influenza A viruses are additionally the major cause of epizootic disease and human pandemics. In the past 96 years five confirmed human pandemics have occurred with the most devastating one in 1918 (“Spanish influenza”). This pandemic was caused by an avian origin H1N1 virus which circulated since then in humans and was also the origin of the following pandemics in 1957 (“Asian influenza”, H2N2), 1968 (“Hong Kong influenza”, H3N2), 1977 (“Russian influenza”, H1N1) and in 2009 (swine origin H1N1 influenza) [2–4].

These pandemics were typically caused by the introduction of a virus possessing an HA subtype new to the human population. The emergence of such a new virus strain is

facilitated by the genetic flexibility of influenza A viruses. The segmented genome allows them to exchange genes between different strains upon co-infection of a host so that novel viruses emerge constantly with a new composition of segments and subtypes (reassortment or "*antigenic shift*") [5,6]. Furthermore, the high mutation rate during viral replication due to the infidelity of the viral polymerase results in multiple mutations in individual genes ("*antigenic drift*"). In some cases these point mutations produce selective advantages for the virus such as better binding and/or replication efficiency or by allowing them to escape pre-existing immunity [7,8]. Of the past pandemics only human adapted H1N1 and H3N2 viruses still circulate in the human population as so called seasonal influenza A viruses (see above). A new influenza variant appeared in 2011 by reassortment of the pandemic H1N1 virus with an H3N2 swine influenza virus. However, this virus only transmitted from pigs to humans and rarely between humans which is considered as prime condition for pandemicity.

In the last decades major poultry epizootics caused by viruses of H5, H7 and of H9 subtypes have caught public attention due to repeated spillover infections in humans. In particular, the great bird flu which has its origins in the 1996 epizootic in China and re-emerged in 2003 raised major concerns for the outbreak of a new human pandemic. 661 human cases including 387 deaths have been reported from 2003 until 2014 (WHO). Fortunately, this virus has so far only transmitted from birds to humans. Spread among humans has only been observed in rare cases. However, only last year, in March 2013, human cases with the newly identified avian H7N9 virus raised new public concern. The virus has emerged from reassortment of several avian strains, mainly from H7N3 and H9N2 viruses in Asia. Although less pathogenic than the H5N1 virus (137 cases, 45 fatalities) it was shown to contain signs of mammalian adaptation in some of the viral genes of avian origin and transmitted more readily from animals to humans [9]. Again sustained human-to-human transmission has fortunately not been observed.

The continuing circulation of these avian viruses in birds and the associated spillover infection in humans and other mammals pose a constant risk for the development of a new human pandemic. Although influenza viruses have been extensively studied since the 1930s which is reflected by the high amount of knowledge that has been gained over the last century, properties that contribute to the success of novel avian strains in the human host are still not clearly defined.

1.1.2 Structure and morphology of influenza A virus

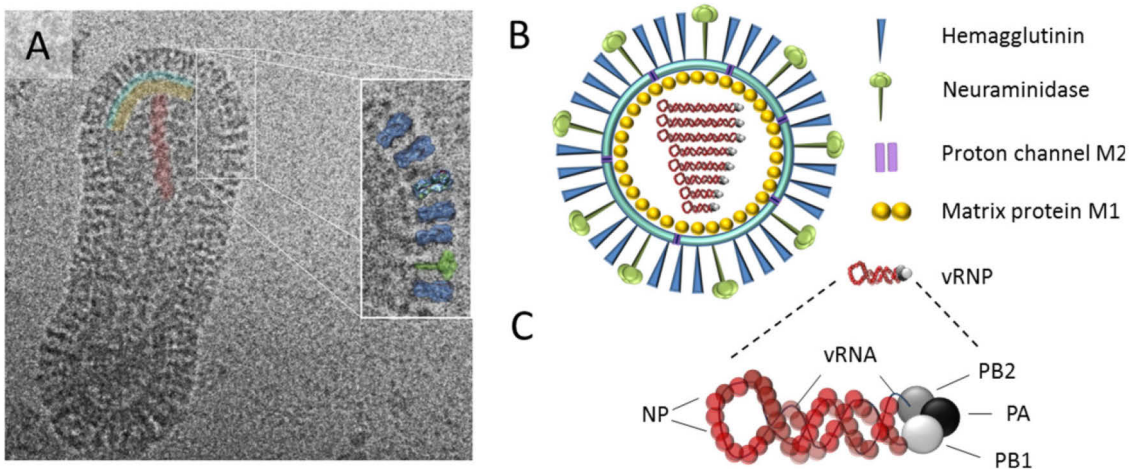

Figure 1.1: Structure and morphology of influenza A viruses.

(A) Transmission electron micrograph of an influenza A/X-31. Regions of the lipid membrane (turquoise) and of the M1 capsid (yellow) as well as one RNP (red) are colorized. In the magnified section of the electron micrograph HA and NA were overlaid with surface representations of the corresponding crystal structures filtered to an EM-comparable resolution (attainable by 3D-TEM-reconstruction techniques)[1]. (B) Schematic representation of an influenza A virus particle. The spike proteins hemagglutinin (HA, blue), neuraminidase (NA, green) and the proton channel protein M2 (purple) are embedded in the lipid envelope (turquoise) of the virus. The membrane is lined with the M1 capsid protein at the inside (yellow). The viral genome consists of eight ribonucleoprotein particles (RNPs, red). (C) Enlargement of a vRNP segment. Each segment is formed by viral RNA (vRNA), the nucleoprotein (NP) and the viral polymerase proteins (PB1, PB2 and PA, colored in white, gray and black, respectively).

Influenza A viruses are enveloped viruses with pleomorphic morphology forming spherical structures of ~100 nm in diameter as well as filamentous virions reaching up to ~20 µM in length (Figure 1.1). In the lipid bilayer three integral membrane proteins are inserted: the antigenic glycoproteins HA and NA, and the multi-functional, proton-selective ion channel M2. Beneath the membrane the matrix protein M1 forms a protein layer which is essential for viral stability and integrity [10,11]. The single stranded negative-sense RNA is divided into eight segments, each encoding for at least one viral protein [12] (summarized in Table 1.1). Each segment is encapsulated by viral proteins into ribonucleoprotein complexes (vRNPs) [13,14] (Figure 1.1 C). The terminal sequences are bound by the trimeric viral RNA dependent polymerase complex (PB1, PB2 and PA) whereas the rest of the sequence is bound by multiple copies of nucleoprotein (NP) which upon binding oligomerizes into a double helical, rod-shaped structure [15,16]. Being capable of transcription and replication in the absence of other viral proteins these vRNPs are the minimal replicative units of influenza

[1] The transmission electron micrograph was obtained from Dr. Kai Ludwig, Research Center of Electron Microscopy, Free University Berlin

and other orthomyxovirions. A full set of viral RNPs is sufficient to initiate infection [17–21]. Due to the membrane and RNP-binding activities of M1 the vRNPs are integrated into the viral membrane and by that M1 is also a determinant of virus morphology [11,22–24] (see 1.1.3.2).

Table 1.1: Viral proteins encoded by the eight vRNPs of influenza A virus.

vRNP segment	Viral protein	Main protein function**	Size in amino acids	References
1	PB2	Cellular mRNA cap recognition and binding	759	[25,26]
2	PB1	RNA dependent RNA polymerase; RNA chain elongation	757	[26]
	PB1-F2*	Virulence factor; pro-apoptotic activity	90	[27]
	N40*	unknown; rescues viral replication in presence of PB1-F2	718	[28]
3	PA	Endonuclease; Cleavage of capped mRNAs (cap snatching)	716	[29]
	PA-X*	Repression of cellular RNA polymerase II gene expression	252	[30]
	PA-N155*	unknown; probably promote viral replication	568	[31]
	PA-N182*	unknown; probably promote viral replication	535	[31]
4	HA	Cell receptor binding, viral membrane fusion	560	[32]
5	NP	Component of vRNP complex; vRNA binding, nuclear import and replication	498	[33,34]
6	NA	Cleavage of terminal sialic acids (release of progeny virus)	465	
7	M1	Matrix protein; Determinant of virus structure; involved in nuclear export of vRNPs, assembly and budding	252	[10,11,24,35]
	M2	Proton selective ion channel; important for vRNP uncoating and virus budding	97	[36,37]
	M42*	unknown; can functionally replace M2 in M2-deficient viruses	99	[38]
8	NS1	Antiviral response inhibition	217	[39,40]
	NS2/NEP	Nuclear export protein; M1 binding and vRNP export	121	[41,42]
	NS3*	Unknown; replicative gain-of-function in the mouse model	174	[43]

*auxiliary proteins

**for a more detailed description see Vasin *et al*. 2014 [12].

1.1.3 Replication cycle of influenza A viruses

Transcription and replication of influenza A viruses take place in the nucleus and thus viral RNPs have to be transported from the cell periphery to the center of the cell for RNA synthesis. This involves passage of the nuclear envelope which is a tightly regulated process (see 1.1.3.3). However, it provides the virus with several advantages for transcription and

replication. Before import into and export from the nucleus the viral RNA is encapsulated in RNPs and thus remains hidden from antiviral host response factors such as the cytoplasmic RNA receptor retinoic acid inducible gene 1 (RIG-I) [44,45]. In addition, transcription inside the nucleus at the site of host transcription allows the virus to associate with the host RNA polymerase II (pol II) for mRNA synthesis and processing (splicing). Thus, the virus hijacks the host machinery thereby expanding its coding capacity [12] and at the same time inhibiting host gene expression by subsequent degradation of pol II [46,47].
The individual steps of the influenza A virus replication cycle can be divided into (i) binding and uptake, (ii) endocytic transport and fusion, (iii) nuclear import and replication, (iii) protein synthesis and nuclear export and (iv) viral assembly and budding. These steps are illustrated in Figure 1.2 and described in detail below.

1.1.3.1 Binding and uptake

Influenza A virus entry is mainly mediated by binding of the viral HA to the terminal sialic acids (SAs) of host cell glycoproteins [32] triggering endocytosis of the virus. Of the different existing entry mechanisms that have been identified [48–50] influenza A viruses were found to enter cells primarily by clathrin-mediated endocytosis (CME) [51–53]. Electron micrographs and live viral tracking additionally revealed a clathrin- and caveolin-indpendent entry pathway, especially for those of filamentous morphology, which was only discovered in 2011 as macropinocytosis [54,55].
Virus internalization is not a simple process and seems to be highly cell-dependent. Recent studies suggest that post-attachment factors and associated host-specific signaling factors additionally to SA binding are required to trigger endocytic uptake of the virus [56–58]. For example, binding to the epidermal growth factor (EGF) receptor was shown to promote internalization of the virus by activating receptor tyrosine kinases [59]. Furthermore, the ability of influenza viruses to infect cells independent of SA binding suggests a more host-specific uptake mechanism which may require the activation of cellular signaling molecules by yet undetermined co-receptors [60–62].

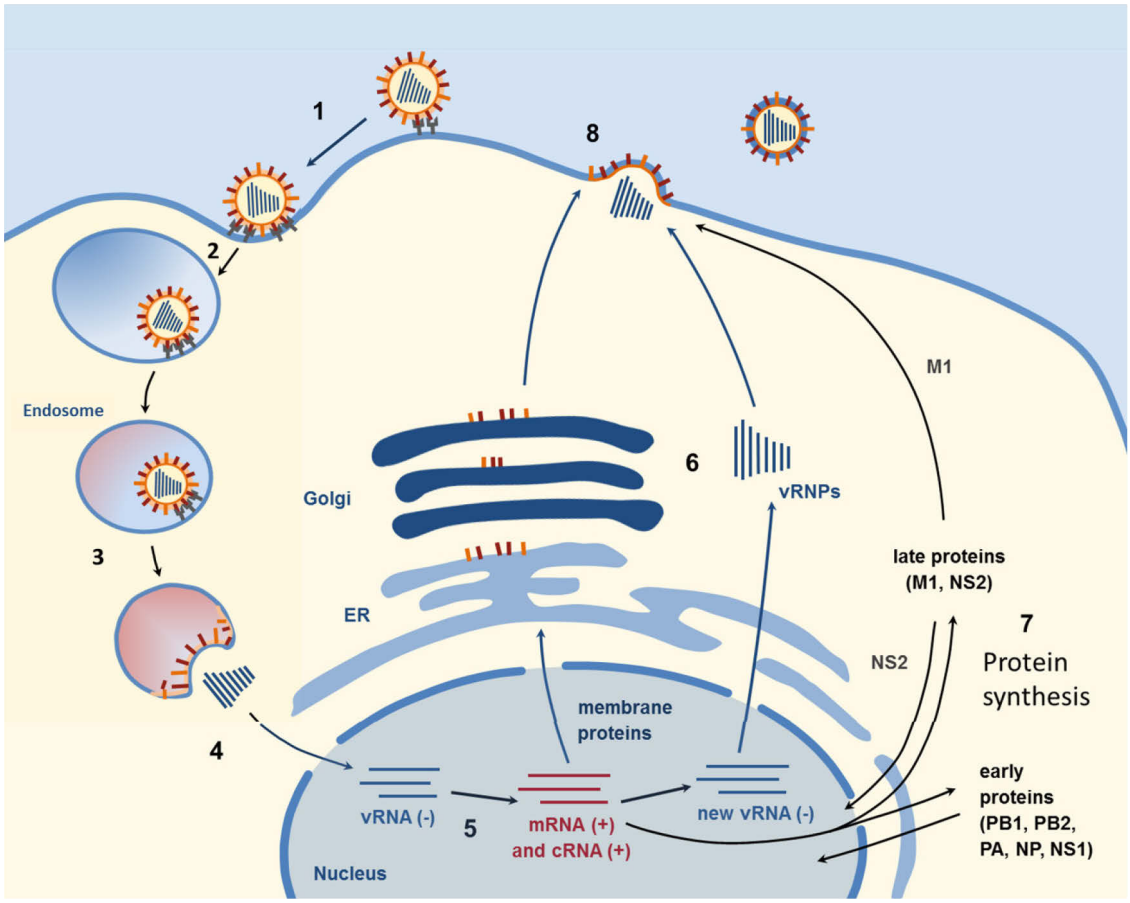

Figure 1.2: Replication cycle of influenza A viruses.
After the virus has bound to sialic acid containing receptors via HA (1) it gets endocytosed (2) and is transported within the endosome along microtubules (3). The declining endosomal pH triggers a conformational change of HA mediating the fusion of the viral and the endosomal membrane. As a consequence, the RNPs are released into the cytoplasm and are finally transported into the nucleus (4). There the viral RNA is transcribed into mRNA and new viral RNA (via cRNA intermediate) (5). From the newly synthesized mRNA viral membrane proteins (HA, NA and M2) are produced at the endoplasmic reticulum(ER) and travel through the Golgi apparatus to the plasma membrane of the cell (6). Other early (PB1, PB2, PA, NP and NS1) and late (M1 and NS2) viral proteins are also translated and transported back into the nucleus where new ribonucleoprotein particles (vRNPs) are formed with the nucleoprotein (NP) and the trimeric polymerase complex (PB1, PB2, PA) (7). These new vRNPs, as well as M1, are also transported to the plasma membrane, where assembly of new viral particles takes place which subsequently bud from the plasma membrane (8).

1.1.3.2 Endocytic transport and penetration

Transport inside endocytic vesicles enables the virus to circumvent the meshwork of microfilaments and cytoplasmic crowding on their way from the cell periphery to the perinuclear region. Travelling inside these cellular vesicles also prevents early detection by the antiviral immune response and allows the virus to release its genome in close vicinity to the nucleus [48,50,51]. Apart from these advantages resulting from endosomal transport along microtubules, the associated pH drop due to endosomal maturation from early endosomes to lysosomes is essential for release of the viral RNPs into the cell [49]. The low pH environment activates the proton channel M2 [63] resulting in the acidification of the viral interior and, as a consequence, in M1 dissociation (vRNP uncoating) [64,65]. At a specific pH HA is induced to undergo a conformational change triggering fusion of the viral with the endosomal membrane (see 1.4.2) which results in the ejection of the viral genome into the cytoplasm of the cell [32,66].

The exact functional compartment where influenza A virus membrane fusion occurs has long been unknown [67]. Early endosomes (EEs) can develop to recycling endosomes (REs), from where endocytosed material is transported back to the cell surface, or to late endosomes (LEs) and lysosomes (Lys). Rab GTPases are involved in targeting and formation of vesicles and were found to determine vesicle specificity [68] by their association with specific endosomal compartments (Rab5 associates with EE, Rab7 and Rab9 with LE, Rab11 and Rab4 with RE) [48,69]. Influenza virus infectivity was significantly inhibited in Rab5 and Rab7 dominant-negative mutants suggesting that both, early and late endosomes are required for trafficking and infection of influenza A viruses [67]. Indeed, tracking of labeled viruses in living cells revealed that an initial acidification step is essential for subsequent virus fusion in late endosomes [70]. Also recently, sequential exposure to early and late endosomes [71] as well as the influx of K+ ions [72] were reported to be required for proper vRNP uncoating and infection implying an excellent adaptation of the influenza A virus to the endosomal maturation pathway in mammalian cells.

1.1.3.3 Nuclear import and replication

After release of the RNPs by membrane fusion they are transported to the nucleus by diffusion where they are shuttled through the nuclear pore complexes (NPCs) by binding to nuclear transport receptors (karyopherins) [73]. These karyopherins import and export structures larger than 20-30 kDa (such as vRNPs) with the help of Ran GTPases [74]. Binding to importins occurs via nuclear localization signals (NLSs) which are present on viral proteins [75] mediating rapid import with a half time of only 10 min [33]. Interestingly, only the NLSs of M1 and NP proteins but not of the polymerase subunits in packaged RNPs are

recognized by the importins, a fact that appears to be essential for regulating the import of incoming and the export of newly synthesized vRNPs [74]. In particular, it was found that M1 prevents re-import of new vRNPs and is also required for the export of vRNPs to the cytosol [35,73]. Transport into the nucleus was found to occur by diffusion [76].
Replication of new viral RNA (vRNA) and transcription of mRNA for translation of viral proteins are two distinct modes of RNP function, however both include copying the negative sense viral RNA (vRNA) to a positive sense reverse complement (mRNA and cRNA) [77]. Initially, the m7GpppXm-cap of host mRNA is bound by PB2 enabling endonucleolytic cleavage 10-13 bases downstream of the 5'cap by the viral polymerase acidic subunit (PA) (cap snatching) [29]. The resulting short RNA fragment serves as primer for the production of 5`-capped and 3'-polyadenylated mRNAs by PB1. Then, vRNA is transcribed into a perfect copy of its template (cRNA) without a cap or polyadenylation signal which again serves as template for the synthesis of new vRNA [34]. Transcription dominates early in infection whereas replication occurs more common as infection progresses. Factors controlling the switch from transcription to replication are still unknown however the source of polymerase and the accumulation of NP and virus-generated small RNAs have been suggested to play a role in this process [78].

1.1.3.4 Protein synthesis and nuclear export

Translation of the viral proteins occurs mainly in the cytoplasm of the cell. The first transcribed proteins are NP and the polymerase subunits (early proteins) as well as M1 and NS2 (NEP) which are subsequently imported back to the nucleus [79]. Newly synthesized vRNA, NP and the PA-PB1-PB2 complex assemble into new RNPs. However, export of vRNPs is only possible when bound to M1 (see above) and to the small nuclear export protein (NEP) [35,42]. Both contain nuclear export signals thus interacting with Crm1 which mediates export by binding to Ran-GTP. Nuclear export is also regulated by other mechanisms with the best understood one being the slow accumulation of NEP due to mRNA splicing [80]. Also phosphorylation of M1, NP and NEP as a result of HA accumulation at the plasma membrane [81] and the activation of the apoptotic pathway and as a result of caspase 3 have been proposed to promote vRNP export [82].
The exported vRNPs attach to Rab11 associated recycling endosomes (RE) which are then transported from the microtubule organizing center (MTOC) to the plasma membrane where viral assembly and budding takes place [83–85]. Recent evidence suggests that the vRNPs already assemble into complexes to be packaged on their way to the plasma membrane due to association with Rab11 positive vesicles [86]. HA, NA and M2 are synthesized by ribosomes at the endoplasmic reticulum (ER) (late proteins). As integral membrane proteins

they follow the secretory pathway including posttranslational modifications in the ER and the Golgi apparatus, from where they are transported to the apical plasma membrane.

1.1.3.5 Assembly and budding

As infection progresses, viral proteins are increasingly enriched at the apical plasma membrane. HA and NA concentrate in lipid raft domains where they are thought to initiate the budding process of progeny virus by inducing curvature of the membrane [87]. M1 and M2 are also required for virus budding in infected cells but how these viral proteins interact to induce bud formation and membrane scission is still not completely understood [88].
The current model suggests that M1 binds to the cytoplasmic tails of HA and NA [89] inducing M1 polymerization [90,91]. However, evidence was recently provided that M1 multimerizes upon binding to the plasma membrane in the absence of other viral proteins [92]. The matrix protein was also proposed to be responsible for subsequent filament formation [11,22–24] and for recruitment of vRNPs and M2 to the viral budozone [10]. Finally, the channel protein M2 concentrates at the boundary phase between raft and bulk plasma membrane at the neck of the budding virion. There it is thought to induce membrane scission by insertion of its amphipathic helix and resulting generation of positive curvature [37]. After completed membrane scission the new influenza virus particles are still tethered to the plasma membrane by HA-SA interaction. Only final cleavage of sialic acid receptors by neuraminidase leads to the release of budded virions from the cell surface [93]. Evidence has been achieved that both, spherical as well as filamentous particles only contain one copy of each vRNA segment [94]. Thus, a highly selective mechanism of genome packaging has been proposed which seems to depend on functional, *cis*-acting packaging signals at either end of the vRNA segment [95,96]. A recent study on vRNP assembly reported the co-localization of vRNPs in Rab11 associated vesicles (REs) in the cytoplasm before arrival at the budding site [86]. This study supports the previous idea of specific inter-vRNA interactions leading to the arrangement in a so called “7+1” configuration as revealed by electron tomography [97]. However, the exact gene sequences involved in direct vRNA-vRNA base pairing are currently unknown and seem to differ among virus strains [98], a fact that might substantially influence the emergence of reassortant viruses [6,99].

1.2 Membrane fusion

1.2.1 Biological significance

Membrane fusion is the merger of two initially separated lipid membranes into a single continuous bilayer. This uniting mechanism plays an essential role for numerous functions in eukaryotic cells and for the formation of multicellular organisms. Intracellular fusion is fundamental for the distribution of lipids and proteins to different organelles (vesicular transport) as well as for intracellular communication by synaptic transmission. Extracellular fusion of two neighboring cells, also referred to as cell-cell fusion, is detrimental for developmental processes such as fertilization (fusion of a sperm with an oocyte) and tissue generation (e.g. myoblast fusion to form a muscle) [100–102].
However, also viral pathogens make use of this membrane uniting mechanism enabling host cell infection and the spread of disease [103–106]. Invasion by enveloped viruses including pathogens such as influenza, HIV and Ebola requires the fusion of their host cell derived lipid bilayer with the cellular membrane in order to deliver their viral genome into the host cell. Also the dissemination of non-enveloped reoviruses was found to depend on viral fusion of infected and non-infected cells [107].

1.2.2 The fusion-through-hemifusion pathway

Despite the high diversity of cell-cell, virus-cell and intracellular fusion processes and involved proteins a common fusion pathway was found to exist in which hemifusion turned out to be a key intermediate [102,108–112]. The hemifusion intermediate is characterized by a lipid connection of the outer membrane leaflets while the inner leaflets remain distinct. Several models have been suggested for this fusion-through-hemifusion pathway with the most prevalent one depicted in Figure 1.3. Five steps have been proposed: (1) Local membrane bending creates a first site of contact. (2) Dehydration of this initial contact induces monolayer rupture establishing a local lipid connection between the two bilayers (hemifusion fusion stalk). (3) Subsequent radial expansion of the stalk results in a hemifusion diaphragm (HD) (4) Disruption of this diaphragm leads to the formation of a small fusion pore which allows for mixing of aqueous luminal contents. (5) A final enlargement of this pore leads to the complete fusion of membranes which is irreversible [109,113–115]. Alternatively, it has been proposed that the fusion stalk directly decays into a fusion pore omitting the stage of HD formation [116–118]. In any case, the hemifusion stalk is the most reliable intermediate structure which has been commonly found by modeling approaches and was confirmed experimentally [119].

Another important intermediate structure in the fusion-through-hemifusion pathway is the fusion pore which is characterized by the lipid connection of outer and inner leaflets allowing for the mixing of aqueous contents which have been initially separated by the membranes. Both, hemifusion and fusion pore formation have been analyzed by electrophysiological approaches [120–123] and fluorescence assays monitoring lipid mixing (hemifusion) or lipid and content mixing (fusion pores) [108,124–126]. In these studies reversibility of the hemifusion intermediate was reported as well as reversible fusion pore opening, so called "pore flickering" [120], before its irreversible expansion. In general, the fate of two lipid bilayers - if they transit into a fusion stalk, a "restricted" or "unrestricted" hemifusion diaphragm, or into a small or expanded fusion pore - mostly depends on the type of fusion protein and its surface density [127]. However, several other factors such as lipid composition, lateral membrane tension and curvature of the fusing membranes have a substantial influence on the required energy at different stages of fusion.

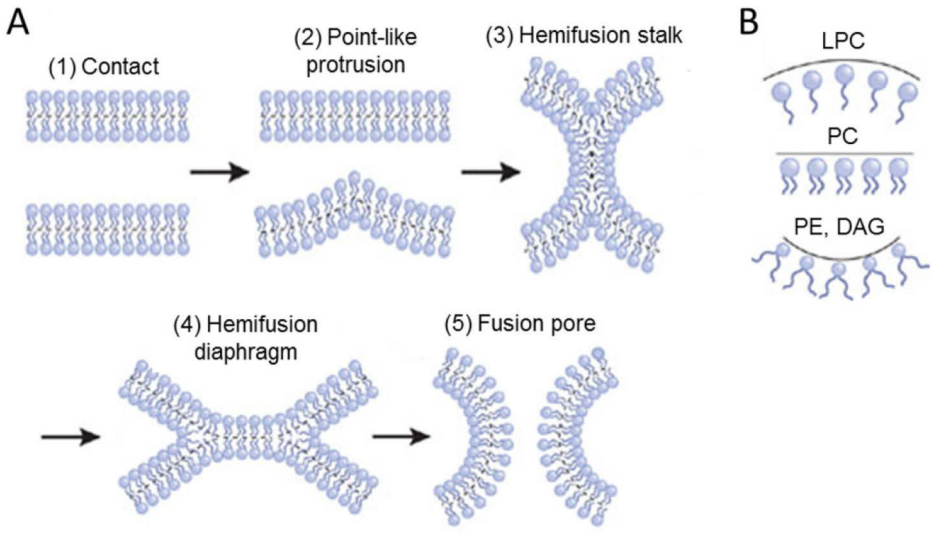

Figure 1.3: The fusion-through-hemifusion pathway and the lipid character in fusion.
(1) After a first pre-fusion contact (2) point-like protrusions minimize the energy of the hydration repulsion between the proximal leaflets of the membranes coming into immediate contact. (3) A hemifusion stalk is formed with proximal leaflets fused and distal leaflets unfused. (4) Stalk expansion yields the hemifusion diaphragm (HD). (5) A fusion pore forms either in the HD bilayer or directly from the stalk. Dashed lines show the boundaries of the hydrophobic surfaces of monolayers. (B) Monolayers formed by inverted cone–shaped lysophosphatidylcholine (LPC) and by cone-shaped phosphatidylethanolamine (PE) and diacylglycerol (DAG). Cylindrical phosphatidylcholine (PC) forms an almost flat monolayer (adapted from Chernomordik et al. 2008) [119].

1.2.3 Role of lipids for membrane fusion

Early studies on protein-free liposome and flat bilayer fusion in the presence of divalent cations have shown that the stage of membrane fusion largely depends on the lipid composition of the monolayers (114). Lipid molecules with relatively small polar heads (e.g.

phosphatidylethanolamine (PE) and diacylglycerol (DAG)) were shown to promote hemifusion due to their cone shaped structure which induces spontaneous negative curvature of the membrane (Figure 1.3 B). In contrast, those with larger polar heads and small hydrophobic moieties such as lysophosphatidylcholine (LPC) are molecules of inverted shape disturbing the leaflet configuration within the stalk and the HD thus inhibiting hemifusion. At the same time these inverted-shape-lipids promote fusion pore formation due to the induction of opposite curvature at the edge of the fusion pore [114]. Thus, the effect of the respective lipid depends on the monolayer of the membrane where it is inserted. The promoting effect of PE on the formation of the hemifusion intermediate as well as of LPC on pore formation was also found for viral [125,129–131] and intracellular fusion [132,133] supporting the role of lipids for the fusion of biological membranes.

1.2.4 Role of membrane tension

Another player driving the fusion of lipid bilayers is membrane tension. The minimal distance of artificial bilayers under normal conditions is 2-3 nm due to hydration of the lipid head groups [134]. Dehydration of these protein-free membranes brings them into very close contact (<1nm) generating a large amount of energy from intermembrane repulsion which is thought to be relaxed upon hemifusion [135–137]. Experimentally this can be achieved by direct dehydration [137] or by the addition of calcium ions or polyethylene glycol (PEG) [138,139]. Also other studies have proposed that the generation of membrane stresses at the fusion site initiate stalk formation [140–142]. In addition, simulations and experiments revealed that lateral tension in the external monolayers promotes stalk expansion and that opening and expansion of fusion pores is driven by the tension in the whole bilayers resulting from the forming HD [112,143–146].

1.2.5 Role and types of fusion proteins

The activation energy of the fusion process has been estimated to be in the range of 40 kcal/mol, most of which is required for enlargement of the initial fusion pore [147–149]. This energy is thought to be generated by the reversible or irreversible conformational change of one [150] or several fusion proteins [151,152] which bring the membranes in close apposition and drive the membrane rearrangements resulting in complete fusion [147,153,154].

Due to the simplicity of viral structures the fusion proteins of enveloped viruses have already been studied in depths and thus represent the best studied class of fusogens. Also the

intracellular fusion machinery composed of several proteins of the SNARE[2] family has already been well characterized [100]. All of these fusion proteins are anchored in the membrane via a transmembrane anchor and establish a connection to the opposing bilayer, either by insertion of a hydrophobic anchor peptide (viral fusion) or by zippering up with another protein which is anchored in the opposed membrane by a transmembrane domain (TMD) (SNARE-mediated fusion). Of the proteins responsible for developmental fusion reactions only very few have been identified [102]. The fusion mediating mechanism of these so-called fusion failure (FF) proteins has only been discovered very recently. As demonstrated for the epithelial fusion failure protein EFF-1 it resembles that of the intracellular fusion machinery [155]. Although there are major differences in the pre-fusion structures of viral and cellular proteins driving membrane fusion, the conserved hairpin structure of these fusogens in the post-fusion state as well as the detection of a hemifusion intermediate in all processes suggests a conserved mechanism of coupling between protein and membrane rearrangements [119].

1.3 Viral fusion proteins

Enveloped viruses contain a lipid bilayer which protects the nucleocapsid and the genetic information from the environment. In order to mediate a new infection the genome has to be released by fusion of the viral with the cellular membrane. In contrast to cellular fusion, where the respective fusion proteins have to be present on both fusing membranes, the viral fusion machinery is exclusively provided by the virus and drives membrane fusion in the absence of an external energy source [100].

Depending on the viral family, the transition from the pre- to the post-fusion conformation is triggered by binding to one or multiple receptors at the plasma membrane (neutral pH) or, after endocytic uptake, by protonation in the acidic endosomal compartment (low pH) [103,105]. Critical histidines have been suggested as key residues, which upon protonation trigger the structural rearrangements in the acidic pH environment of endosomes, however only a few potential pH sensors have been identified to date [156–163]. Avian α-retroviruses even require a two-step fusion activation process (receptor binding followed by low pH) and fusion by severe acute respiratory syndrome (SARS) Coronavirus S and Ebola virus GP proteins is only initiated following enzymatic cleavage by endosomal enzymes such as cathepsins [105,164–166] (see Table 1.2). In any case, the induced conformational change involves common structural rearrangements for all fusion proteins (Figure 1.4). These are, first, the insertion of hydrophobic peptides or loops, referred to as fusion domains, into the target membrane (pre-hairpin intermediate) and second, the refolding of the extended

[2] SNAP receptor; SNAP, soluble N-ethylmaleimide-sensitive factor (NSF) attachment protein

conformation into the characteristic hairpin fold positioning the TMD and the fusion domain at the same end of the rod-like structure [167]. If the pre-hairpin intermediate is monomeric or a homotrimer of several fusion subunits is still a matter of debate [168]. Recruitment of several pre-hairpins to the fusion site followed by a sequence of refolding steps to the energetically most stable hairpin structure is thought to help bringing the membranes into increasingly close contact and progress through hemifusion to fusion pore formation and finally to the enlargement of the fusion pore, which allows passage of the viral genome into the cytoplasm [105].

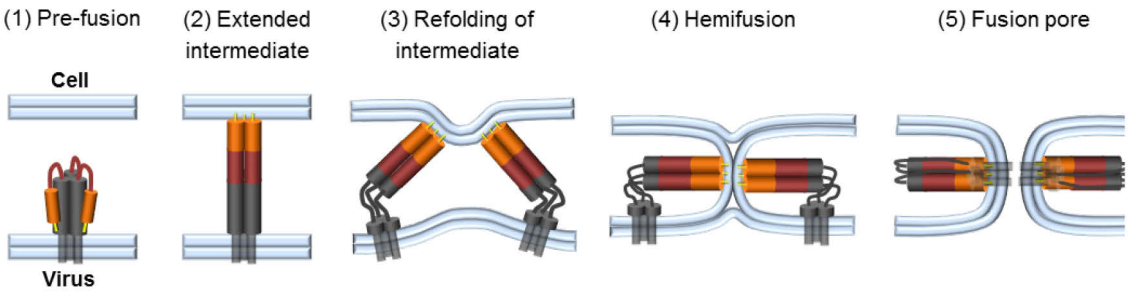

Figure 1.4: Schematic representation of events in membrane fusion promoted by a viral fusion protein. (1) The fusion protein in the pre-fusion conformation with the fusion peptide (yellow) at the N-terminal end of the cleaved structure. (2) Extended intermediate: The protein opens up, the fusion peptide or loop interacts with the target bilayer. (3) Refolding of the intermediate: A C-terminal segment of the protein folds back along the outside of the trimer core pulling the membranes into the hemifusion intermediate (4). As the hemifused bilayers open into a fusion pore (5) the final zipping up of the C-terminal ectodomain segments results in the fully symmetric, post-fusion conformation, preventing the pore from resealing (adapted from Harrison *et al*., 2008) [106].

1.3.1 Features of fusion and transmembrane domains

The fusion and the transmembrane domain of viral fusion proteins play an essential role in the process of membrane fusion. Insertion of the fusion peptide or loop of 10-30 nucleotides in length into the target membrane brings the two bilayers in close proximity which is usually disfavored due to strong hydration repulsion forces [134,169]. Furthermore, this step is important for translating the force resulting from protein refolding to membrane merger [167]. However, some of the viral fusion proteins (vesicular stomatitis virus G (VSV G) and fusion-associated small transmembrane (FAST) proteins of non-enveloped viruses) are not able to transfer a significant amount of energy to the target membrane required for membrane tilting [107,170]. Hence, there has been emerging evidence that additional to membrane anchoring the fusion peptides or loops induce membrane curvature by intercalation with the target membrane generating local membrane stresses which then initiate the formation of a fusion stalk [103,154,171–173]. Korte *et al.* demonstrated that the absence of negatively charged

Glu residues of the HA fusion peptide affected its interaction with lipid membranes probably by allowing better access to the bilayer [173]. Similarly, the kink in the fusion peptide and the conserved N-terminal glycine ridge were shown to be of functional importance for membrane insertion and perturbation [174,175].

A local deformation of membranes has also been suggested to result by the local concentration of TMDs in the membrane [176]. Indeed, isolated peptides derived from the transmembrane domain of SNARE proteins [177] as well as from VSV G [178] alone promoted fusion. Interestingly, mutations increasing the stability of their α-helical structures decrease the fusogenic activity of the TMD peptides suggesting that a certain structural flexibility is essential for fusogenicity [177,178]. A certain length requirement as well as the importance of (semi)conserved glycine motifs within the TMDs of viral proteins have also been reported [178–182]. Since GPI-anchoring of HA [121,125,126,183], VSV G [184] and HIV Env [185,186] as well as mutation or truncation of TMDs resulted in an arrest at the hemifusion stage or at the transient fusion pore intermediate, it is commonly believed that TMDs play a major role in the transition from the hemifusion or fusion pore intermediate to the final enlargement of fusion pores [187]. As a consequence, lateral interactions between the TMDs were suggested to be involved in the recruitment of viral fusion proteins to the fusion site, which is essential for fusion pore enlargement [188–190]. Another possibility involves the stabilization of the post-fusion structure by interactions of the fusion peptide with the transmembrane domain late in fusion as suggested by Li *et al.* [175].

1.3.2 Classes of viral fusion proteins

Based on common structural motifs in the post-fusion conformation (α-helical coiled-coil, β-sheet structures or both) viral fusion proteins have been classified into three groups: class I, class II and class III fusion proteins [191] (summarized in Table 1.2). Class I and II viral fusion proteins are synthesized as inactive precursors which have to be proteolytically cleaved to gain fusion competence. This priming step yields metastable spring-loaded structures [192–194], which upon receptor binding or activation by low pH transit into thermodynamically highly stable hairpin conformations. The soluble fusion subunits of HA and F expressed without the TMD were found to spontaneously fold into their hairpin configuration rather than to its native one [195–197] explaining the irreversible nature of class I and II refolding. In contrast, class III fusion proteins do not require proteolytic cleavage and the transition of the pre- to the post-fusion state is reversible [131].

1.3.2.1 Class I fusion proteins

Viral class I fusion proteins include proteins of major pathogens such as influenza virus HA, human immunodeficiency virus (HIV) Env, the SARS coronavirus spike (S) and the Ebola virus glycoprotein (GP). Among these influenza virus HA and paramyxovirus F (Figure 1.5) represent the best characterized proteins. They have been crystallized first in their pre- and post-fusion conformation and thus most information about class I proteins was obtained from these structures [196,198–200]. Proteolytic cleavage of these class I fusion proteins results in the rescue of the initially buried fusion peptide. In the cleaved, metastable structure it is located at (e.g. HA2) or near the N-terminus (e.g. F1) of the fusion subunit [105]. The metastable structures of class I fusion proteins are activated by different fusion triggers to undergo the conformational changes resulting in the six-helix bundle (6HB) that is characteristic to this class of fusion proteins. Some require low pH (e.g. influenza HA) or binding to one (e.g. paramyxovirus F) or multiple receptors (HIV Env) or even both (avian retroviruses). The 6HB is composed of central N-terminal α-helical coiled-coil structures however its size and position varies significantly among different proteins [201].

1.3.2.2 Class II fusion proteins

Viral class II fusion proteins are mostly represented by the fusion proteins of flavivirus E and alphavirus E1 proteins [202]. The E proteins of the flaviviruses such as tick borne encephalitis (TBEV), dengue and west nile virus have similar structures as do the E1 proteins of alphaviruses (e.g. semliki forest (SFV)). In general, this class of fusion proteins displays a molecular architecture completely different from that of class I proteins (Figure 1.5). After proteolytic cleavage of the associated chaperone protein (p62 for E1, prM for E) [194,203], they form hetero- or homodimeric structures running parallel to the membrane and covering the icosahedral viral envelope [202]. Another striking difference is that the three domain architecture of these glycoproteins consists primarily of β-sheet structures. Furthermore, the fusion domains are internal loops at the tips of β-strands rather than terminal peptides as it is the case for most class I fusion proteins [204].
All class II fusion proteins identified to date are activated by protonation at low pH mediating their transition from the pre-fusion dimer through a monomeric or trimeric pre-hairpin intermediate to the post-fusion trimer. Once triggered, E1 of SFV and E of TBEV were found to form ring structures of five or six trimers suggesting a cooperative mechanism of membrane fusion [172,205]. Interestingly, also the recently solved crystal structure of rubella virus E1 from the rubivirus genus of *Togaviridae* has similar features [206] and a class II fusion protein was additionally discovered in the unrelated *Bunyaviridae* family [207]. In contrast, the fusion machinery of closely related hepatitis C and of pestiviruses such as

bovine diarrhea virus of the *Flaviviridae* family were suggested to define a new structural class of fusion proteins due to distinct folds of its surface glycoproteins and the lack of typical structural hallmarks for fusion [208].

1.3.2.3 Class III fusion proteins

The glycoproteins of rhabdo- and herpesviruses combine features of class I and class II fusion proteins and thus were assigned to class III of viral fusogens [152,209]. The successful crystallization of the pre- and post-fusion structures of VSV G further advanced understanding of this new class of fusion proteins [170,210]. As class I proteins they have a trimeric structure in the pre-and post-fusion state and form a central α-helical core in the hairpin structure (Figure 1.5). However, in striking similarity to class II fusion proteins, each fusion subunit contains two fusion loops which are located at the tip of an elongated β-sheet. VSV G mediates both, receptor binding and membrane fusion in the endosomal compartment at low pH whereas the gB protein of herpesviruses requires prior receptor binding to gD to be activated for fusion [105].

In contrast to all class I and II viral proteins the fusion loop of VSV G is very short and discontinuous not allowing for stable anchoring the viral membrane. Furthermore, it is exposed, not hidden in the oligomer interface [170]. Since the pre-fusion structure is not meta-stable, the refolding of G is reversible which allows for regeneration of the native structure after transport through the acidic Golgi complex. The structural rearrangements from the pre- to the post-fusion state also include a pre-hairpin intermediate. Thus, there is a pH-dependent equilibrium between three different states of the protein that is shifted toward the post-fusion state at low pH [211,212].

Table 1.2: Classes and triggers of viral fusion proteins.

Virus family	Viral glycoprotein	Fusion unit	Fusion trigger
	Class I		
Orthomyxo-viridae	Influenza A virus HA	HA2	low pH
	Influenza C virus HEF	HEF	
Paramyxo-viridae	Human parainfluenza virus F	F1	binding of single receptor
	Newcastle disease virus F	F1	
	Respiratory syncytial virus F	F1	
Coronaviridae	SARS coronavirus S	S2	binding of single receptor [a,b]
Retroviridae	HIV- 1 Env	gp41	binding to multiple receptors
	Moloney Murine leukemia virus Env	TM	binding of single receptor by subunit
	Avian α-retrovirus Env	TM	receptor binding followed by low pH
Filoviridae	Ebola virus GP	gp2	low pH [b]
	Class II		
Togaviridae	Semliki forest virus E1/E2	E1	low pH
	Chikungunya virus E1/E2	E1	
	Sindbis virus E1/E2	E1	
	Rubella virus E1/E2	E1	
Flaviviridae	Tick borne encephalitis virus E	E	low pH
	Dengue virus E	E	
	West nile virus E	E	
	Japanese encephalitis virus E	E	
Bunyaviridae	Rift valley fever virus Gc		
	Class III		
Rhabdoviridae	Vesicular stomatitis virus G	G	low pH
Herpesviridae	Herpes simplex virus gD, gB, gH/L	gB	binding to single receptor [c]
	Class IV [d]		
Flaviviridae	Bovine diarrhea virus E	E1/E2?	unknown
	Hepatitis C virus E	E1/E2?	unknown

[a] for some types followed by low pH

[b] low pH is required for cleavage by endosomal proteases which activate GP at acidic conditions

[c] receptor binding by gD activates gB for fusion; gH/gL are also involved in fusion

[d] to be proven

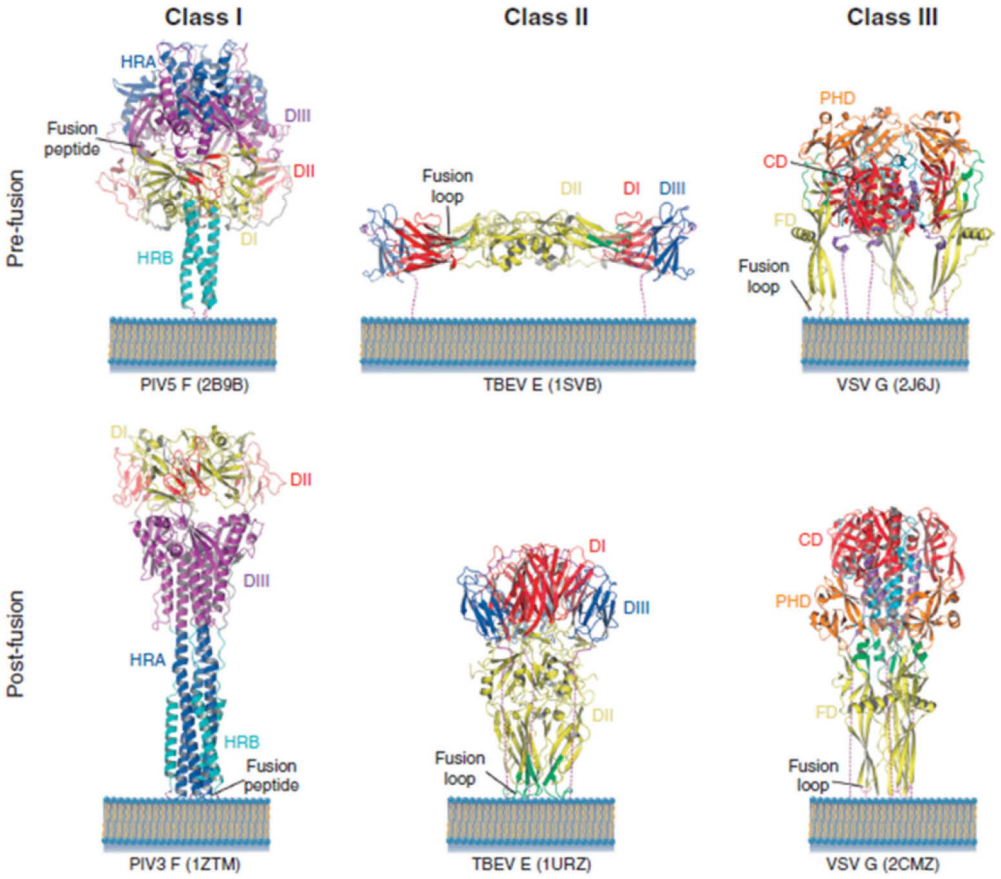

Figure 1.5: Ribbon illustrations of representative members of the three classes of viral fusion glycoproteins in their pre- and post-fusion conformations.
The paramyxovirus F protein (class I) consists of a large C-terminal fragment (F1) and a small N-terminal fragment (F2). F1 is the fusion subunit containing the hydrophobic fusion peptide near the N terminus and two hydrophobic, heptad repeat regions (HRA and HRB). The globular head contains three domains per subunit (DI, DII and DIII) that extend around the trimer axis. In the pre-fusion form, a large cavity formed by DI and DII is covered by DIII which contains the HRA and the fusion peptide. At low pH the fusion peptide is exposed and inserts into the target membrane. Subsequent refolding and assembly of HRA and HRB into a 6HB (post-fusion) induces membrane fusion [196,200]. The monomer of flavivirus E protein (class II) also consists of three domains: the β-sandwich domain (DI) which organizes the structure, an elongated domain (DII) which bears the fusion loop at its tip and an Ig-like domain (DIII) [213]. The protein responds to acidic pH exposure with a hinge motion that exposes and inserts the hydrophobic fusion loop into the cell membrane. The protein then folds back on itself, directing the fusion loop towards the transmembrane anchor. Formation of additional trimer contacts between the stem-anchor and the ectodomain leads to fusion of the viral and cellular membranes (post-fusion form) [202]. Domains of the rhabdovirus G protein (class III) are colored and named according to Roche *et al*. [152]. Only the central domain (CD) that was initially ascribed to two domains (DI and DII) is depicted as a single domain which remains as a rigid block during the transition [168]. The overall architecture of G in its pre-fusion state resembles a tripod. Each monomer is composed of a fusion domain (FD) with the fusion loops pointing toward the viral membrane and a pleckstrin homology domain (PHD). Exposure to low pH causes a 94° rotation around the hinge between FD and PHD and the repositioning of PHD at the top of the trimerization domain (blue) (post-fusion form) [170,210]. Dash lines represent the unresolved segments at the C-termini of the ectodomain connecting them to the TM domain. Respective PDB codes of each protein are shown in parentheses (from Baquero *et al*., 2013) [168].

1.3.3 Cooperativity in viral fusion

Early data on influenza virus HA mediated fusion indicated that the stage of fusion pathway reached largely depends on the density of HA molecules at the cell surface [127]. Only at the highest number of activated HAs an expanding fusion pore was formed whereas its decrease arrested fusion at the (unrestricted) hemifusion stage. Furthermore, a ring-like organization of fusion proteins around the fusion site was reported to restrict lipid mixing but at the same time supports fusion pore formation [127]. Kozlov *et al.* suggested that an interconnected protein coat around the fusion site deforming the membrane in an opposite direction resulting in the lateral membrane tension is not only needed for pore expansion but as well for early stages of membrane fusion [214]. Also experimentally it could be demonstrated that activated fusion proteins outside of the contact zone are required in order to achieve fusion pore expansion [215]. All of these studies suggest a cooperative process of HA-mediated membrane fusion, whereas only one single HIV Env protein was shown to be required for full fusion of membranes [150].

Cooperative interactions during fusion were also suggested for class II viral fusion proteins since the fusion inducing proteins of SFV [172], TBEV [205] and the newly identified E1 of rubella virus [206] form hexagonal lattices of five or six trimers at the surface of liposomes. For class III rhabdoviral G mediated fusion a minimal number of 15 spike proteins was found to be required [216].

The actual number of HA molecules required for the formation of a fusion pore has long been unknown as well as if aggregation occurs before or after acidification in the late endosome. Different models and experimental setups were used yielding quite distinct results. Three trimers were proposed by Danieli *et al.* [188] using HA expressing cells and labeled red blood cells (RBCs) as target membranes. This result could be confirmed by Floyd *et al*. using a rather new single-virion-imaging technique [217]. In contrast, Blumenthal *et al*. reported the requirement of six trimers for an expanding fusion pore [190]. Also others suggested that aggregates of at least six [218] or eight trimers [189] are required of which only two or three trimers undergo the fusion inducing conformational change [189,218]. A very recent study combining low pH-induced fusion kinetics of individual virions with computer simulation revealed that contact with the target membrane is established by independently triggered HA molecules [219]. Subsequent engagement of three or four extended intermediates and their cooperative fold-back was reported to induce the fusion of membranes.

1.4 The influenza virus HA

1.4.1 Structure of the HA protein

HA is a homotrimeric glycoprotein covering around 90 % of the viral membrane. The first crystal structure of HA at neutral pH was obtained by bromelain cleavage of HA of A/Hong Kong/1968 (BHA) yielding the water soluble ectodomain of the glycoprotein [220]. It is comprised of a globular region of antiparallel β-sheets (HA1, head domain) and the central, triple-stranded coiled-coil of α-helices (HA2, stem domain) (Figure 1.8 A). The membrane-distal HA1 globular head is the receptor binding domain which contains the receptor binding pocket and the highly variable loops for antigenic binding. HA2 is crucial for stabilizing the trimeric conformation and for anchoring the protein in the membrane by its TMD. Furthermore, HA2 is the fusion inducing subunit of the protein which carries the fusion peptide at its N-terminus [221,222].
The post-fusion structure was resolved by low pH incubation of BHA and subsequent digestion with trypsin and thermolysin (TBHA2) [198]. However, using this approach only information about the HA2 subunit could be obtained. As typical for class I fusion proteins, the post-fusion state of HA2 is mainly composed of α-helical structures forming a 6HB with the fusion peptide and the TMD positioned at the same end of the trimer (Figure 1.8 B).

1.4.1.1 Folding, transport and cleavage activation

In infected cells HA is synthesized as fusion-inactive precursor protein (HA0) by membrane-bound ribosomes in the ER. The precursor of approximately 560 amino acids gets co-translationally inserted into the membrane following signal peptide cleavage and core glycosylation. With the help of chaperones these precursor proteins are assembled into non-covalently linked homotrimers which are subsequently transported through the Golgi apparatus to the plasma membrane [223,224]. In the Golgi the trimeric proteins undergo further post-translational modifications such as trimming of carbohydrate side chains, terminal glycosylation and acylation [225–227]. In addition, H5 and H7 subtypes containing a polybasic cleavage site are intracellularly cleaved by proteolytic enzymes before arrival at the plasma membrane, whereas all other HA subtypes have a monobasic cleavage site which is typically targeted by trypsin-like proteases of the extracellular space. In any case, cleavage results in the two subunits HA1 and HA2, which remain disulfide linked [228], and the generation of the highly conserved fusion peptide at the HA2 N-terminus, the pre-condition for membrane fusion activity [229–231]. The liberated peptide with its positively charged N-terminal amino group gets buried in a negatively charged cavity at the oligomer

interface of HA2 where it forms stabilizing interactions with other conserved residues such as Asp109 and Asp112 [232].

1.4.2 The fusion inducing conformational change

After cleavage of the HA0 precursor the protein assumes a metastable structure that can be induced by the acidic pH in the endosome to undergo an irreversible conformational change mediating fusion of the viral with the endosomal membrane [193,233]. As described in section 1.3.1 the fusion peptide, as well as the TMD play an essential role in this process. Structural elements which were identified to undergo a major transition at acidic pH are the B loop which connects the long α-helix (helix A) in the stem domain with the shorter helix at the outside (helix C) and residues 106-112 of HA2, a part of helix A [198]. Cryo-EM studies and the characterization of HA mutants locking the protein in (mostly) reversible intermediates further advanced the current understanding of the HA conformational change.
The generally accepted model suggests three major steps (Figure 1.6 C): (1) Protonation of specific residues results in the dissociation of intra-trimeric and inter-subunit contacts and thus of HA1 monomers allowing water to enter the ectodomain [234,235]. (2) Interaction of water with sequences that have originally been shielded from water triggers the B loop to undergo a loop-to-helix transition [236]. Thereby the fusion peptide gets exposed and inserts into the endosomal membrane resulting in the extended coiled-coil conformation of the three monomers. (3) The extended intermediate then collapses due to refolding of helix A into a loop which draws the fusion peptide towards the transmembrane region promoting membrane merger through hemifusion and fusion pore formation [106,198]. In support of this model partial opening of the HA1 monomers was observed by cryo-EM for the trimeric ectodomain (BHA) [234] as well as of HA in intact virus particles [64] upon incubation at low pH. Furthermore, mutations in the B-loop (F63P, F70P) inhibiting fusion by the incomplete formation of the extended coiled-coil intermediate emphasized the importance of a fully extended conformation for complete fusion [237].

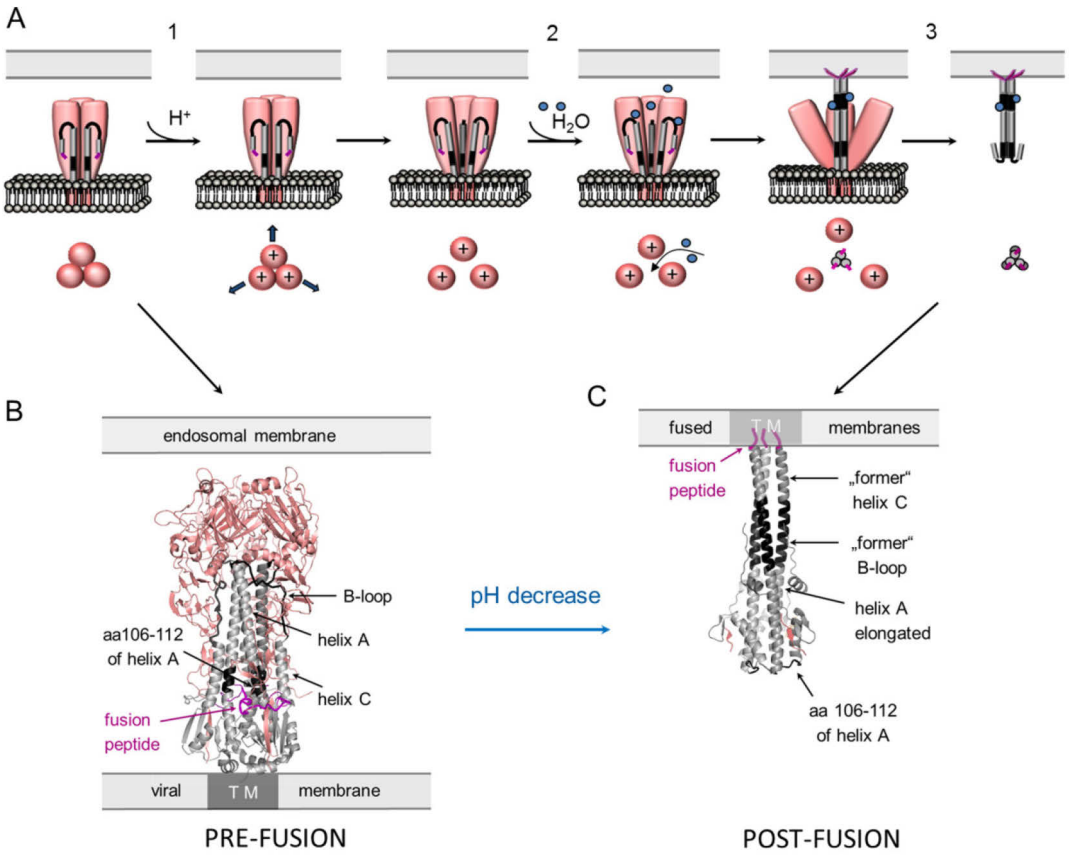

Figure 1.6: Conformational change of the influenza virus HA at acidic pH (5.0–6.0).
(A) The steps of conformational change are illustrated (HA1 in pink, HA2 in gray and black, fusion peptide in purple). Upon acidification in the endosome protonation of HA1 leads to the dissociation of the HA1 monomers (1). Water can enter triggering the structural transition of the B-loop into a helix and liberating the fusion peptide which inserts into the endosomal membrane yielding the extended intermediate conformation of HA (2). Refolding of amino acid residues (aa) 106–112 of the helix A into a loop finally mediates the apposition of the two membranes triggering fusion (hairpin conformation of HA) (3). (B) Corresponding secondary structures of trimeric HA of A/X-31 (H3N2) at neutral (PDB ID: 2YPG) and low pH (hairpin structure, PDB ID: 1HTM) are shown in cartoon representation (H1 in pink, HA2 in gray) with structural elements undergoing a conformational change highlighted in black. TM is the transmembrane region of HA.

1.4.3 Determinants of host range and pathogenicity

1.4.3.1 Receptor binding specificity

Before mediating virus-endosome fusion HA initiates attachment of the virus to the cell surface by binding to sialic acid (SA) cell receptors (see 1.1.3.1). SA is the general term for N-acetyl-neuraminic acid, which inserts into the receptor binding pocket at the top of the HA1 subunit. The pocket, also referred to as receptor binding site (RBS) is formed by three domains, the 130-loop (residues 134-138), the 190-helix (residues 188-195) and the 220-loop (residues 221-228) (Figure 1.7). Only some of the residues of the pocket directly interact with the receptor sialic acid. In the H3 subtype Y98, W153, E190, Y195 and H183 were identified to interact through hydrogen bonds with the side chains of SA [238,239]. Three of these residues (Y98, W153 and H183) are highly conserved throughout all HA subtypes except from the recently identified H17 and H18 subtypes of bat derived H17N10 and H18N11 [240].

Rogers *et al.* [241] was the first to discover that human and avian influenza viruses display differences in the receptor specificity of HA which is determined by the kind of linkage between the carbohydrate (mostly galactose) and its terminal SA. Whereas avian HA have a preference for SA that are linked to galactose (Gal) by α-2,3-linkage (α-2,3-SA), the RBS of human HA preferentially binds to α-2,6 linked SA (α-2,6-SA). This difference in cell receptor binding is considered as major interspecies barrier since it was found to be an important determinant of host range and cell and tissue tropism [242–246]. The preference of avian HA to bind to α-2,3-SA matches the occurrence of this sugar on epithelial cells in the respiratory and intestinal tract of birds. In contrast, the upper respiratory tract (URT) of humans consists primarily of α-2,6-SA-glycans and thus might not be infected with avian influenza viruses [247]. However, the lower respiratory tract (LRT) contains a higher percentage of α-2,3-SA- than α-2,6-SA-glycans and was shown to be more readily infected by avian influenza viruses [248,249]. Interestingly, young children seem to express more α-2,3-SA and a lower level of α-2,6-SA in the respiratory tract than adults [250].

The specificity of HA for α-2,6-SA or α-2,3-SA has been found to mainly depend on the amino acid composition of its RBS. Adaptation of H2 and H3 subtypes to human type receptors has been shown to involve mutations Q226L and G228S (H3 numbering) [251–253] whereas for human adapted H1 the substitutions E190D and/or L225D were responsible for a switch in receptor specificity [254,255]. These mutations did not only confer α-2,6-SA binding and human infection but also the ability of these viruses to transmit between humans [253,256,257]. Interestingly, the introduction of mutations Q226L and G228S in H5 and H7 subtypes also increased the ability of these mutant subtypes to bind to human type receptors [258–260]. Increased α-2,6-SA binding was also reported for

mutations N224K and Q226L resulting from experimental adaptation of recombinant H5N1 to ferrets [261]. Structural studies revealed that these mutations in the 220-loop resulted in a "widening" of the RBS allowing for insertion of the human type receptor with *cis* linkage instead of the avian *trans* motif [262] (Figure 1.7 B and C). In particular, the Q226L substitution facilitated binding to α-2,6-SA while α-2,3-SA binding was reduced.

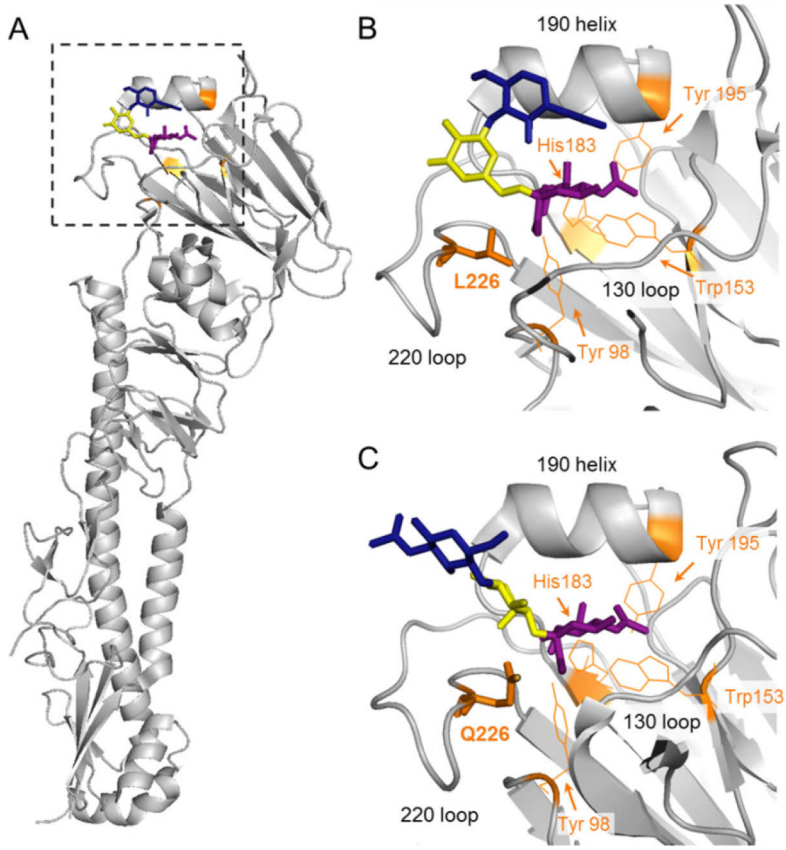

Figure 1.7: Receptor binding site of influenza virus HA in complex with the human or avian type receptor. (A) Cartoon representation of human influenza virus HA monomer in complex with the human-type receptor (PDB ID: 2YPG). In the magnification the RBS of (B) human adapted H3 (PDB ID: 2YPG) and of (C) avian H5 (PDB ID: 4BH1) are shown in complex with their preferred receptor analog. The 190-helix, 220- and 130-loop are displayed with conserved residues (Tyr98, Trp153, His183 and Tyr195) represented as orange lines. N-acetyl-glucosamine (NAG, blue) and galactose (Gal, yellow) of the receptor are shown which are linked to sialic acid (violet) in α-2,6- (A, B) or α-2,3-linkage (C), respectively. HA from human influenza A/X-31 H3N2 has leucine at position 226 (orange stick) facilitating binding to the human type receptor (2-galactose (2-Gal) in *cis* conformation) (A, B) whereas HA from avian H5N1 has a glutamine at position 226, favoring the *trans* motif of avian type receptors (C).

1.4.3.2 Cleavage by host proteases

The number of activated HA molecules undergoing a conformational change is important for successful fusion of the viral with the endosomal membrane (see 1.3.3). Therefore, the efficiency of HA0 cleavage is an important determinant of fusogenicity and pathogenicity [263–267]. Cleavage of the HA protein occurs at the C-terminal end of a single basic residue (R/K) for all HA subtypes followed by removal of the basic residue by a carboxypeptidase C-type enzyme [268]. However, the amino acid sequence of the cleavage site differs among HA subtypes, and accounts for the grade of host invasion [229,230,269] (Figure 1.8).

The monobasic cleavage site of low pathogenic strains (LPAIV) depends on cleavage by trypsin-like serine proteases (e.g. cellular trypsin and tryptase Clara) secreted form epithelial cells that are present only in respiratory or intestinal tissues. Infection is therefore restricted to these organs [267]. In contrast, the polybasic cleavage site of some H5 and H7 subtypes is intracellularly cleaved by subtilisin-like proteases such as furin and PC6 which are ubiquitously distributed [270,271]. Thus, infection with such highly pathogenic avian influenza virus (HPAIV) strains results in non-restricted virus spread in the whole organism and as a consequence in a higher degree of virulence than LPAIV which cause only localized infections.

The efficiency of cleavage has also been reported to depend on additional factors beyond the cleavage site. Residues in the flanking region have been shown to influence the efficiency of cleavage [272] and only recently, subtype specific differences in the cleavage efficiency of HA independent of mono- or polybasic character were reported [273]. These differences were not only ascribed to variations in the cleavage site flanking regions but also attributed to the kind of protease that is present in the infected cell as well as sequence specific targeting of the cleavage site [269]. For example, the cleavage efficiency of blood proteases such as plasmin, urokinase, plasma kallikrein and thrombin was found to differ between and within individual HA subtypes, which was attributed to the presence of bacterial proteases promoting the pathogenicity of influenza viruses and the development of pneumonia synergistically [274,275]. In addition, influenza virus infection was shown to up-regulate cellular trypsins, metalloproteinases and cytokines, and also ATP depletion in various infected cells which was suggested to change organ tropism of seasonal IAV and, as a consequence, resulting in severe disease [276].

In the mammalian airway epithelium type II transmembrane serine protease TMPRSS2 and TMPRSS4 as well as the human airway trypsin-like protease (HAT) were suggested to activate human adapted virus strains in the natural setting of the lung [277]. However, recent data indicate that TMPRSS2 also cleaves HA0 in the secretory pathway within the cell including the highly pathogenic H5 HA [273,278]. Also other members of this family were found to activate highly pathogenic HA subtypes: MSPL and TMPRSS13 [279]. Furthermore, Galloway *et al*. identified differences in the TMPRSS2-mediated HA cleavage profiles

compared to those obtained with HAT and trypsin [273] suggesting that also other factors beyond the cleavage site region and the kind of activating protease might influence the cleavage of HA.

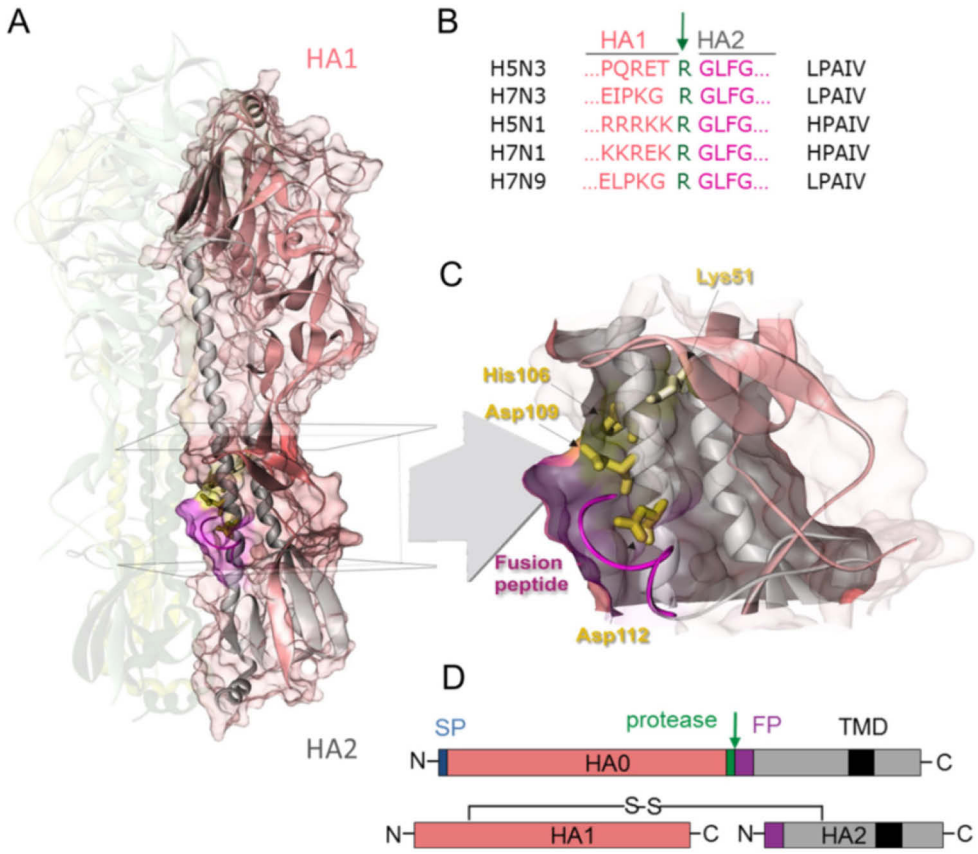

Figure 1.8: The cleavage site of the influenza virus hemagglutinin.
(A) Cartoon representation of the cleaved HA trimer with two monomers colored in green and yellow (transparent) and one monomer colored in pink (HA1) and gray (HA2), respectively. (B) The mono- and polybasic cleavage site of low (LPAIV) and highly pathogenic (HPAIV) avian viruses. Cleavage occurs at the C-terminal end of a single basic residue (R/K, green) for all HA subtypes. The first ten N-terminal amino acids of the fusion peptide are highly conserved (purple). (C) Magnification of the fusion peptide region with conserved residues represented as yellow sticks. After cleavage the fusion peptide of HA2 (purple) gets buried in a cavity at the oligomer interface of HA2 where it forms stabilizing interactions, e.g. with negatively charged residues Asp109 and Asp112. (D) Schematic representation of HA before and after cleavage (SP, signal peptide; FP, fusion peptide; TMD, transmembrane domain; -S-S- disulfide bond).

1.4.3.3 The acid stability of HA

The conformational change of HA, and thus membrane fusion, do not only depend on the efficiency of cleavage and endosomal acidification inside cells but also on the stability of the protein itself. In the absence of a target membrane the irreversible conformational change of HA leads to the inactivation of its membrane fusion activity. Therefore, the pH threshold of conformational change provides a marker for the acid stability of the protein. Exposing HA to increased temperature leads to the biochemically identical conformational change and thus, the stability of HA can be measured over a range of different pH values or temperatures [261,280]. The acid stability has been shown to differ among HA subtypes [273,281,282] as well as between viruses of the same subtype [283–285]. This divergence is ascribed to structural variations in the protein ectodomain that have been identified by comparison of the various crystal structures [284,286–289]. However, the biological significance of HA stability has not yet been fully clarified but it seems to be another hallmark of HA affecting the infection potential of the whole virus.

1.4.3.3.1 Stabilizing interactions and potential triggers of conformational change

The meta-stable HA1-HA2 structure resulting from HA0 cleavage is stabilized by the HA1 domain acting like a “clamp” on HA2 thereby preventing its refolding at neutral pH [193,290]. Several ionic interactions between HA subunits and monomers contribute to the stabilization of this structure and the protonation of key residues located in these critical interface regions is thought to trigger the structural rearrangements leading to membrane fusion [162,245,291]. Analysis of a variety of so called “fusion mutants” has revealed the importance of some key residues and their interactions at several domain and subunit interfaces which are partially conserved throughout HA subtypes [162,284,285,291–298].
One of the most studied regions includes the fusion peptide and the pocket where it is intercalated. The first ten N-terminal residues of the fusion peptide and some residues in the fusion peptide pocket are highly conserved. Accordingly, amino acid deletions or substitutions in the peptide or the cavity surrounding it disturb these balanced interactions significantly affecting the fusion activity of HA [162,173,291,292,297]. For example, highly conserved residues Asp109 and Asp112 of the pocket could act as potential triggers for the release of the fusion peptides since mutation of these residues significantly altered the pH dependent fusion of HA [162,292,297] and of mutant viral particles [219]. In contrast, mutations in the fusion peptide affecting the pH dependence of HA can as well be ascribed to its ability to interact with the target membrane (see 1.3.1). Other regions of structural importance are the HA1-HA1 interface as well as the region around the inter-helical loop B of

HA2 which undergoes a loop-to-helix transition upon protonation. Locking the HA1 monomers by the introduction of disulfide bonds [183,299] or salt bridges [295] inhibited any conformational change of HA and abolished its ability to induce fusion demonstrating the essential role of globular head dissociation in the overall fusion mechanism. Furthermore, several mutational studies demonstrated the importance of interactions at the contact area of HA1 and HA2 such as a conserved tetrad salt bridge [295], interactions of conserved phenlyalanines of the B loop [237] and of helix 110 in the HA1 domain [284,300]. However, residues which, upon protonation, trigger the destabilization of these regions remain essentially unknown.

1.5 Aims of thesis

Human infection with influenza A viruses is still one of the major health problems causing seasonal epidemics and as a consequence millions of cases of disease annually. In addition, avian influenza A viruses pose an ongoing risk to the human population due to their high pandemic potential [301,302]. Vaccination is currently the most effective method for preventing influenza infection however requires constant surveillance of circulating strains and annually changing vaccine formulations. In the case of a pandemic, a fast supply of high amounts of vaccine for the whole population is therefore critical. Furthermore, approved therapeutic drugs might soon become useless due to increasing emergence of resistant strains [303].

The influenza virus HA mediates the first crucial steps of viral entry and thus serves as major target for new antiviral strategies. New developments aim to inhibit the fusion inducing conformational change of HA [304–306], which is already quite well understood. However, critical residues that are protonated at low pH inducing the structural rearrangements remain essentially unknown. The identification of such conserved protonable residues and better understanding of sequential structural rearrangements within HA may facilitate the discovery of new drugable domains for the development of new broad-spectrum antivirals. Histidines have been proposed to function as molecular “switches” in class I and II viral fusion proteins due to their unique characteristic to get protonated and thus charged in the same acidic pH range as these viral proteins are activated (pK_a~6.0) [156,158,159,163]. Thus, one of the aims was to identify critical histidines for their ability to act as pH sensors in the influenza virus H5 HA. We focused on His184 due to its high conservation grade within and among different subtypes (except H17 and H18) and its central position at the HA1-HA1 interface. Furthermore, it has already previously been proposed to function as molecular switch of the HA conformational change [163]. Likewise, we addressed His110 as potential pH sensor of H5 HA. Being located close to the B-loop at the HA1-HA2 interface His110 possibly triggers the structural rearrangement of this domain upon its protonation. However, different to

His184 it is only conserved within certain subtypes (H2, H5, H13 and H16). To illustrate His184 and His110 as possible molecular switches at low pH these two histidines were characterized by comprehensive experimental and computational methods for their influence on pH dependent conformational change and fusion of H5 HA.

Due to its pivotal role in viral entry the HA protein is also a major determinant for the pathogenicity of avian influenza viruses in the human host. Binding to α-2,3- or α-2,6-SA cell receptors determines host specificity whereas the high pathogenicity of some circulating H5N1 strains depends on the cleavage site within HA. In 2003-2004 a more aggressive form of the highly pathogenic H5N1 virus evolved which did not only result in massive bird-die offs in Asia, Africa and Europe, but also in an accumulating number of human spill-over infections.

Apart from mutations in the RBS of HA resulting in increased α-2,6-SA binding, adaptation to the mammalian host has been suggested to require additional mutations preserving the acid stability of the HA protein and thus of the whole virus. A glutamate-to-arginine (E216R) mutation in H5 HP was identified which is located at the HA1-HA1 interface close to His184 where it might affect its pK_a and thus the acid stability of H5 HA [295]. Thus, the charge was exchanged in H5 HP and H5 LP and the effect on pH dependent conformational change and fusion was determined.

However, little is known about the consequences of an altered acid stability for virus infection and its role for host adaptation. Therefore, another aim was to assess the effect of an altered acid stability of HA on intracellular fusion and host-specific infection efficiency of the virus. To this end recombinant viruses containing a destabilizing mutation in the H3 subtype were produced on the basis of the A/WSN/1933 (H1N1) plasmid system [19]. The pH threshold of fusion of wild type and mutant viruses was measured using a traditional fluorescence dequenching assay and the infectivity of these viruses was assessed in different cell lines. Virus labeling in combination with high-resolution microscopy further allowed us to observe fusion on the single virus level and assess the fusion kinetics of wild type and mutant viruses inside living cells.

In summary, in this thesis we aimed to identify critical amino acids that are involved in triggering the fusion inducing conformational change of HA and of mutations in the H5 subtype which might alter its acid stability thereby contributing to the evolution of the highly pathogenic H5N1 virus in 2003/04. Analyzing the effect of an altered acid stability on viral fusion and infectivity allowed us to gain more insight on the role of acid stability for host-specific virus infection.

2 Material and Methods

2.1 Material

2.1.1 Technical equipment

Fluorescence spectrophotometer Fluoromax 4	Horiba Jobin Yvon GmbH, Unterhaching, D
Biophotometer plus	Eppendorf, Hamburg, Germany
Centrifuge Avanti J-20XP (Rotor JLA10.500)	Beckmann Coulter GmbH, Krefeld, D
Ultracentrifuge Optima L-100K (Rotors: 45Ti, 70.1Ti, SW40Ti, SW60)	Beckmann Coulter GmbH, Krefeld, D
Confocal Microscope	FluoView-1000, Olympus, Hamburg, D
Incubator	Heraeus, Berlin, D
Semi-Dry Transfer cell "TransBlot SD"	BioRad, Munich, D
Thermo cycler "My Cycler"	BioRad, Munich, D
Odyssey Scanner	LICOR Biosciences, Bad Homburg, D
FACS Aria II	BD Biosciences, Heidelberg, D
Imager	INTAS Science Imaging Instruments GmbH, Göttingen, D
CASY ® cell counter Model TTC 45/60/150	OLS Omni Life Sciences, Bremen, D

2.1.2 Biological material

2.1.2.1 Cell Lines

CHO-K1 cells (Chinese hamster ovary cells)	ATCC number: CCL-61
MDCK (Madin Darby canine kidney cells)	ATCC number: CCL-34
A549 (human epithelial cells)	ATCC number: CCL-185
Df-1 (chicken embryo fibroblasts)	ATCC number: CRL-12203

2.1.2.2 Influenza virus strains

A/Aichi/2/1968 (H3N2) from eggs
A/WSN/1933 (H1N1) from recombinant plasmid system
A/chicken/Vietnam/P41/2005 (H5N1)
A/teal/Germany/Wv632/2005 (H5N1)

2.1.2.3 Bacteria

DH5α (*E.coli)*	F- endA1 recA1 hsdR17(rk- mk+) supE44 λ- thi-1 gyrA(Na1) relA1 Φ80 lacZΔMΔ(lacZY A-argF)

2.1.2.4 Antibodies

Primary antibodies	
Rabbit anti H5 Ab1 and Ab2 antisera	Genosphere Biotechnologies, Paris, France
Mouse monoclonal anti H5N1 (Vn04-2, -9 and -16)	Biomol, Hamburg, Germany
Mouse polyclonal Anti GFP	Roche
Mouse monoclonal anti influenza A NP	Millipore
Mouse monoclonal anti β-actin	Sigma

Secondary antibodies	
Anti-mouse Alexa Fluor 568	Life technologies
Anti-rabbit Cy3	Life technologies
Anti-rabbit Alexa 488	Life technologies
Goat anti-mouse IgG conjugated to HRP	Life technologies
Goat anti mouse IRDye 680	LICOR Biosciences
Goat anti rabbit IRDye 800	LICOR Biosciences

2.1.3 Plasmids and Oligonucleotides

Plasmids pEYFP-H3, pCAGGS-*Esp*-blue (pCAG) and pHW2000-*Esp*-blue (pHW) were used for cloning (Figure 2.1). The vector pEYFP-H3 is based on plasmid pEYFP-N1 which was provided by Dr. Michael Veit. The HA of A/Aichi/2/1968 (X-31) was inserted into the multiple cloning site (MCS) by Dr. Christian Sieben (Humboldt University Berlin) using restriction sites *NheI* and *SacII*. The resulting plasmid pEYFP-H3 was used as template for molecular cloning and for expression analysis. Plasmids pCAGGS-*Esp*-blue and pHW2000-*Esp*-blue containing the reporter gene lacZ were kindly provided by Dr. Volker Czudai-Matwich (Marburg). The plasmids for the production of recombinant virus particles based on A/WSN/1933 (H1N1) genetic background (pHW2000 1 - 8) were also obtained from Dr. Michael Veit (Free University, Berlin) (Table 2.1).
The protocol for insertion of HA into pCAG was adapted from Dr. Volker Czudai-Matwich [307]. For cloning of highly (H5 HP) and low (H5 LP) pathogenic H5 HA proteins forward and reverse primers contained *BsmBI* restriction sites (correspond to *Esp3I* restriction sites) whereas for cloning of H3 HA proteins *BsaI* restriction sites were used. Mutations into H3 HA and highly and low pathogenic H5 HA were inserted by overlap extension PCR (see 2.2.1.8). In Table 2.2 used oligonucleotide primers for cloning H3 and H5 HA gene sequences into the respective plasmids and for the introduction of mutations into H3 and H5 HA are listed.

Table 2.1: Plasmids used in this study.

Plasmid	Insert	Source
pcDNA3	H5 from A/chicken/Vietnam/P41/2005	provided by Dr. Timm Harder
pEYFP-N1	H3 from A/X-31	provided by Dr. Christian Sieben
pCAGGS-*Esp*-blue	lacZ	provided by Dr. Volker Czudai-Matwich
pHW2000-*Esp*-blue	lacZ	provided by Dr. Volker Czudai-Matwich
pHW2000 1-8	Viral genes of A/WSN/1933	provided by Dr. Michael Veit
pTM1-H3	H3 from A/X31	provided by Dr. S. Rachakonda
pTM1-H3 T212E-N216R	H3 mutant	provided by Dr. S. Rachakonda

The viral cDNA of H3 HA gene was obtained by reverse transcription from viral RNA of influenza virus A/Aichi/2/1968 (H3N2) according to Hoffmann *et al.* [308]. The H3 cDNA was amplified using H3 HA specific primers and cloned into pHW using the *BsaI* restriction sites [307]. The viral H5 LP gene sequence was also synthesized from viral RNA and cloned into pHW by overlap extension PCR [309,310].

2.1.4 Enzymes

Restriction enzymes	
NheI	New England Biolabs (NEB)
BamHI	New England Biolabs (NEB)
SacII	New England Biolabs (NEB)
Esp3I	Fermentas
BsaI	Fermentas
DpnI	Fermentas
Phosphatase	
CIP (Calf intestine phosphatase)	NEB
Ligase	
T4-DNA ligase	NEB / Fermentas
Polymerase	
Phusion High-Fidelity DNA Polymerase	Finnzymes
Taq DNA polymerase	Peqlab
Superscript II reverse transcriptase	Life technologies

2.1.5 Reagents

Standard chemicals were purchased from Sigma, Roth and Merck; others are listed below.

Chemicals	
TPCK Trypsin	Sigma
Neuraminidase from *Clostridium perfringens*	Sigma
Mowiol	Roth
SYBR safe DNA gel stain	Life technologies
Roti safe	Roth
PageRuler ™ Prestained Protein Ladder	Fermentas

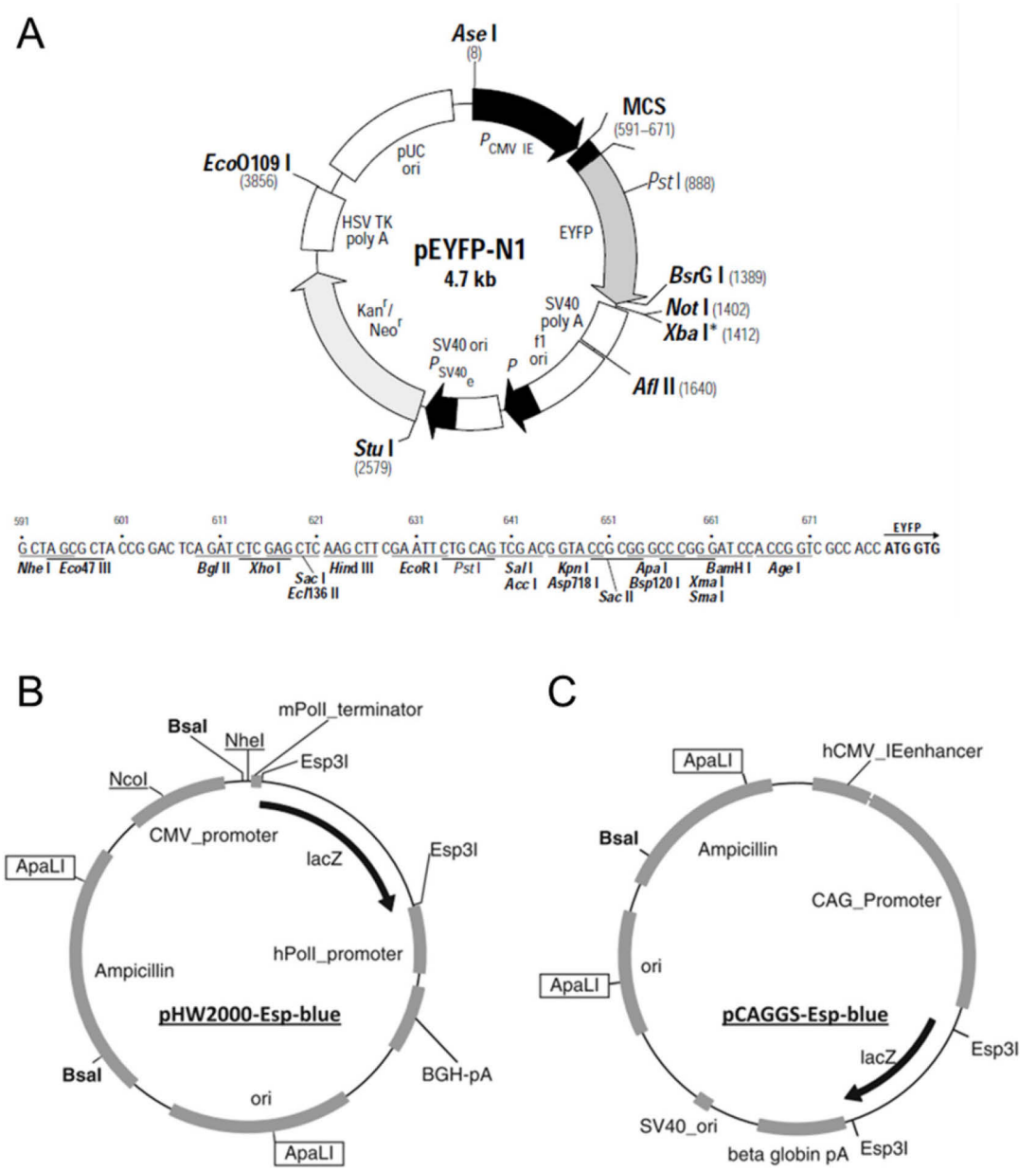

Figure 2.1: Vector maps of pEYFP-N1, pHW2000-*Esp*-blue and pCAGGS-*Esp*-blue.
. (A) Restriction Map and Multiple Cloning Site (MCS) of pEYFP-N1. Unique restriction sites are marked in bold. (B) Vector map of pHW2000-*Esp*-blue. The plasmid contains the human polymerase I (hpol I) and the mPol I terminator for the generation of viral negative strand RNA and the CMV promoter for the generation of mRNA for the production of viral proteins. (C) Protein expression in pCAGGS-*Esp*-blue is driven by the hCMV-IEenhancer. Both, pHW2000-*Esp*-blue and pCAGGS-*Esp*-blue have the gene encoding for lacZ between the *Esp3I* restriction sites (adapted from Czudai-Matwich *et al*., 2013).

Table 2.2: Oligonucleotides used in this study.

Primer name	Insert	Purpose	Sequence[a]
Fw HA-X31 (C. Sieben)	H3 HA	Cloning into pEYFP	GGCCGCTAGCATGAAGACCATCATTGCTTT *NheI* H3 HA
Rev HA-X-31 (C. Sieben)	H3 HA	Cloning into pEYFP	CCGCCCGCGGAATGCAAATGTTGCACCTAA *SacII* H3 HA
NheI-H5 fw	H5 HA	Cloning into pEYFP	GCCGCGCTAGCATGGAGAAAATAGTGCT *NheI* H5 HA
BamHI-H5YFP rev	H5 HA	Cloning into pEYFP	CGCGGGGATCCAATGCAAATTCTGC *BamHI* H5 HA
BsaI-H3 pCAG fw	H3 HA	Cloning into pCAG	TATTGGTCTCAGGGAATGAAGACCATCATTGCTTTGAG *BsaI* H3 HA
BsaI-H3 pCAG rev	H3 HA	Cloning into pCAG	GGGTGGTCTCGTATTAATGCAAATGTTGCACCTAATGT *BsaI* H3 HA
BsaI-YFP rev	H3YFP	Cloning into pCAG	GGGT GGTCTCG TATT TTACTTGTACAGCTCGTCCATGC *BsaI* YFP
Bsm-H5 pCAG fw	H5 HP HA	Cloning into pCAG	TATTCGTCTCAGGGAATGGAGAAAATAGTGCTTCT *BsmBI* H5 HA
Bsm-H5 pCAG rev	H5 HP HA	Cloning into pCAG	GGGTCGTCTCGTATTTTAAATGCAAATTCTGCATTG *BsmBI* H5 HA
Uni12	all segments	cDNA-Synthesis from viral RNA	AGCAAAAGCAGG packaging signal
BsaI-H3 pHW fw	HA	Cloning into pHW	TATTGGTCTCAGGGAAGCAAAAGCAGGGG *BsaI* packaging signal HA
BsaI-H3 pHW rev	HA	Cloning into pHW	ATATGGTCTCGTATTAGTAGAAACAAGGGTGTTTT *BsaI* packaging signal HA
pHW-H5 fw	H5 HA	Generation of amplicon for cloning into pHW	GAAGTTGGGGGGGAGCAAAAGCAGGGGG pHW backbone packaging signal HA

pHW-H5 rev	H5 HA	Generation of amplicon for cloning into pHW	CCGCCGGGTTATTAGTAGAAACAAGGGTG pHW backbone packaging signal HA
H5 LP Seg fw	H5 LP HA	Amplification of H5 LP cDNA	AGCAAAAGCAGGGGTCTAATTTGTC packaging signal H5 LP HA
H5 LP Seg rev	H5 LP HA	Amplification of H5 LP cDNA	AGTAGAAACAAGGGTGTTTTTAACTACAATCTA packaging signal H5 LP HA
T212E-N216R fw	H3 HA	Introduction of mutation into H3 HA	AGAAGCCAGCAAGAAATAATCCCTAGGATCGGGTCCAG AC
T212E-N216R rev	H3 HA	Introduction of mutation into H3 HA	GTCTGGACCCGATCCTAGGGATTATTTCTTGCTGGCTTC T
H5 HP R216E fw	H5 HP HA	Introduction of mutation into H5 HP	GGGACATCAACACTAAACCAGGAGTTGGTACCAAGAATA
H5 HP R216E rev	H5 HP HA	Introduction of mutation into H5 HP	TATTCTTGGTACCAACTCCTGGTTTAGTGTTGATGTCCC
H5 LP E216R fw	H5 LP HA	Introduction of mutation into H5 LP	AGGTCAGTACCAAGGATAGCTACTAGACCC
H5 LP E216R rev	H5 LP HA	Introduction of mutation into H5 LP	GGGTCTAGTAGCTATCCTTGGTACTGACCT
H184N fw	H5 HP HA	Introduction of mutation into H5 HP	GTGGGGGATTCACAATCCTAATGATGCG
H184N rev	H5 HP HA	Introduction of mutation into H5 HP	CGCATCATTAGGATTGTGAATCCCCCAC
H184A fw	H5 HP HA	Introduction of mutation into H5 HP	G TGGGGGATTCACGCTCCTAATGATGCG
H184A rev	H5 HP HA	Introduction of mutation into H5 HP	CGCATCATTAGGAGCGTGAATCCCCCAC
H184R fw	H5 HP HA	Introduction of mutation into H5 HP	GTGGGGGATTCACCGTCCTAATGATGCG
H184R rev	H5 HP HA	Introduction of mutation into H5 HP	CGCATCATTAGGACGGTGAATCCCCCAC

H184D fw	H5 HP HA	Introduction of mutation into H5 HP	GTGGGGGATTCACGATCCTAATGATGCG
H184D rev	H5 HP HA	Introduction of mutation into H5 HP	CGCATCATTAGGATCGTGAATCCCCCAC
H110Y fw	H5 HP HA	Introduction of mutation into H5 HP	GACTATGAAGAATTGAAATACCTATTGAGCAG
H110Y rev	H5 HP HA	Introduction of mutation into H5 HP	CTGCTCAATAGGTATTTCAATTCTTCATAGTC
H110G fw	H5 HP HA	Introduction of mutation into H5 HP	GACTATGAAGAATTGAAAGGCCTATTGAGCAG
H110G rev	H5 HP HA	Introduction of mutation into H5 HP	CTGCTCAATAGGCCTTTCAATTCTTCATAGTC
H110R fw	H5 HP HA	Introduction of mutation into H5 HP	GACTATGAAGAATTGAAACGCCTATTGAGCAG
H110R rev	H5 HP HA	Introduction of mutation into H5 HP	CTGCTCAATAGGCGCTTTCAATTCTTCATAGTC
H110E fw	H5 HP HA	Introduction of mutation into H5 HP	GACTATGAAGAATTGAAAGAGCTATTGAGCAG
H110E rev	H5 HP HA	Introduction of mutation into H5 HP	CTGCTCAATAGCTCTTTCAATTCTTCATAGTC

[a]Restriction sites are highlighted in green with used restriction enzyme indicated below. The C-terminal and N-terminal ends of the gene of interest and packaging signals required for the production of recombinant viruses are labeled in yellow and in gray, respectively. Changes in the nucleotide sequences for the generation of mutations are marked in cyan.

Fluorescent Markers	
octadecylrhodamine B (R18)	Life technologies
1,1-dioctadecyl-3,3,3,3-tetramethylindocarbocyanine perchlorate (DiI)	Life technologies
4,6-diamidino-2-phenylindole (DAPI)	Life technologies
Hoechst 33342	Life technologies
FITC/Rhodamine-dextran (10.000 kDa)	Life technologies
Propidium iodide	Sigma

2.1.6 Tissue culture reagents

DMEM with/without phenol red	PAA
PBS with/without Ca2+ Mg2+ (PBS+)	PAA
EMEM	PAA
0.05 % Trypsin + 0.2 % EDTA in PBS-	PAA
L-Glutamine (200 mM)	Biochrom AG
10 % Fetal Bovine Serum (FBS)	PAA

2.1.7 Kits

Qiagen Plasmid Mini Kit	QIAGEN
QIAquick Gel Extraction Kit	QIAGEN
Qiagen Plasmid *Plus* Maxi Kit	QIAGEN
Qiagen OneStep RT-PCR Kit	QIAGEN
Micro BCA protein assay kit	PIERCE
Invisorb Spin Virus RNA Mini Kit	STRATEC Molecular GmbH

2.1.8 Culture media

Mammalian cell culture media	
Culture medium	DMEM + phenolred, 10 % FBS, 1 % Penicillin-Streptomycin, 2 mM L-Glutamine
Cell detachment	Trypsin/EDTA
Cryo medium	20 % FBS, 10 % DMSO
Selection medium	DMEM, 10 % FBS, 1 % Penicillin-Streptomycin, 250-500 µg/ml Geneticin

Bacteria medium and plates	
LB-medium	1 % Bacto™ Tryptone, 0.5 % Bacto™ Yeast Extract, 0.5 % NaCl, in ddH2O, pH 7.0
Ampicillin-LB-plates	1 % Bacto™ Tryptone, 0.5 % Bacto™ Yeast Extract, 0.5 % NaCl, 1.5 % Agar, 100 µg/ml Ampicillin in ddH2O, pH 7.0
Kanamycin-LB-plates	1 % Bacto™ Tryptone, 0.5 % Bacto™ Yeast Extract, 0.5 % NaCl, 1.5 % Agar, 50 µg/ml Kanamycin in ddH2O, pH 7.0

Virus infection and cultivation	
Infection medium	DMEM, 0.2 % BSA
Virus cultivation medium	DMEM, 0.1 % FBS, 0.2 % BSA, 2 mM Glutamine, 1 %Penicillin/Streptomycin, 4 µg/ml TPCK Trypsin
Agarose semi-solid medium	0.4 % sea-plaque agarose in EMEM supplemented with 0.1 % FBS, 0.2 % BSA, 2 mM glutamine, 1 % penicillin/streptomycin and 4 µg/ml TPCK Trypsin
$TCID_{50}$ infection medium	DMEM, 50mM HEPES, 1 % BSA, 1 % Penicillin/Streptomycin

2.1.9 Buffers

SDS PAGE and Western blot	
10x PBS	40 g NaCl, 1 g KCl, 7,1 g Na2HPO4 2H2O, 1 g KH2 PO4 in 500 ml ddH_2O
10x Running buffer	30 g Tris-Base, 144 g Glycin, 10 g SDS in 1 l ddH_2O
4x sample buffer reducing	25 % β-mercaptoethanol, 5 % SDS, 0,05 % Blue Bromophenol, 25 % Glycerin, 12.5 % 1 M Tris-HCl buffer pH 6,8
4x sample buffer non-reducing	5 % SDS, 0,05 % Blue Bromophenol, 25 % Glycerin, 12.5 % 1 M Tris-HCl buffer pH 6,8
1.5 M Tris-HCl, pH 8.8	181.71 g of Tris-base in 1 l ddH_2O, pH iadjusted with 2 M NaOH
0.5 M Tris-HCl, pH 6.8	60.57 g of Tris-base in 1 l ddH_2O, pH adjusted with 2 M NaOH
Blocking buffer	0.1 % Tween-20, 5 % dry Milk, 1 x PBS in ddH2O
Odyssey blocking solution	2 % Fish Gelatine, 1 % Ovalbumin 10 mM Tris pH 7.5, 150 mM NaCl in 400 ml ddH_2O
Transfer buffer	40 % Running buffer, 20 % Methanol, 6 ml SDS (10 %), in 1 l ddH_2O
Washing buffer	0.1 % Tween-20 in PBS-
Lysis-Buffer for trimer formation assay (with DSP)	50 mM NaOH, 150 mM NaCl, 1 % NP 40, 5 mM Iodoacetamide, 1 mM PMSF
RIPA-Buffer	1 % Triton X-100, 1 % Desoxylat, 0.1 % SDS, 0,15 M NaCl, 20 mM Tris,10 mM EDTA, 10 mM Iodoacetamide, 1 mM PMSF, in ddH_2O, pH 7.4
Resolving gel (10 %)	4 ml Acrylamide/Bisacrylamide (30 %), 2.5 ml 1.5 M Tris-HCl (pH 8.8), 100 µl SDS (10 %), 3,3 ml ddH_2O, 4 µl TEMED, 100 µl APS (10 %)
Stacking gel (5 %)	0.5 ml Acrylamide/Bisacrylamide (30 %), 0.75 ml 0.5 M Tris-HCl (pH 6.8), 30 µl SDS (10 %), 1,7 ml ddH_2O, 3 µl TEMED, 30 µl APS (10 %)
TNE-Buffer	25 mM Tris-HCl pH 7.4, 150 mM NaCl, 5 mM EDTA, 1 % Triton X-100, 0.2 mM PMSF in ddH_2O

Immunostaining	
Blocking solution	0.2 % BSA in PBS+
Permeabilization (FACS)	0.2 %Saponin in PBS+
Permeabilization (microscopy)	0.1 % Triton-X, 0.2 % BSA in PBS+
Fixative	4 % paraformaldehyde (+0.1 % glutaraldehyde) in PBS+

TCID 50	
Fixative	80 % acetone in PBS-
Wash buffer	0.3 % Tween-20 in PBS-
Antibody diluent	0.3 % Tween-20, 5 % w/v milk in PBS-
Substrate	o-phenylenediamine dihydrochloride (OPD) in 0.05 M citrate buffer
Stop solution	0.5 M sulfuric acid

Virus-ghost fusion	
Hemolysis buffer	10 mM Na_2HPO_4 + 2 H_2O, 1.76 mM KH_2PO_4, pH 7.4
Fusion buffer	10 mM sodium acetate*3H_20, 150 mM NaCl, pH 7.4
pH adjustment	250 mM citric acid in ddH_20
Membrane disruption	20 % Triton-X

RBC fusion assay	
Fusion buffer	10 mM HEPES, 10 mM MES,100 mM NaCl in PBS+, pH 7.4-5.0
HA activation	4 µg/ml TPCK Trypsin, 0.5 U/ml Neuraminidase in PBS+

2.2 Methods

2.2.1 Molecular cloning

2.2.1.1 Polymerase chain reaction (PCR)

The polymerase chain reaction (PCR) is an *in vitro* method for the amplification of a specific DNA sequence. For the DNA synthesis, a thermo-stable polymerase, two specific oligonucleotide primers, which flank the region of interest in the target DNA (template), and a mix of deoxynucleotides (dNTPs) are required. The reaction is carried out in a thermocycler machine which is able to switch very fast and accurately between temperatures. It is initiated by a denaturation step, where the template DNA strand is separated, followed by primer annealing to the separated strands so that the 3' OH ends face each other and an extension step where both primers are elongated past the other primer site resulting in two new template strands. Thus, in each cycle the number of DNA sequences is doubled and depending on the number of cycles about a million-fold (2^{20}) amplification of the desired DNA sequence can be obtained [311]. In the table below the required reagents and a typical reaction scheme for the amplification of the HA sequence are shown. The temperature in each step depends on the used polymerase and the thermal stability of the primers (essential for the annealing temperature) whereas the length of the DNA template determines the extension time (Table 2.3).

Table 2.3: Scheme of a typical PCR reaction

PCR reagents		PCR reaction		
50 ng Template	1.0 µl	**Cycle**	**Temp. [°C]**	**Time [min]**
Polymerase	0.2-0.5 µl	Initial denaturation	98°C	0.5
10 µM Primer fw	1.5 µl	*Denaturation	98°C	0.5
10 µM Primer rev	1.5 µl	*Annealing	55°C	0.5
10 mM dNTPs	0.4 µl	*Extension	72°C	2.5
5x Buffer	6.0 µl	Final Extension	72°C	10.0
ddH_2O	add up to 30 µl	Cooling	12°C	∞
Total volume	30 µl			

*Denaturation, annealing and extension steps were repeated 30-35 times in this order.

2.2.1.2 Purification of the PCR product

In order to make sure, that the correct DNA sequence was amplified by PCR, the reaction mix is run on a 1 % agarose gel next to a standard DNA ladder. For visualization of the DNA, 1x SYBR green or Roti safe were added before loading onto the gel. Both are DNA binding dyes and fluoresce upon UV exposure. The presence and size of the product was verified (HA: ~1700 bp) and in case of successful DNA synthesis the PCR product was cut out of the gel and purified from side products using the QiaQUICK Gel Extraction Kit. The purified DNA was collected in 30 µl ddH_2O.

2.2.1.3 Restriction and Ligation

The PCR product is inserted in to the desired vector using restriction enzymes, which cut the DNA within specific sequences, so called restriction sites, and produce overlapping or blunt ends. Since both, the PCR product ("insert") and the plasmid, where the gene of interest should be inserted, are cut with the same enzymes, these can be subsequently linked using an enzyme called DNA ligase which catalyzes the formation of a phosphodiester bond. The plasmid is additionally treated with calf intestine phosphatase (CIP) which removes the phosphate groups at both ends of the vector preventing re-ligation of the "empty" vector and thereby promoting insertion of the gene of interest. The reaction mixture for enzymatic cleavage contains a selected buffer for optimized enzyme activity and the reaction is performed at least 1 h at 37°C. For cloning the H5 HA gene sequence into the pmYFP vector, the enzymatic cleavage of vector and insert was performed with two enzymes, *NheI* and *BamHI,* at 37°C over-night in a total volume of 10-50 µl. The reaction mixture for digestion of the plasmid additionally contained 1 µl of CIP. After digestion, enzymes were inactivated at 60°C for 20 min and DNA binding dye was added to both reactions. These were subsequently run on a 1 % agarose gel and digested products (vector and insert) were purified from the gel as described above. For efficient ligation vector and insert are mixed in a vector: insert-ratio of at least 1:3 which is calculated based on the number of base pairs (bp):

$$\text{ng of insert} = \frac{\text{50 ng of vector x bp of insert}}{\text{bp of vector}} \text{ x } \frac{3}{1}$$

Depending on the type of DNA ligase and the efficiency of the reaction, the ligation is performed at room temperature for 1 h, at 16°C for 3 h or at 4°C over-night in a total volume of 10µl. For the insertion of H3 and H5 HA gene sequences into pCAGGS- and of H3 HA into

the pHW2000-Esp-blue the protocol of Czudai-Matwich was used [307], which combines enzymatic cleavage and ligation in one step (Table 2.4).

Table 2.4: One-step cloning of HA into pCAGGS and pHW2000

Reagents	Volume
10 ng pCAGGS-Esp-blue	0.5 µl
10 ng insert	1.0 µl
100 mM ATP	0.5 µl
100 mM DTT	1.0 µl
Esp3I	1.0 µl
T4 DNA Ligase	1.0 µl
10x Tango Buffer	2.5 µl
ddH_2O	17.5 µl
Total volume	25.0 µl

This is only possible using the *Esp3I* or the *BsaI* restriction enzyme (Fermentas). Both have an optimal activity at 37°C, similar to the T4 DNA ligase with an optimal activity of 16 - 37°C (Fermentas). The reaction was incubated for 1 h at 37°C followed by an additional incubation at 65°C for the inactivation of enzymes. To obtain higher yields of ligated plasmids another 0.5 µl ATP and of DNA ligase were added and the reaction mix was incubated at room temperature over-night.

2.2.1.4 Transformation

The ligated plasmids were then transformed into *E.coli* DH5α. 1-5 µl of ligation reaction were mixed with 50 µl chemically competent bacteria and incubated for 30 min on ice. The transformation proceeds by a heat-shock of 45 sec followed by a fast transfer on ice for 2 min. For the regeneration of bacteria 600 µl of pre-warmed LB-medium were added and the reaction mixture was incubated at 37°C for 1 h in a thermo shaker before plating the cells on LB-plates containing 50 µg/ml kanamycin (LB-Kan) or 100 µg/mg ampicillin (LB-Amp) for selection. The plates were incubated at 37°C over-night.
Plasmids containing the gene for ampicillin resistance (pCAGGS-, pHW2000-*Esp*-blue) were transformed using Z-competent transformation into *E.coli* DH5α. Ligated plasmids and 50 µl competent bacteria are incubated for 2 min on ice before plating them on pre-warmed LB-Amp plates.

2.2.1.5 Plasmid purification from bacteria culture

After incubation of the transformed bacteria over-night at 37°C single-colonies were picked from the plates and inoculated in 3 ml LB medium containing 100µg/ml ampicillin. Cultures were incubated at 37°C with continuous shaking 13-16 h and plasmid DNA was extracted on

the next day using the QIAGEN Plasmid Mini Kit. Purified plasmid DNA was sent for sequencing or used for further cloning.
To obtain higher yields of plasmid DNA (e.g. for transfection of mammalian cells) 100 ml LB-Amp medium were inoculated with 200 µl over-night culture as described above. Plasmid DNA was extracted after 13-16 h using the QIAGEN Plasmid *Plus* Maxi Kit and collected in 400 µl ddH_2O.

2.2.1.6 Isolation of viral RNA and cDNA synthesis

Viral RNA was isolated from supernatant of infected cells 24h post-infection using the Invisorb Spin Virus RNA Mini Kit from STRATEC Molecular GmbH. Subsequently, viral cDNA was synthesized from the viral RNA and the viral HA gene sequence for cloning into the pHW2000-*Esp*-blue plasmid for reverse genetics was amplified from the gained cDNA in one PCR reaction using the One Step RT-PCR Kit from Qiagen.

2.2.1.7 Cloning by target-primed plasmid amplification

Established systems for the generation of influenza viruses solely from plasmids [19,312,313] require prior cloning of influenza gene sequences into the plasmids using the *BsmBI* restriction sites. However, as described above, the insertion of target sequences into circular vectors by restriction and ligation is laborious and time-consumable. Furthermore, many viral genes contain internal restriction sites for all available enzymes of this type (*BsaI, BsmBI, Esp3I*) generating a compatible overhang. Additionally, for reverse genetics of influenza viruses it is essential that the inserted cDNA is transcribed to viral RNA of precise length without additional terminal nucleotides. An alternative method for cloning, which is independent of restriction enzyme cleavage, is the overlap extension PCR or target-primed plasmid amplification [309,310]. It is based on a modified Quick change mutagenesis protocol for the integration of entire PCR amplicons between two neighbored nucleotides or by exchange of an entire vector region [314]. The two strands of the amplicon serve as mega primers. Each mega primer anneals to the complementary site in the plasmid and is then elongated from its 3'-end by the DNA polymerase (Figure 2.2).
Primers pHW-H5 fw and rev were used to generate the PCR amplicon, which is the cDNA of HA with overlapping ends complementary to the sites in the vector where it shall be inserted. The PCR amplicon was gel purified as described in 2.2.1.2 and used for cloning into the vector pHW2000-Esp-blue following the protocol of Stech *et al*. [309]. Briefly, the plasmid was amplified using the PCR amplicon as mega primers as shown in . The PCR product was digested with DpnI, an enzyme which only targets methylated DNA sequences from bacteria and thus only digests the template plasmid (37°C, 1h). The digested product (which should

contain the viral cDNA) was transformed into bacteria as described in 0 and colonies were screened for plasmid carrying the cDNA of the viral HA.

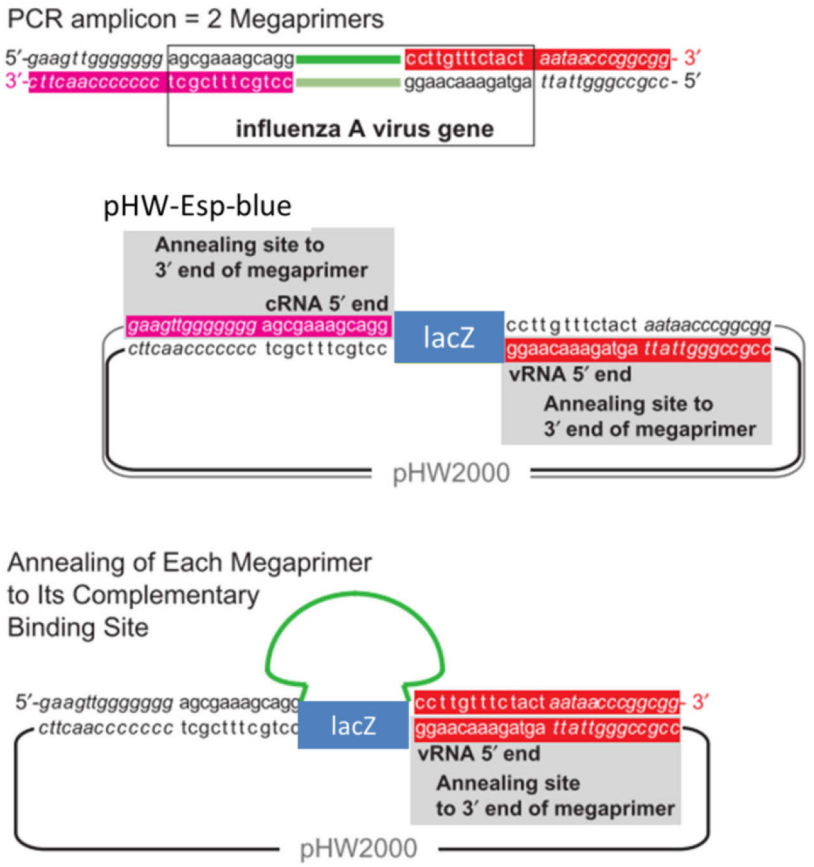

Figure 2.2: Schematic representation of the principle of target-primed plasmid amplification.
The two strands of the PCR amplicon serve as mega primers. Each 30-end of the mega primer anneals to the complementary annealing site within the plasmid pHW2000 and is elongated during target-primed plasmid amplification leading to replacement of the lacZ marker by the viral gene. The two newly synthesized strands hybridize to nicked circular molecules (from Stech *et al.* 2008) [309].

Table 2.5: Typical PCR reaction for the insertion of genes by target primed plasmid amplification

PCR reagents		PCR reaction		
150 ng pHW2000-*Esp*-blue	1.0 µl	**Cycle**	**Temp. [°C]**	**Time [min]**
2 units Phusion Polymerase	1.0 µl	Initial denaturation	98°C	0.5
150 ng PCR amplicon	1.0 µl	*Denaturation	98°C	0.5
10 mM dNTPs	1.0 µl	*Annealing	48°C	1.0
5x Buffer	10.0 µl	*Extension	72°C	5.5
ddH_2O	34.5 µl	Final Extension	72°C	10.0
Total volume	50 µl	Cooling	12°C	∞

2.2.1.8 Site-directed mutagenesis by overlap extension PCR (AB-PCR)

Overlap extension PCR is primarily used in molecular biology to introduce mutations or splice smaller DNA fragments into one large polynucleotide [315]. Four primers are needed which are employed in two PCR reactions (PCR I and II): two complementary ones (a1 and b1), which contain the mutation and two oligonucleotides which flank the gene of interest (a2 and b2) and contain restriction sites for subsequent cloning (Figure 2.3). In the first reaction two DNA fragments (A and B) with overlapping ends, which contain the nucleotide changes, are generated and gel purified. These fragments are combined in a subsequent 'fusion' reaction (AB-PCR) in which the overlapping ends anneal, allowing the 3' overlap of each strand to serve as a primer for the 3' extension of the complementary strand. The resulting fusion product is amplified further by PCR, gel purified and cloned into the desired plasmid. Sequencing was performed by GATC Biotech AG.

2.2.2 Cell culture

2.2.2.1 Thawing, freezing and sub-culturing of cells

1 ml of cell suspension was quickly thawed at 37°C in the water bath and transferred to 10 ml DMEM supplemented with 10 % FBS, 2 mM glutamine and 1 % penicillin/streptomycin (DMEM full medium). After centrifugation at 1000 rpm for 3 min at room temperature (RT), the cell pellet was resuspended in 12 ml DMEM full medium and transferred to a T75 cell culture flask. Cells were cultivated at 37°C and 5 % CO_2 until they reached 80 % confluence. For sub-culturing of confluent cells, the medium was aspirated and cells were washed using 5 ml PBS. Cells were detached with 2 ml Trypsin/EDTA and the reaction was blocked after 2 to 20 min (depending on the cell line) by the addition of 10 ml DMEM full medium. For a 1:12 dilution 1 ml of the cell suspension was transferred to a new flask and 11 ml of DMEM full medium were added. The stable-transfected cell line CHO-K1-H3mYFP was sub-cultured in DMEM full medium supplemented with 500 µg/ml Geneticin.
For freezing of cells, detached cells were centrifuged at 1000 rpm for 3 min at 4°C and the cell pellet was resuspended in 5 ml cold freezing medium which is composed of 1.5 ml cryo-medium and 3.5 ml DMEM full medium (1:3). 1-1.5 ml aliquots in cryo-vials were stored at -80°C over-night before transferring them to the liquid nitrogen tank for long-time storage.

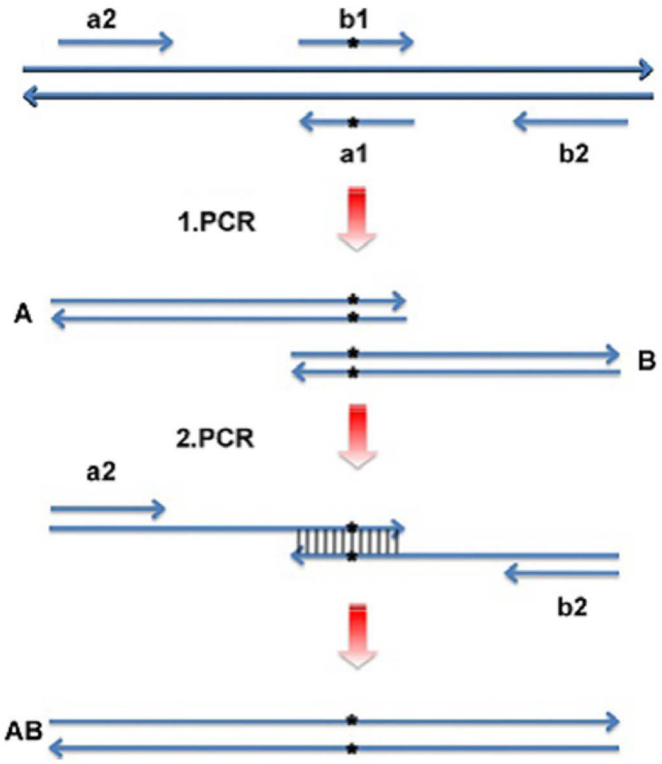

Figure 2.3: Schematic illustration of an overlap extension PCR reaction for the introduction of mutations. Two PCR reactions are preformed generating two DNA strands with overlapping ends containing the nucleotide changes. These anneal in the subsequent reaction and serve as primers for the extension of the complementary DNA strand (AB-PCR).

2.2.2.2 Transient transfection

Cells were transfected at 90 % confluence using Turbofect (Fermentas) according to the manufacturer's protocol. Briefly, for a 35 mm dish 4 µg of plasmid-DNA were mixed with 400 µl pure DMEM and 6 µl Turbofect reagent and the mixture was incubated for 15-20 min at RT. The medium was aspirated from the cells and the Turbofect-DNA complexes and DMEM full medium were added resulting in a final volume of 2 ml. The dishes were swirled were carefully to distribute the complexes in the whole dish. Cells were incubated at 37°C and 5 % CO_2 for 24 or 48 h and then treated as indicated for each experiment.

2.2.2.3 Stable transfection

For stable transfection of CHO-K1 cells with the plasmid pmYFP-H3 the transfection reagent Lipofectin (10 µl for 35 mm dish) and the selection antibiotic Geneticinsulfate (G418) were used. Lipofectin and plasmid-DNA (4 µg) were each separately incubated with 100 µl pure DMEM for 45 min at RT before mixing and additional incubation for 15-20 min. The cells were washed twice with pure DMEM and then the Lipofectin-DNA complexes and 1.8 ml

pure DMEM were added. After 24 h incubation at 37°C and 5 % CO_2 the medium was exchanged with DMEM full medium and cells were incubated another 24 h or more until cells were confluent. At 90 % confluence cells were split into a 94 mm dishes in dilutions 1:10, 1:20 and 1:50 and grown in the presence of 500 µg/ml G418. At about 50 % confluence fluorescent (and thus resistant) colonies were picked and transferred into a 24 well plate with a cover slip. Again cells were grown until confluence in DMEM full medium containing 500 µg/ml G418. Then, the cells on the cover slip are fixed with 4 % paraformaldehyde and imaged for detection of fluorescent protein expression. Positive clones are transferred to T25 and subsequently to T75 flasks prior to freezing. For further cultivation of stable transfected cell lines DMEM full medium containing 500 µg/ml G418 is used.

2.2.3 Protein biology

2.2.3.1 Expression of wild type and mutant HA proteins at the cell surface

2.2.3.1.1 Selection of expression system

In order to study conformational change and membrane fusion of wild type and mutant HA proteins, high expression levels at the cell surface of CHO cells are required. A plasmid expressing the H3YFP fusion protein (pEYFP-H3) was obtained from Dr. Christian Sieben of the Molecular Biophysics group which was constructed by cloning HA of the influenza virus strain A/X-31 (H3N2) into the pEYFP-N1 plasmid (Life technologies) using the restriction sites *NheI* and *SacII* resulting in the H3YFP fusion protein (H3 carrying YFP at its C-terminus). However, expression of HA proteins in mammalian cells is typically performed using the pCAGGS expression plasmid which contains a hybrid CMV-chicken β-actin promoter.

To compare the levels of H3YFP expression obtained with the different plasmid systems the H3YFP fusion protein was subcloned into the pCAGGS-*Esp*-blue (pCAG) plasmid which was provided from Dr. Volker Czudai-Matwich (Institute of Virology, Philips University Marburg) [307]. Expression levels of H3 HA fusion proteins depending on the expression system were compared by analyzing the YFP-fluorescence of transfected cells using confocal microscopy and flow cytometry. Expression of H3YFP was indeed higher using the pCAG plasmid as observed by confocal microscopy (Figure 2.4 A). Quantification of the mean fluorescence intensity (MFI) of H3YFP expressed in CHO cells yielded a 3 times higher fluorescence intensity as analyzed by flow cytometry (Figure 2.4 B). Hence, for expressing HA proteins at the cell surface the pCAG plasmid was used in all subsequent experiments. Furthermore, different transfection reagents were tested for their ability to successfully deliver the gene

encoding plasmids into the cells. Turbofect (Fermentas) and Lipofectamine 2000 (Life technologies) showed the same efficiency with 34 and 36 % of transfected cells, respectively (Figure 2.4 C). Due to less cytotoxicity and easier handling Turbofect was used as transfection reagent in all subsequent experiments.

2.2.3.1.2 Cleavage activation of low pathogenic HA

HA is synthesized as HA0 precursor protein which needs to be cleaved into HA1 and HA2 after trimerization resulting in the release of the fusion peptide. Highly pathogenic HA proteins (H5 HP) carry a polybasic cleavage site which is cleaved by intracellular proteases in the course of transport to the cell surface. In contrast, low pathogenic HA proteins (H5 LP) have a monobasic cleavage site which can only be cleaved extracellularly by trypsin-like proteases. Thus, before acidification, the low pathogenic HA proteins (H3 and H5 LP) were treated with 4 µg/ml TPCK trypsin for 5 min at room temperature for cleavage activation. The reaction was stopped by the addition of DMEM full medium.

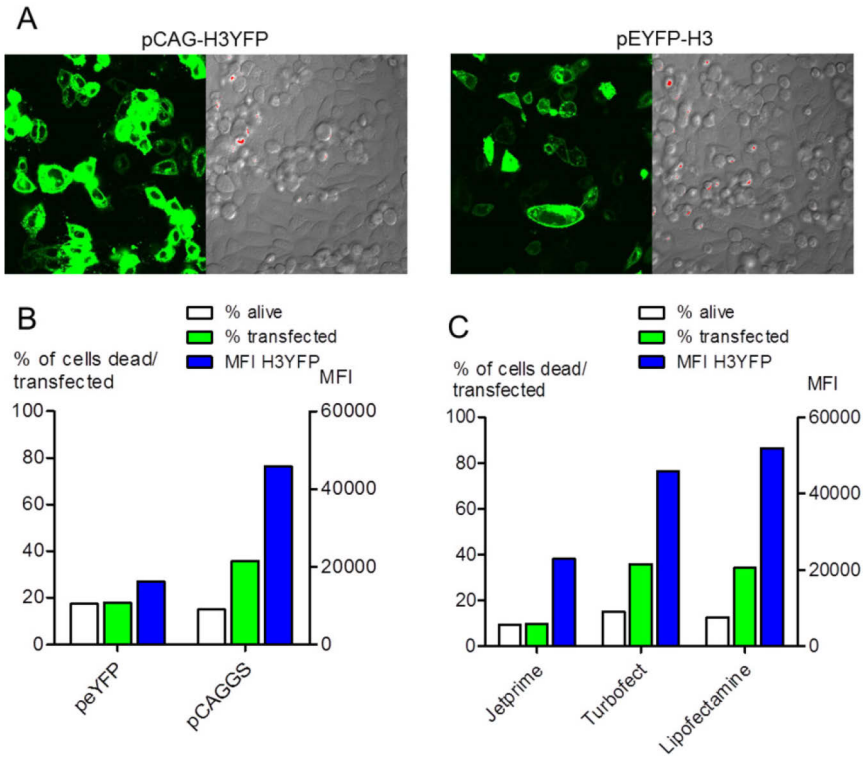

Figure 2.4: Selection of expression plasmids and transfection reagents for HA expression using YFP as reporter.
(A) Representative images of H3YFP expressed in CHO cells from the pCAG or pEYFP plasmid, respectively. (B) Quantitative analysis of H3YFP expression from different plasmids in CHO cells by flow cytometry. (C) Quantitative analysis of H3YFP expression in CHO cells using different transfection reagents.

2.2.3.2 Expression analysis

2.2.3.2.1 Expression and cleavage analysis by SDS PAGE and Western Blot

Expression and cleavage of mutant proteins was analyzed by SDS PAGE and Western blotting and by Immunostaining and flow cytometry (see 2.2.3.5) using the mouse monoclonal Vn04-2 antibody (dilution 1:1000). 48 h post-transfection cells were washed twice with PBS- and detached using 2 mM EDTA. After centrifugation at 385 g for 5 min the cell pellet was resuspended in 100 µl PBS-. Samples were divided and reducing or non-reducing loading dye was added, respectively. Samples were incubated at 60°C (non-red.) or 95°C (red.) for 5 min before loading on a 10 % SDS PAGE. Proteins were transferred on a nitrocellulose membrane by semi-dry western blotting for 1.5 h and membranes were incubated for 1 h at room temperature in Odyssey blocking buffer. H5 HA was detected with primary Vn04-2 antibody (1:1000, at 4°C over-night) and secondary LICOR goat anti-mouse IRDye 680 (1:20 000, 1h at RT). Uncleaved H3YFP was taken as control which was detected using the mouse polyclonal anti GFP antibody (1:1000) and equal loading of wells was confirmed using the mouse polyclonal anti β-actin antibody (1:3000).

2.2.3.2.2 Trimer formation assay

To increase the yield of detectable trimers, 3, 3-dithiobissuccinymidylpropionate (DSP) was used for the analysis of trimer formation of H5 wild type and mutant proteins. DSP covalently links the three monomers within a trimer which can be subsequently detected by SDS PAGE and Western blotting using the monoclonal anti H5 Vn04-2 antibody (dilution 1:1000). 48 hours post-transfection cells in a 6 well plate were lysed by the addition of 250 µl ice-cold lysis buffer. After an incubation of 10 min cells were scraped off and shaken for 30 min at 4°C. Cells were centrifuged at 12 000 g for 30 min and supernatants were treated with 0.8 mM DSP in DMSO for 15 min at 15°C. The reaction was stopped by addition of 20 mM ammonium chloride and after addition of loading dye and incubation at 60°C for 5 min samples were subjected to a 6 % SDS PAGE and Western blot analysis under non-reducing conditions. H5 HA proteins were detected using antibodies Vn04-2 and LICOR goat anti mouse IRDye 680 as described above. Samples without DSP reagent were taken as controls for the respective protein.

2.2.3.3 Adjustment of pH *in vitro*

The HEPES fusion buffer was adjusted with 1 M NaOH and 1 M HCl before adding the buffer to the HA expressing cell monolayers. In the red blood cell fusion assay cells were incubated

for 5 min with the buffer of the respective pH at 37°C with a subsequent re-neutralization step for 2 min at 37°C. For conformational change analysis by flow cytometry cell monolayers were incubated for 15 min with fusion buffer before re-neutralization.

2.2.3.4 Red blood cell fusion assay

Fresh human red blood cells (RBCs) were double labeled with the lipoid dye octadecyl rhodamine B chloride (R18) and the content marker Calcein (Molecular Probes, Life technologies). HA expressing CHO-K1 cells were treated with 0.5 U/ml neuraminidase and with 4 µg/ml TPCK trypsin (if required) followed by incubation with DMEM supplemented with 10 % FBS. CHO-K1 cells carrying the activated HA proteins were then incubated with the double labeled RBCs for at least 30 min to induce binding of the RBCs to HA at the cell surface. After the incubation time samples were washed three times with PBS+ to get rid of unbound RBCs and analyzed for RBC binding and, after low pH incubation, for fusion under the fluorescence microscope (Olympus Fluoview FV-1000).

2.2.3.5 Immunostaining and flow cytometry

The expression of the HA proteins at the cell surface was quantified at neutral pH using the Vn04-2 antibody (dilution 1:1000). The conformation of HA at different pH was assessed using the monoclonal antibodies Vn04-9 or Vn04-16 (dilution 1:500) which have been previously described to preferentially bind the neutral (Vn04-9) or low (Vn04-16) pH conformation of H5 HA [297,316]. 48 h post-transfection cells growing in 24 well plates were incubated with neutral (pH 7.0) or low pH (pH 5.0-6.6) for 15 min at 37°C as described above. After re-neutralization with PBS+, cell monolayers were blocked with 0.2 % BSA in PBS+ for 15 min on ice and all subsequent steps were also performed on ice. For expression analysis cells were overlaid with the primary antibody Vn04-2 in 0.2 % BSA in PBS+ whereas for assessing the conformational change primary antibodies VN04-9 and -16 were used. After incubation for 45 min samples were washed three times with 0.2 % BSA in PBS+ and overlaid with a fluorescently labeled secondary anti-mouse antibody for 30 min. Cells were detached using 2 mM EDTA in PBS- following analysis by flow cytometry using the FACS Aria II (BD Biosciences). Expression of mutant proteins relative to the wild type was evaluated by normalizing the median fluorescence intensity (MFI) values of 10 000 cells to that of the highly pathogenic H5 HA wild-type protein. The pH of conformational change was determined as the point at which 50 % change in signal occurred between minimum and maximum of respective Vn04-9/Vn04-16 ratios (Figure 2.5).

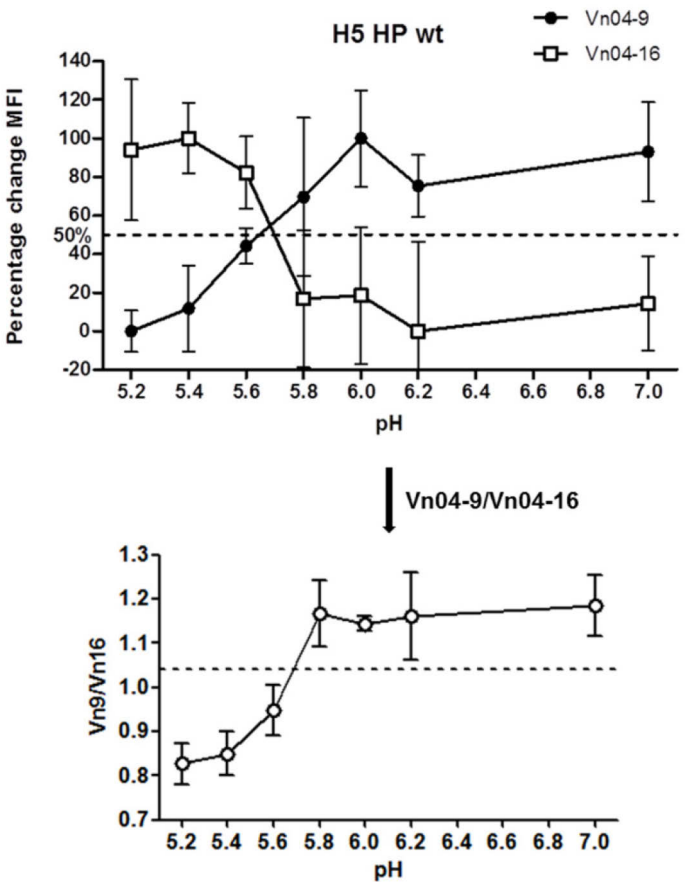

Figure 2.5: Determination of the pH of conformational change for H5 wild type and mutant proteins.
The ratio of Vn04-9- to Vn04-16 binding was calculated and plotted as a function of pH. The pH of conformational change corresponds to the pH of 50 % of change in the Vn04-9/Vn0416-ratio.

2.2.3.6 Computational modeling

Analysis of H3 and H5 crystal structures and computational modeling of mutations was performed by Tim Meyer (Macromolecular Modeling, FU Berlin). His184 mutations were modeled into the crystal structure of highly pathogenic H5 HA (PDB ID: 2IBX). The residue His184 in chain A, C and E was replaced. Missing atoms were added using default internal coordinates of CHARMM22 [317,318]. To obtain reasonable interactions of the mutated residue with its environment, the model was geometry optimized with CHARMM [318] using the CHARMM22 [317] force field. The influence of the solvent was considered implicitly with a dielectric constant of 80 by using the GBSW Generalized Born module [318] of CHARMM. To obtain the correct protonation state for the histidines at neutral pH an electrostatic energy calculation was also performed by Tim Meyer using the software Karlsberg+ [319].

2.2.4 Virology

2.2.4.1 Construction of pHW plasmids for the production of recombinant WSN H3 viruses

To produce recombinant WSN viruses containing H3 wild type or mutant HA instead of H1 HA, new pHW plasmids were constructed containing the respective HA segment. Each segment is composed of the viral cDNA which carries additional non-coding regions (NCR) at the 3' and 5' end (cRNA). These NCRs include conserved packaging signals which are crucial for vRNP synthesis.

The viral RNA of the segment encoding H3 HA was extracted from A/Aichi/2/68 (X-31, H3N2) and the viral cRNA (including NCRs) was synthesized by reverse transcription using the Uni12 primer followed by amplification with H3 HA specific primers containing the *BsaI* restriction sites [308]. These restriction sites were used for cloning the cRNA of H3 HA into the pHW plasmid. The T212E-N216R mutation was inserted using an adapted Quick change mutagenesis protocol from Stratagene. Correct insertion of the segments was confirmed by sequencing (GATC Biotech AG, Germany).

2.2.4.2 Production of recombinant viruses

For the production of recombinant viruses the eight-plasmid-system was used [19]. The pHW plasmids containing the cDNA encoding for all 11 viral proteins of A/WSN/1933 (H1N1) were kindly provided by Dr. Michael Veit (Free University Berlin). These plasmids contain the viral cDNA sequences encoding all required viral proteins of A/WSN/1933 (H1N1). The cDNA sequence in each plasmid is inserted between the pol I promoter (p_{Ih}) and the pol I terminator (t_I) (Figure 2.6). This pol I transcription unit is flanked by the pol II promoter (p_{II}CMV) of the human cytomegalovirus and the polyadenylation signal of the gene encoding bovine growth hormone (a_{II}BGH).

To obtain recombinant WSN H3 viruses the plasmid encoding H1 HA was exchanged for the newly constructed plasmids encoding the H3 wild type or H3 T212E-N216R yielding WSN H3 wt and WSN H3 T212E-N216R mutant viruses, respectively. HEK-293T cells were simultaneously transfected with 0.5 µg of each plasmid in a 35 mm dish. After 6 h of incubation at 37°C and 5 % CO_2 the medium was exchanged with virus cultivation medium (DMEM with 0.1 % FBS, 0.2 % BSA, 2 mM glutamine, 1 % penicillin/streptomycin and 4 µg/ml TPCK Trypsin). After 2 days the virus was harvested by centrifugation of the cell supernatant at 2000 rpm to get rid of cell debris.

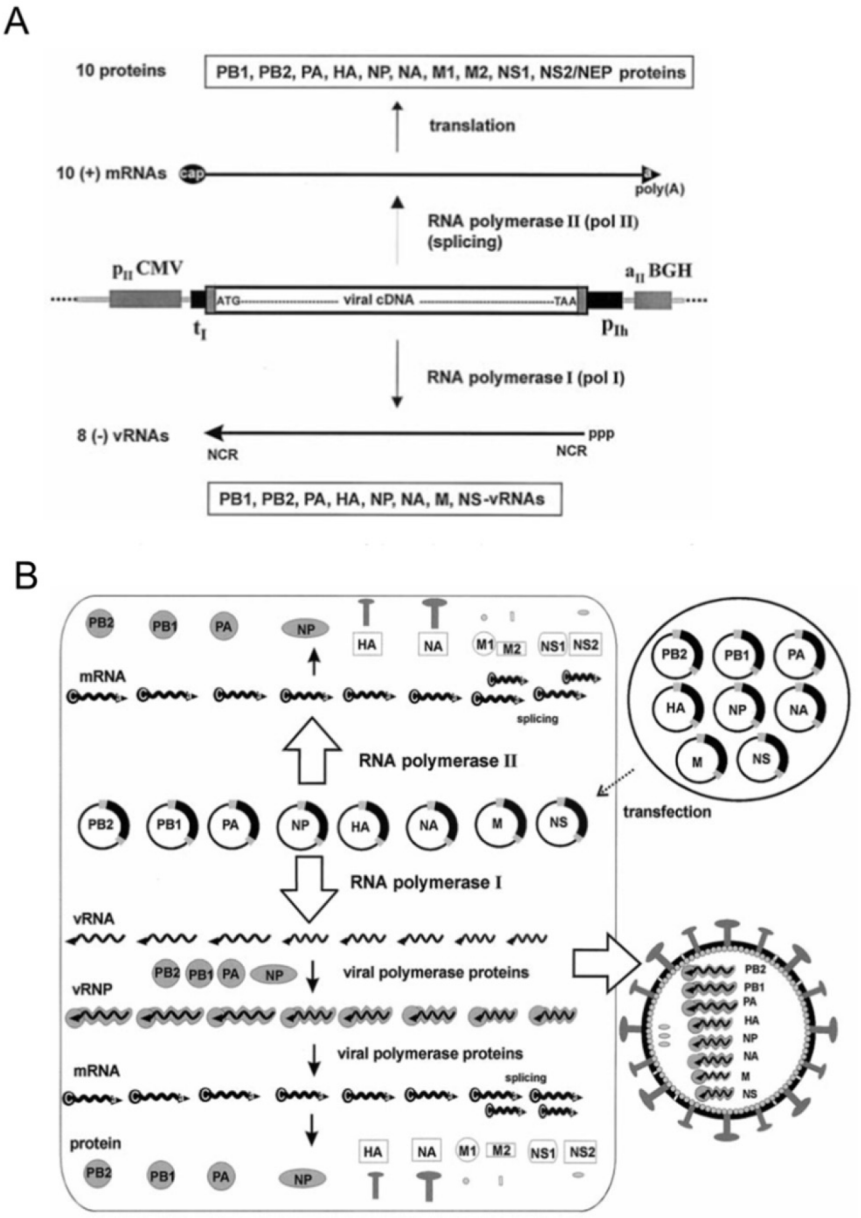

Figure 2.6: Schematic representation of the pol I-pol II transcription system and the generation of recombinant viruses from the eight plasmid system.
(A) The viral cDNA of each of the eight influenza virus segments is inserted between the pol I promoter (pIh) and the pol I terminator (tI). This pol I transcription unit is flanked by the pol II promoter (pIICMV) of the human cytomegalovirus and the polyadenylation signal of the gene encoding bovine growth hormone (aIIBGH). After transfection of HEK-293T cells with the eight expression plasmids, two types of molecules are synthesized. From the human pol I promoter, negative-sense vRNA is synthesized by cellular pol I. Transcription by pol II yields mRNAs with 5' cap structures and 3' poly(A) tails; these mRNAs are translated into viral proteins (B). After packaging of vRNPs and transport to the cell surface, new infectious recombinant viruses are produced which can be harvested and amplified in MDCK cells (from Hoffmann *et al*. 2000) [19].

For amplification of recombinant viruses MDCK cells were infected in 6 well plates with 1 ml of 1:1, 1:10 and 1:100 dilutions of the cleared supernatant containing the virus. After 1 h incubation at 37°C and 5 % CO_2 the medium was exchanged with virus cultivation medium. The virus was harvested after 48 h or when at least 70 % of cell death (CPE) was observed. Virus-containing supernatants were titrated using a $TCID_{50}$ assay (see 1.1.1.1.4) and stored at -80°C. For further amplification MDCK cells were infected with virus-containing supernatant in T75 and T175 flasks at an MOI of 0.01.

2.2.4.3 Concentration and purification of recombinant viruses

For of extra- and intracellular fusion measurements a concentrated and purified virus suspension is required. Therefore, the cell supernatant was (ultra-)centrifuged at 100 000 g for 2 h at 4°C. After drying of the pellet for 5-10 min the pellet was “swollen” in 200-500 µl TNE buffer and for 15 min at 4°C before resuspension. To get rid of cellular proteins and other vesicles, which are also present in the supernatant, the concentrated virus suspension was loaded on a 20-60 % sucrose gradient and centrifuged for an additional 4 h at 100 000 g at 4°C. The virus was carefully removed from the gradient and washed in 30-50 ml PBS-. After pelleting for 1.5 h at 100 000 g at 4°C the virus was resuspended in a small volume (200-300 µl) PBS- as described above.

2.2.4.4 Virus quantification and titration

1.1.1.1.1 Protein quantification

Total protein concentration of viruses can be taken as measure of virus concentration in the concentrated and purified virus suspension since the viral membrane is covered by its spike proteins HA and NA. Thus, the protein or virus content respectively was determined using the BCA protein assay kit. Briefly, samples are diluted 1:10, 1:20 and 1:50 and incubated with the BCA reagent according to the manufacturer’s protocol for 30 min hours at 37 ºC. After cooling of samples the absorbance is measured at 562 nm on a spectrophotometer. Protein concentration of the unknown samples is determined based on a standard curve of bovine serum albumin (BSA).

1.1.1.1.2 Hemagglutination assay

Another known assay for the determination of virus concentration in the sample is the hemagglutination assay (Figure 2.7). The virus titer is assessed based on the ability of HA to

agglutinate red blood cells (RBCs), which carry the sialic acid cell receptor at the surface. As each of the agglutinating molecules (HA) attaches to multiple RBCs, a lattice-structure will form in the presence of virus which can be observed from the top. If the virus concentration is too low or no virus is present at all the RBCs form a pellet at the bottom of the well. To assess the hemagglutination titer of a sample two-fold dilutions are prepared in 96- round or v- bottom well plates in PBS-. Then human or chicken RBCs (1 % in PBS-) are added to the samples followed by incubation for 30 min up to an hour at room temperature. The viral titer is then determined based on the last viable "lattice" structure found (approximately the HA titer multiplied by 10^7).

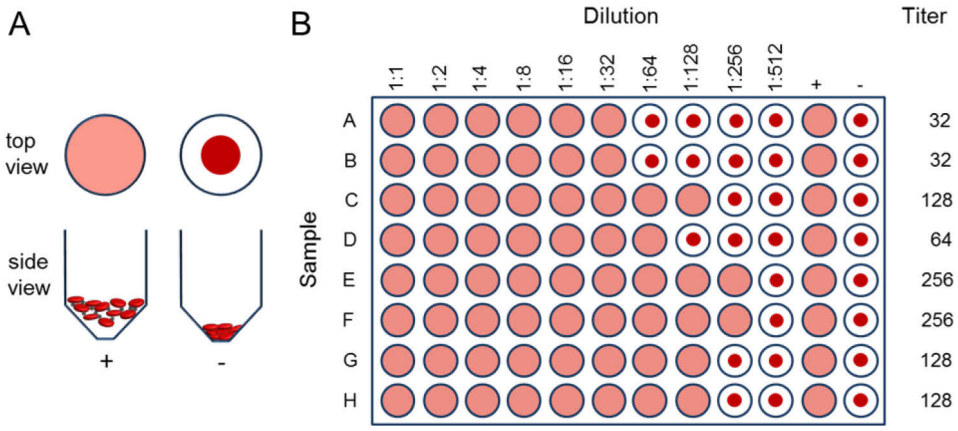

Figure 2.7: Schematic depiction of the hemagglutination assay.
(A) Influenza viruses bind to erythrocytes (RBCs, red) via their envelope protein hemagglutinin resulting in the formation of a lattice (hemagglutination positive, +). If the virus concentration is too low or no virus is present at all the RBCs form a pellet at the bottom of the well (hemagglutination negative, -). (B) To assess the concentration of influenza viruses in a sample, two-fold dilutions are prepared in a 96-well round bottom or v-bottom plate. After incubation with RBCs the hemagglutination titer is determined by the last dilution where a lattice structure can still be observed.

1.1.1.1.3 Plaque Assay

Both above mentioned assays determine the total protein or hemagglutinin concentration in the sample and thus do not give any measure of viral infectivity. In contrast, in the plaque assay the number of infective particles within the sample is determined based on the CPE. Confluent monolayers of MDCK cells are infected with the virus at varying dilutions (usually in 10-fold) and covered with a semi-solid medium, such as agar or carboxymethyl cellulose which prevents the virus from spreading indiscriminately. When a cell of the monolayer gets infected, this cell will lyse and spread the infection to adjacent cells so that after repeated cycles of lysis and infection a plaque will emerge which can be discriminated by eye from the

surrounding monolayer. The number of plaque forming units per unit volume (Pfu/mL) is calculated by multiplying the number of plaques with the dilution factor and applied volume.
Briefly, MDCK cells were seeded in 6 well plates to a confluence of 90-100 % and infected with 10 fold –dilutions of recombinant viruses as described in 2.2.4.1. After 1 h cells were washed two times with PBS+ and overlaid with agarose semi-solid medium (0.4 % sea plaque agarose in EMEM supplemented with 0.1 % FBS, 0.2 % BSA, 2 mM glutamine, 1 % penicillin/streptomycin and 4 µg/ml TPCK Trypsin).

1.1.1.1.4 50 % Tissue Culture Infectious Dose ($TCID_{50}$)

The $TCID_{50}$ is an endpoint dilution assay which quantifies the amount of virus required to infect 50 % of inoculated tissue culture cells. Thus, this assay can be used to determine the amount of infectious virions in a sample irrespective of their ability to replicate. Several methods can be used to assess the $TCID_{50}$. In this study infected cells were assessed by ELISA [320].
Briefly, virus samples were diluted in ½ log_{10} steps in a 96 well plate (4-8 replicates). 1.5 $x10^4$ MDCK cells were washed in virus diluent (DMEM supplemented with 1 % BSA, 1 % P/S and 20 mM HEPES) and added to the virus. After 20h of infection cells were washed in PBS+ and fixed with 80 % ice-cold acetone (10 min) following staining using the primary mouse influenza anti NP antibody (Millipore) and the secondary Goat anti-mouse IgG antibody (Life technologies) which is conjugated to horseradish peroxidase. After addition of the substrate σ-phenylenediamine dihydrochloride (OPD) and color formation the reaction was stopped by the addition of 0.5 M sulfuric acid and absorption was measured on the plate reader. The $TCID_{50}$ was calculated using the Reed and Muench method [321].

2.2.4.5 Infection studies

The infectivity of recombinant viruses was assessed in MDCK and A549 cells. Therefore, 2 $x10^5$ cells growing on glass cover slips were infected with the respective virus at an MOI of 0.1 as determined by $TCID_{50}$. 20h post-infection cells were fixed with 4 % PFA and 0.1 % glutaraldehyde in PBS+ (10 min), perforated using 0.1 % Triton-X (5 min) and then stained against the influenza virus NP protein using the primary mouse influenza anti NP antibody (Millipore) and the secondary Anti mouse Alexa488 (Life technologies). Nuclei were stained using DAPI (14nM). Images were taken at the confocal microscope (Olympus Fluoview 1000) and the number of infected cells in percent of total cells in each image was analyzed using the cell image analysis software Cell Profiler (Broad Institute, Cambridge, USA).

2.2.4.6 Fluorescence dequenching assay

To assess the pH threshold of fusion for wild type and mutant recombinant viruses the fusion efficiency of these viruses was assessed by fluorescence dequenching in the pH range from 5.0 to 6.5 using red blood cell ghosts as target membrane (Figure 2.8).

1.1.1.1.5 Preparation of red blood cell ghosts

Purified human erythrocytes (Blutbank, Charité) were washed three times in PBS (2000 g, 10 min). One volume of erythrocytes (RBCs) was resuspended in 10 times the volume ice cold hemolysis buffer. The cells were lysed for 30 - 50 min on ice and centrifuged for 20 min at 5000 g. The lysed RBCs were incubated on ice for 10 min with occasional stirring. These lysis-washing cycles were repeated until the pellet appeared white. The cells were washed in PBS, pelleted and stored at 4 C with 0.02 % sodium azide.

1.1.1.1.6 Virus labeling with R18

100 µl of concentrated and purified virus (~10^6 Pfu) were labeled with 1 µl of 2 mM R18 by incubation for 30 min up to 1 h on ice. To get rid of non-incorporated R18 the virus-dye mixture was centrifuged at 100000 g for 5 min and virus-pellet was resuspended in 100 µl PBS.

1.1.1.1.7 Measurement of pH dependent fusion by fluorescence dequenching

For the fusion measurement 10 µl of labeled virus were bound to a 1:10 dilution of red blood cell ghosts (5-10 mg ghosts/ml) in 40 µl of PBS for 20 min at room temperature. Unbound virus was removed by centrifugation for 5 min at 5000 g and ghosts with bound viruses were resuspended in 40 µl PBS. The virus-ghost suspension was subsequently added to 1.96 ml of pre-warmed sodium acetate fusion buffer in a cuvette and the fluorescent emission at 590 nm was recorded by using a Horiba Yobin Yvon FluoroMax. After 100 seconds 250 mM citric acid was added to decrease the pH from neutral to acidic inducing fusion. The fluorescence increase due to R18 dequenching was measured for 500 sec. The maximal dequenching of R18 was achieved by addition of detergent (0.5 % Triton-X in ddH_2O). The fusion efficiency obtained at the specific pH was calculated by the formula

$$FDQ = \frac{F(t) - F(0)}{Fmax - F(0)} \times 100$$

with F(0) as the fluorescence signal of quenched R18 (before the onset of fusion), Fmax, the maximal dequenching signal of R18 (after addition of Triton-X 100), and F(t), the signal obtained 500 sec after the onset of fusion.

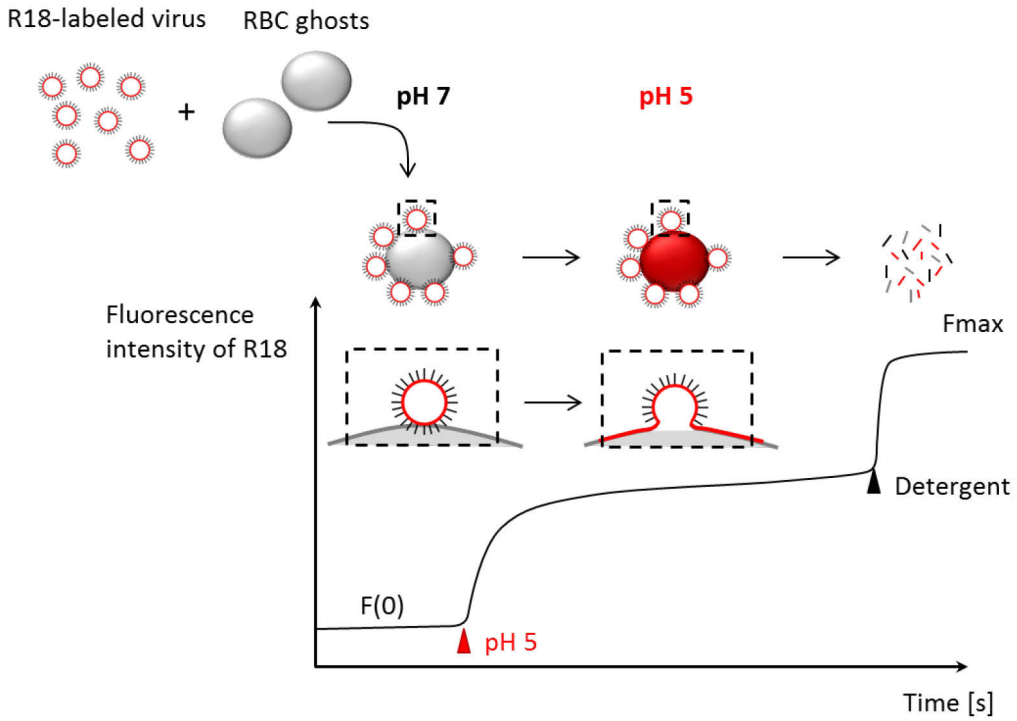

Figure 2.8: Fluorescence dequenching assay.
Influenza viruses are labeled with R18 at self-quenched concentration. The labeled viruses bind to red blood cell ghosts due to the presence of SA receptors at the cell surface. After incubation for 20 min at RT with RBC ghosts unbound viruses are removed by centrifugation and the virus-ghost suspension is transferred to a glass cuvette containing pre-warmed fusion buffer (pH 7.4). The fluorescence is detected (ex = 560nm; em = 590 nm) in a spectrofluorometer (F(0)). By the addition of citric acid (0.25 µM) the pH is lowered triggering the fusion of membranes (pH 6.5-5.0). The fusion reaction is finally stopped by the addition of detergent (0.5 % Triton X-100) to obtain maximum R18 dequenching (Fmax).

2.2.4.7 Intracellular fusion assay

In contrast to bulk fusion assays as described above imaging of single events of virus-endosome fusion gives information of the time-point and exact site of fusion inside living cells [53,70,106]. Sakai *et al.* reported a dual wavelength imaging approach [322] facilitating the quantification of numerous single fusion events by a color shift from the red fluorescent R18 (here DiI) to the green fluorescent DiO. In the labeled virus, the green fluorescence is suppressed by both, self-quenching of DiO and fluorescent resonance energy transfer

(FRET) from DiO to DiI, whereas the red fluorescence from R18 is partly self-quenched. Upon membrane fusion of the viral with the endosomal membrane and dilution of both dyes, self-quenching and FRET is removed resulting in a dramatic increase of the green fluorescence which is plotted as a function of time (Figure 2.9 A)[322][322].

1.1.1.1.8 Virus labeling with DiO and DiI

33 µM DiO and 67 µM DiI were mixed in a ratio of 1:3 in Ethanol. 100 µg of the concentrated and purified virus suspension (100 µl of 1 mg/ml stock, ~10^6 Pfu) were diluted in PBS+ to a final volume of 1 ml in 2 ml round bottom Eppendorf tubes. 6 µl of the DiO/DiI mixture were added under vigorous mixing on the vortexer (final concentrations: 0.2 µM DiO and 0.4 µM DiI). The mixture was incubated under continuous shaking for 1 h at room temperature and then put on ice. Viral aggregates were removed by filtration using 0.45 µm pore size filters. Correct labeling was evaluated by measuring the fluorescence emission spectra of samples before and after the addition of 0.5 % Triton-X (Figure 2.9 B).

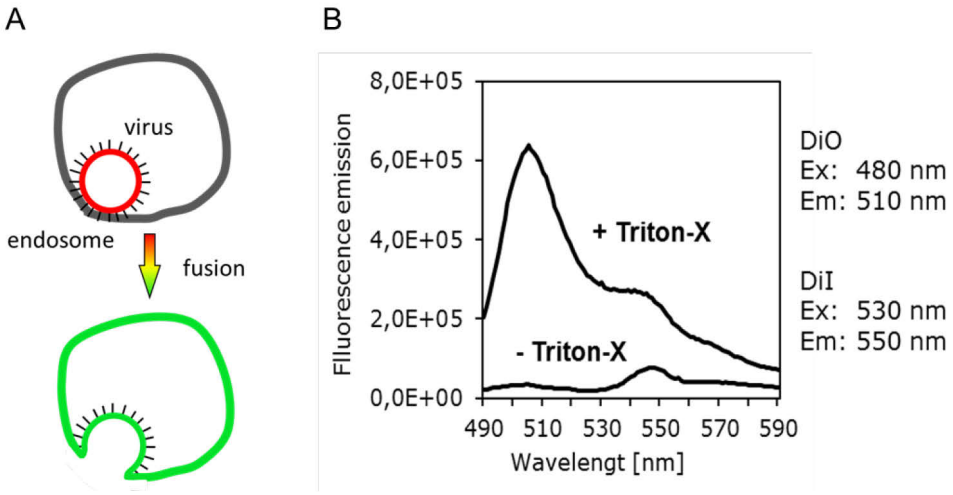

Figure 2.9: Intracellular fusion assay.
(A) Influenza viruses are labeled with 0.2 µM DiO and 0.4 µM DiI. Due to Foerster Resonance Energy Transfer (FRET) and quenching of DiO the labeled particles appear red. Upon fusion with the endosomal membrane FRET is removed and DiO is dequenched so that the fluorescence intensity of DiO increases. (B) Fluorescence emission spectra of DiO/DiI-labeled particles before/after the addition of detergent. The DiO signal in labeled viruses is suppressed due to self-quenching and FRET whereas DiI is only partly quenched (-Triton-X). Upon membrane solubilization with Triton-X the DiO fluorescence is rescued resulting in a significant increase of the DiO signal (+Triton-X).

1.1.1.1.9 Imaging of intracellular virus fusion

Cells were seeded in 35 mm MaTek dishes to reach a confluence of 60-70 % until the onset of the experiment. To label the nuclei cells were incubated 30 min with Hoechst in DMEM full medium. After 2 times washing with PBS+ on ice, 10 µl of labeled and filtered viruses were mixed with 40 µl of 0.2 % BSA in PBS+ and binding of viruses to the cells was induced by incubation for 10 min on ice. Unbound viruses were removed by washing with PBS+ and 1 ml of pre-warmed DMEM full medium without phenol red was added. Cells were immediately transferred to the microscopic stage and imaged every 3 min at 37°C and 5 % CO2 in a climate chamber.

3 Results

3.1 Identification of protonable residues and of pH stability modulating mutations in H5 HP

One of the aims of the present study was to identify critical pH sensors in the influenza virus HA which upon protonation trigger the conformational change of the protein and as a consequence, fusion of the viral with the endosomal membrane. We focused on His184 as potential molecular switch since it has already been previously hypothesized to trigger the conformational change of HA [163]. Indeed, due to its central position at the HA1-HA1 interface protonation of His184 very likely could destabilize inter-monomeric pre-fusion contacts upon protonation (Figure 3.1). Furthermore, His184 is highly conserved among all subtypes (except H17 and H18) and within individual subtypes emphasizing its significance. Likewise, we addressed His110 as a potential pH sensor at the HA1-HA2 interface of H5 HA. His110 is located close to the B loop which is also rearranged at low pH (20, 21) and thus may trigger structural rearrangements of this domain upon its protonation. However, different to His184, His110 is only conserved in H2, H5, H13 and H16 subtypes.

To characterize His184 and His110 as potential pH sensors we substituted these two amino acids for different amino acids and analyzed their effect on the pH dependence of conformational change and membrane fusion. Previous mutational studies of histidines (His17 and His18 of HA1 and His106/111 of HA2) in the HA protein revealed that the effect on fusion largely depends on the substituted amino acids [162,297,323]. Thus, in order to obtain comprehensive results we selected a subset of structurally diverse amino acids as substitutes for His184 and His110[3]. Asparagine was selected for replacing His184 (H184N) since it is structurally most similar to histidine. Therefore, it might be able to interact with neighboring residues at the interface like histidine but does not have the propensity to get protonated at low pH. In contrast, the neutral alanine at position 184 (H184A) was predicted to abrogate any interactions of His184 with neighboring residues which would provide information about the structural significance of histidine at position 184. Arginine with its positive charge was selected to mimic a protonated histidine which, at first glance, should destabilize inter-monomeric interactions. The negatively charged aspartate was chosen as a

[3] Substitutes were selected based on computational prediction of protein stability in collaboration with Qiang Huang, State Key Laboratory of Genetic Engineering, School of Life Sciences, Fudan University, Shanghai and Tim Meyer, Institute of Chemistry and Biochemistry, Free University Berlin.

residue potentially stabilizing the HA1-HA1 interface. Correspondingly, we selected arginine as destabilizing (H110R), glycine as neutral (H110G) and glutamate as stabilizing (H110E) substitutes for His110. Tyrosine (H110Y) was selected due to its reported stabilizing effect on H5 HA when replacing histidine at position 110 [260,324]. All mutant proteins were expressed at the cell surface of CHO cells and the effect of individual mutations on the pH dependence of conformational change and fusion was assessed using two different assays (see 3.3).

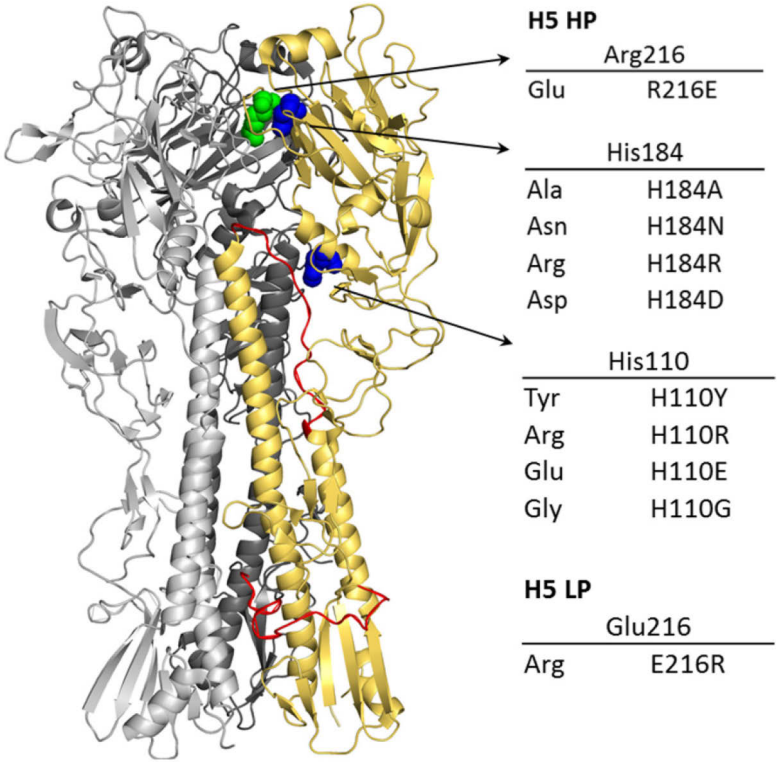

Figure 3.1: Crystal structure of the highly pathogenic H5 HA (PDB ID: 2IBX) in surface and cartoon representation.
Monomers are marked in yellow, light and dark gray. Histidines at positions 184 and 110 (blue) as well as residue at position 216 (green) are depicted as spheres in the yellow colored monomer with selected substitutes for these residues in H5 HP and LP listed in the table next to it. The B-loop and the fusion peptide are marked in red.

Another aim was to identify mutations in the influenza virus H5 HA which might have contributed to the evolution of the highly pathogenic phenotype in 2003-2004. Aligning the sequences of H5 HP and H5 LP we identified a Glu-to-Arg mutation at position 216 in the highly pathogenic H5 HA. Residue 216 is located close to His184 and the exchange of charge might thus affect the pK_a of His184 and as a consequence, the acid stability of H5 HA (Table 3.1). To assess the effect of the present charge at position 216 in the highly and the low pathogenic H5 HA (H5 HP and LP) on the acid stability of the protein, we replaced the

positively charged arginine in H5 HP by the negatively charged glutamate (H5 HP R216E) and glutamate in the low pathogenic subtype (H5 LP) by arginine (H5 LP E216R). Apart from the charged residue at position 216, another charge is present at the HA1-HA1 interface of all H5 and H2 subtypes, where the H3 subtype does not carry any charge at neither position (Table 3.1). Therefore, the effect of these two additionally charges on the acid stability of the H3 subtype was also studied.

Table 3.1: Sequence alignment of H5 HP and LP and of H2 and H3 subtypes.

Consensus sequence H5 HP	N P T T Y I S V G T S T L N Q R L V P R I A T R S K V N
A/Ck/Indonesia/4/2004	. . . . . K . . . . .
A/Ck/Thailand/73/2004	. . . . .
A/Ck/Viet Nam/35/2004	. . . . .
A/Ck/Viet Nam/36/2004	. . . . .
A/Ck/Viet Nam/37/2004	. . . . .
A/Ck/Vietnam/P41/2005	N P T T Y I S V G T S T L N Q R L V P R I A T R S K V N
Consensus sequence H5 LP	N P T T Y I S V G T S T L N Q R L V P E I A T R P K V N
A/Chicken/Hong Kong/1203/97	. . . . .
A/Duck/Hong Kong/p46/97	. . . . .
A/goose/Guangdong/3/1997	. . . . .
A/teal/Germany/Wv632	N P T T Y I S V G T S T L N Q R L V P E I A T R P K V N
Consensus sequence H2	N V G T Y V S V G T S T L N K R S V P E I A T R P K V N
A/duck/Hokkaido/95/01	. . . . .
A/duck/Hong Kong/273/78	. . . . . I . . . . .
A/Japan/305/1957	. . . . . T . . . . .
Consensus sequence H3	Q A S G R V T V S T R R S Q Q T I I P N I G S R P W V R
A/Aichi/2/1968	. . . . .
A/Alaska/04/2013	. S . . . I . . . . K . . . . A V . . . . . R I .
Mutated sequence	Q A S G R V T V S T R R S Q Q E I I P R I G S R P W V R

[a]Strains used in this study are marked in bold. H5 HA of highly pathogenic strains isolated from birds and mammals since 2003/04, carry a positive charge (arginine or lysine, green) at position 216 whereas all low pathogenic virus strains have a negative charge (glutamate, red) at that position. Interestingly, H2 subtypes, like H5 LP, also have Glu at position 216 and Arg at position 212 whereas H3 subtypes do not carry these charges.

3.2 Expression of wild type and mutant proteins at the cell surface

3.2.1 Construction of HA expression plasmids

A fluorescent protein such as YFP or even a smaller tag facilitates the detection of HA, though at the same time may hinder the HA conformational change and thus the ability to induce fusion. Therefore, all wild type and mutant H3 and H5 proteins were cloned into the pCAG vector without the addition of a fluorescent protein or another easily detectable tag using the oligonucleotides listed in Table 3.2. The pcDNA3-H5 plasmid encoding for the H5 HP wild type protein of influenza H5N1 A/Vietnam/P41 as well as the viral RNA of the low pathogenic influenza strain A/teal/Germany/632wv/2006 were obtained from Dr. Timm Harder (Friedrich Loeffler Institute, Insel Riems, Germany).

Table 3.2: Constructs used for HA expression at the cell surface of CHO cells.

Construct	Names of oligonucleotides used for cloning
pCAG-H5 HP	*Bsm-H5* pCAG fw and rev
pCAG-H5 HP R216E	H5 HP R216E fw and rev
pCAG-H5 HP H184A	H5 HP H184A fw and rev
pCAG-H5 HP H184N	H5 HP H184N fw and rev
pCAG-H5 HP H184R	H5 HP H184R fw and rev
pCAG-H5 HP H184D	H5 HP H184D fw and rev
pCAG-H5 HP H110R	H5 HP H110R fw and rev
pCAG-H5 HP H110E	H5 HP H110E fw and rev
pCAG-H5 HP H110G	H5 HP H110G fw and rev
pCAG-H5 HP H110Y	H5 HP H110Y fw and rev
pCAG-H5 LP	Uni12 for cDNA synthesis, pCAG H5 LP fw and rev for cloning
pCAG-H5 LP E216R	H5 LP E216R fw and rev
pCAG-H3YFP	*BsaI*-H3 pCAG fw and *BsaI*-YFP rev
pCAG-H3	*BsaI*-H3 pCAG fw and rev
pCAG-H3 T212E-N216R	*BsaI*-H3 pCAG fw and rev

Both, H5 HP and LP encoding sequences were subcloned into the pCAG plasmid using the *BsmBI* restriction sites [307]. The cDNA of H5 LP was obtained from the viral RNA as described by Hoffmann *et al.* [308] using the One-Step RT-PCR Kit from QIAgen. Thereby the viral cDNA is acquired by reverse transcription using the Uni12 primer and the H5 LP gene sequence is subsequently amplified using H5 specific primers which contained the *BsmBI* restriction sites for cloning into the pCAG plasmid. Mutations into H5 HP and LP were introduced by overlap extension PCR (see 2.2.1.8). H3 HA wild type and T212E-N216R

mutant were amplified from the pTM1-plasmids provided by Dr. Sivaramakrishna Rachakonda and cloned into pCAG using the *BsaI* restriction sites.

3.2.2 Quantification of surface expression

In order to quantify the expression level of all proteins at the cell surface immunostaining and flow cytometry using the Vn04-2 antibody was performed. The antibody was reported to have a broadly neutralizing activity against highly pathogenic H5N1 [316,325] and was shown to bind to cleaved and uncleaved H5 HA [297]. Therefore, antibody binding also serves as indication for correct protein folding of the mutant proteins.
In general, substitution of His184 had a more pronounced effect on HA expression than substitution of His110 or mutation of residue 216 (Figure 3.2). H184R and H184D mutants exhibited a significantly higher (H184R) or lower (H184D) cell surface expression than the H5 HP wild type (p-values < 0.05) whereas mutants H184N and H184A were similarly expressed (p-values > 0.05). His110 as well as the H5 LP E216R and the H5 HP R216E mutants were also similarly expressed as the H5 HP wild type (p-values > 0.05); only the low pathogenic H5 HA and the H110R mutant showed a significantly higher expression (p-values < 0.05). However, the extent of surface expression cannot be simply deduced from reduced or elevated antibody binding but might also indicate a change of the binding epitope. Nevertheless, Vn04-2 binding, trimerization (see 3.2.3), and binding of RBCs (see 3.3.1) to HA expressing cells suggests that the wild type and all generated mutant HA proteins were correctly folded.

3.2.3 Analysis of trimer formation by western blot

Any mutation introduced can also interfere with other processes unrelated to the pH threshold of the fusion mediating conformational change such as protein folding, oligomerization, intracellular transport or maturation. Specifically the highly conserved histidine at position 184 might be indispensable for correct protein folding. Therefore, we analyzed H5 HP and LP mutants for trimer formation and cell surface expression (see below) using the H5 specific antibody Vn04-2. Wild type and mutant proteins were expressed in CHO cells and treated with trypsin (if required). Cells were detached and lysed in non-reducing sample buffer before incubation at 60°C for 5 min. Samples were run on a 10 % SDS PAGE and after transfer to a nitrocellulose membrane antibody Vn04-2 was used to stain against the H5 HA protein.
In our first attempt we could detect monomers, dimers and trimers of all histidine mutants, however not for the proteins with mutation at position 216. To avoid the dissociation of trimers due to processing and increase the yield of detectable trimers we used the

homobifunctional cross-linker DSP and ran the samples on a 6 % SDS PAGE to facilitate subsequent transfer of the trimeric proteins to the nitrocellulose membrane. By using this approach we could also detect trimers for the H5 HP R216E and H5 LP E216R mutants (Figure 3.2 E). Hence, mutation of His184, His110 and residue 216 did not affect trimerization of H5 HA.

3.3 Effect of histidine mutations on the pH dependence of H5 HA

To assess the effect of mutations on the conformational change and fusion activity of H5 HA two methods were used: the red blood cell (RBC) fusion assay and the conformational change assay. In the RBC fusion assay the redistribution of fluorescent dyes from RBCs to HA expressing cells is used as read-out for a fusion inducing conformational change of HA upon low pH incubation, whereas in the conformational change assay the structural rearrangement of HA after low pH incubation is indicated by a change in antibody binding. The advantage of the RBC assay is that fusion of HA expressing cells with labeled RBCs can be directly observed by fluorescence microscopy reflecting the effect of a mutation on the ability to induce membrane fusion. However, being based on visual observation of dye redistribution the assay is prone to subjective error. Furthermore, the actual number of HA molecules undergoing a conformational change cannot be quantified using this assay.
These drawbacks of the RBC fusion assay are compensated by the conformational change assay, where the number of HA molecules which essentially undergo a conformational change is quantified by flow cytometric analysis as described in 2.2.3.5. However, possible rearrangements of HA which do not result in fusion induction cannot be distinguished from the conformational change of HA driving the fusion of membranes. Therefore, using both assays the drawbacks of each assay can be counterbalanced by the other which enables to obtain comprehensive results for each mutant.

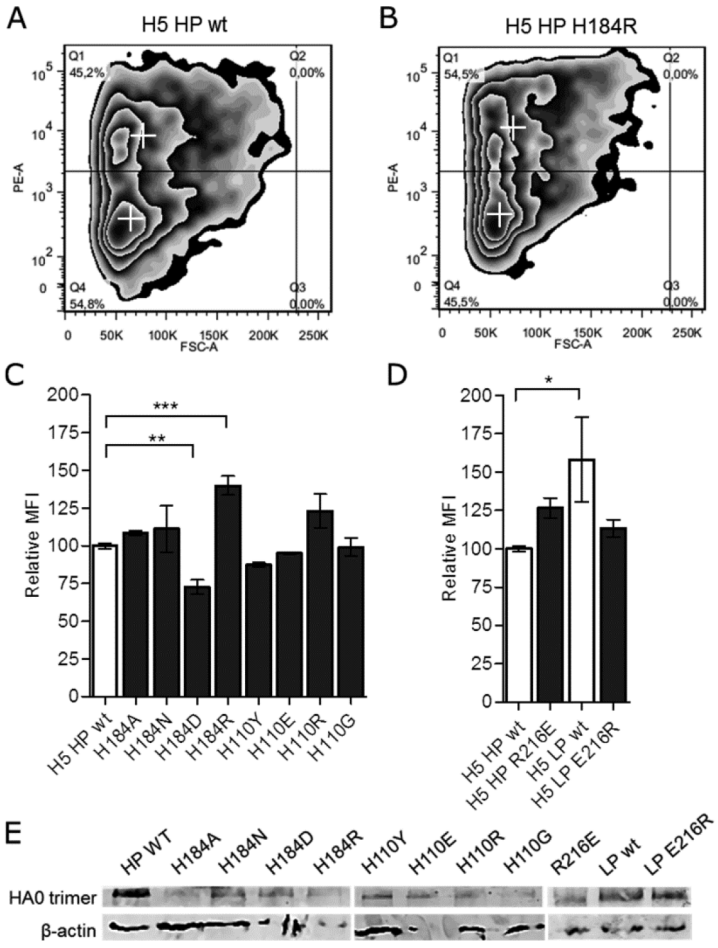

Figure 3.2: Cell surface expression of wild type and mutant HA of H5 HP and LP.
Cell surface expression of mutant proteins was quantified by immunostaining and flow cytometry using the H5 specific antibody Vn04-2. (A) and (B) are example images of flow cytometry measurements using the highly pathogenic wild type (A) and the H184R mutant (B) proteins, respectively. Gate Q1 represents the fluorescent positive cells of each measurement compared to the mock control with white crosses indicating the median fluorescence intensity of the respective gate. (C, D) The median fluorescence intensity (MFI) value of fluorescent cells (gate Q1) in each sample was normalized to the H5 HP wild type protein (relative MFI). Error bars represent the standard error of the mean from triplicate experiments. Significant differences are marked by asterisks with probability values P<0.05 denoted by '*', P<0.01 by '**' and P<0.001 by '***', respectively; one-way ANOVA and Dunnett's multiple comparison post-test was used. (E) Trimer formation of histidine mutants and of highly and low pathogenic H5 HA with mutation at position 216. HA trimers and the cellular protein β-actin were detected by SDS PAGE and Western blotting following incubation with the crosslinking agent DSP.

3.3.1 Effect of mutations on the pH of membrane fusion

The RBC fusion assay is a well-established method to monitor the occurrence of membrane fusion induced by HA via the redistribution of fluorescent dyes upon incubation with acidic pH [237,282,295,326]. To this end, RBCs were labeled with a membrane (R18, red) and a content marker (calcein, green) to distinguish between full fusion (redistribution of both dyes to HA expressing cells) and hemifusion (only redistribution of lipids/R18). The labeled RBCs were bound to HA expressing CHO cells which were previously treated with trypsin (if required) and neuraminidase to prevent binding and fusion with neighboring HA expressing cells (see 2.2.3.4). After removal of unbound RBCs by washing fusion was triggered by incubating the cells in fusion buffer at different pHs ranging from 5.0 to 7.0 at 37°C and 5 % CO_2 following observation under the microscope. Only full fusion of membranes represented by the redistribution of both dyes to an HA expressing cell upon low pH incubation was evaluated as fusion event. The hemifusion intermediate characterized by lipid/R18 mixing without content/calcein mixing was only observed in rare cases and was not rated as membrane fusion event. The 'pH of fusion' corresponds to the highest pH at which full fusion was still observed for at least 50 % of HA expressing cells.

Mutation of His184 to Asn (H184N) and Ala (H184A) shifted the pH of fusion from 5.8 to 6.2 and 6.4, respectively, whereas mutation to Asp (H184D) and Arg (H184R) abolished fusion of H5 HP even at pH 5.0 (Figure 3.3). For H184D the low cell surface expression of the mutant which is also indicated by the low level of RBC binding might explain the absence of fusion at low pH. In contrast, the H184R mutant showed high surface expression and thus higher levels of red blood cell binding than the wild type protein but still did not induce fusion. Thus, arginine at position 184 seems to stabilize the inter-monomeric interactions despite its positive charge which was predicted to disrupt the interfacial contacts.

Also, the exchange of arginine to glutamate (positive against negative charge) in H5 HP caused a shift in the pH of fusion of +0.2 units (6.0 to 0.2) whereas the glutamate to arginine mutation (negative against positive charge) in the H5 LP produced a decrease in the pH threshold of membrane fusion of –0.2 units (6.0 to 5.8), respectively (Figure 3.4). In contrast, mutation of His110 did not show any effect on the pH of fusion except for the histidine-to-tyrosine substitution (H110Y) (Figure 3.3). The latter shifted the fusion pH from 5.9 to 5.6 as also reported by Herfst et al. [260]. Thus, since replacement of His184 and of residue 216 in the highly and the low pathogenic H5 HA had a major impact on the pH of fusion, but mutation of His110 had no effect, we only investigated the role of His184 and of residue 216 for the conformational change of H5 HA in detail (see 3.3.2).

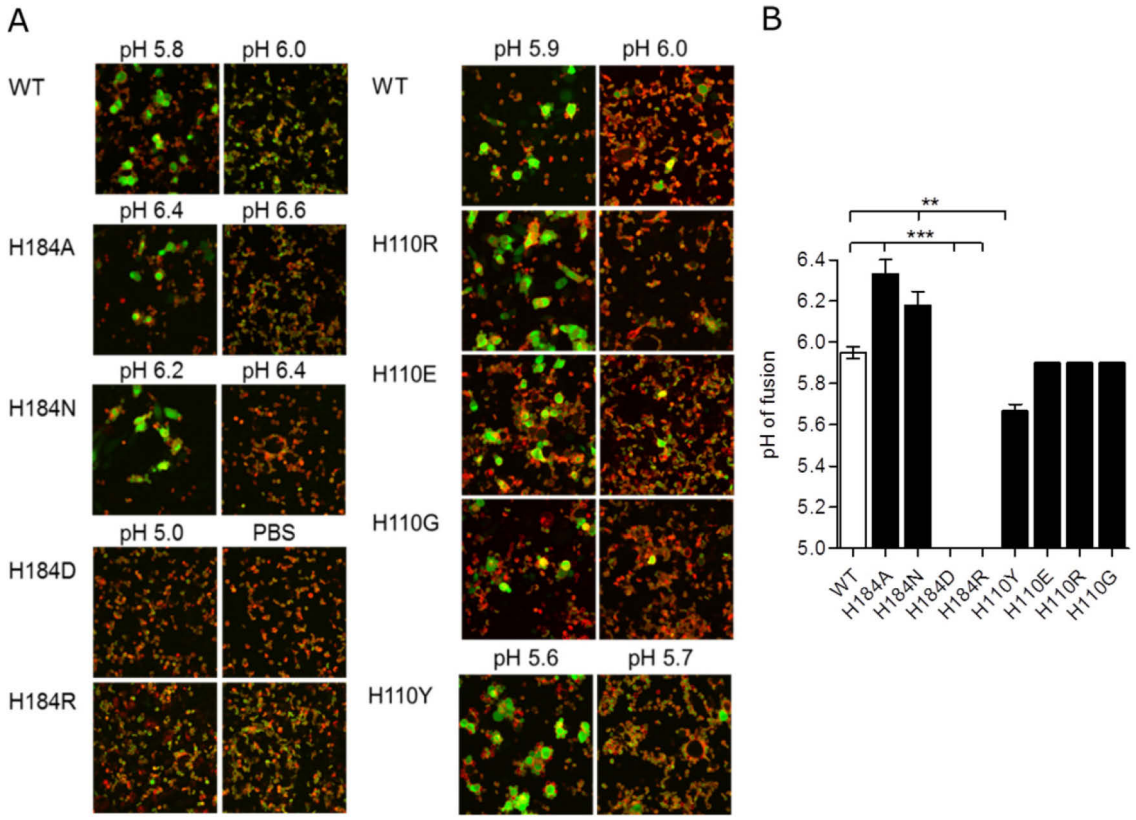

Figure 3.3: pH of membrane fusion for histidine mutants of HA (H5 HP).
(A) Representative images of the RBC fusion assay for wild type (WT) and histidine mutant H5 HA proteins expressed at the CHO cell surface. Only full fusion of membranes represented by redistribution of both, membrane marker (R18, red) and content marker (calcein, green) from RBCs to the HA expressing cells following incubation at the indicated pH at 37°C was rated as fusion event. The pH of fusion was generally assessed in steps of 0.2 pH units. Since for the His110 mutants there was no change in the pH of fusion compared to the wild type (except H110Y) a 0.1 pH unit resolution for these mutant proteins was used. (B) The pH of fusion corresponds to the highest pH at which full fusion was still observed for at least 50 % of HA expressing cells ($n \geq 3$). Error bars represent the standard error of the mean, asterisks denote a statistical difference based on one-way ANOVA and Dunnett's multiple comparison post-test with $P < 0.01$ by '**' and $P < 0.001$ by '***', respectively.

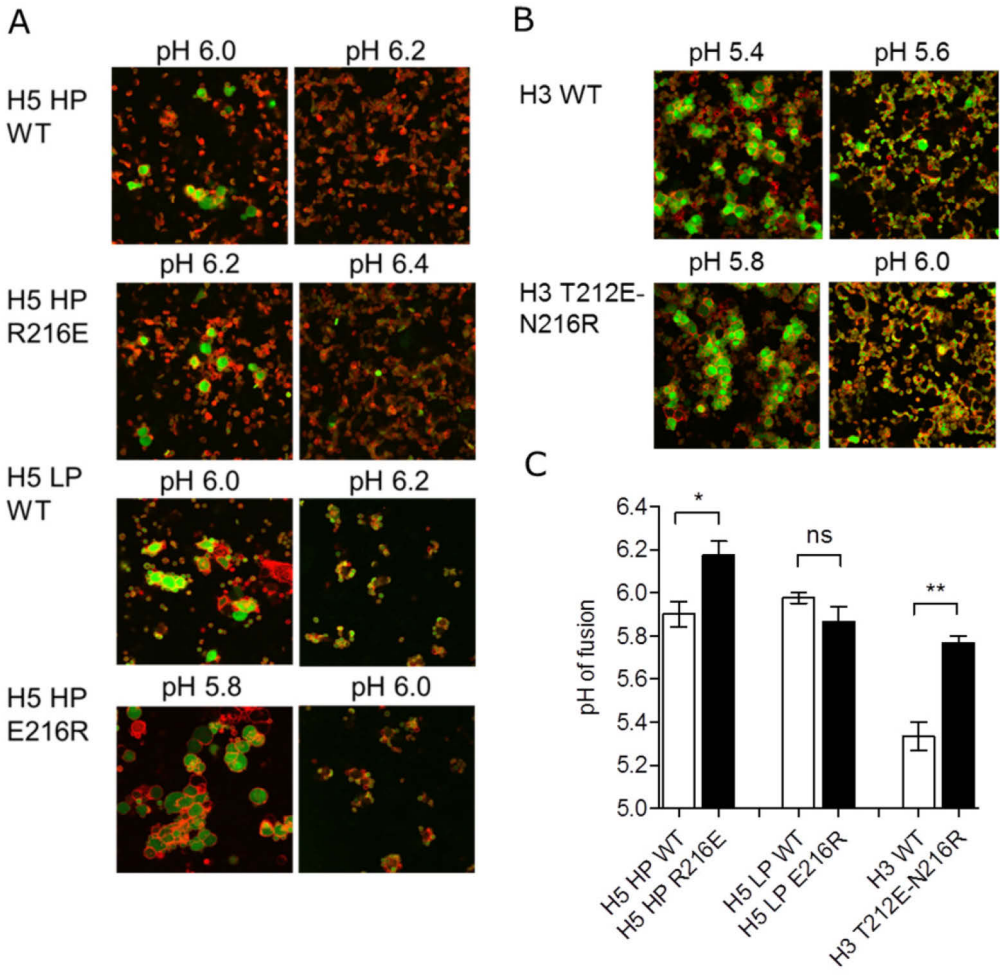

Figure 3.4: Effect of the exchange of charge at position 212 and/or 216 of H5 and H3 HA on the pH of fusion. (A and B) Representative images of the RBC fusion assay for highly and low pathogenic H5 and of H3 wild type and mutant proteins. Only full fusion of membranes represented by redistribution of both, membrane marker (R18, red) and content marker (calcein, green) from RBCs to the HA expressing cells following incubation at the indicated pH at 37°C was rated as fusion event. The pH of fusion was assessed in steps of 0.2 pH units. (C) The pH of fusion corresponds to the highest pH at which full fusion was still observed for at least 50 % of HA expressing cells ($n \geq 3$). Error bars represent the standard error of the mean, asterisks denote a statistical difference with independent t-test associated probability $P<0.05$ denoted by '*' and $P<0.01$ by '**'; 'ns' - non-significant.

Fusion with RBCs was also assessed for the H3 wild type and the T212E-N216R mutant to measure the impact of introducing two additional charges at the HA1-HA1 interface on the acid stability of the protein. Furthermore, a possible difference in the pH dependence of fusion for the HA protein alone compared to the pH dependent fusion efficiency of whole virus particles should be assessed (see 3.5). The H3 wild type exhibited fusion until a pH of 5.4 whereas the T212E-N216R mutant still induced fusion with RBCs at pH 5.8 and hence, 0.4 units higher than that of the wild type. Notably, the introduction of two charges at the HA1-HA1 interface of H3 HA shifted the pH of fusion of the H3 subtype to a similar pH of fusion as H5 LP and HP, where these two charges are naturally present (Figure 3.4).

3.3.2 Effect of mutations on the pH of HA conformational change

Conformation specific antibodies were used to determine the pH dependence of conformational change for H5 HA wild type and mutant proteins. Antibody Vn04-2 was reported to bind equally well to the neutral and the low pH conformation of H5 HA, whereas antibodies Vn04-9 and Vn04-16 were shown to preferentially bind to the neutral (Vn04-9) or the low (Vn04-16) pH conformation, respectively [284,297]. 48h post-transfection HA expressing cells were treated with trypsin (if required) and incubated at the desired pH ranging from 5.0 to 7.4 for 15 min at 37°C. After re-neutralization cells were stained against H5 HA as described in section 2.2.3.5. Median fluorescence intensity (MFI) values of fluorescent cells were measured and normalized to the maximal MFI obtained with the respective antibody (relative MFI).

As depicted in Figure 3.5 we found consistent pH dependent binding for the wild type H5 HP protein as it has been reported previously [284,297]. However, for the H5 HP mutant proteins and H5 LP pH dependent binding was only exhibited by antibody Vn04-9. Binding of antibody Vn04-16 was equal or even lower after incubation at low pH compared to binding after neutral pH incubation suggesting that this antibody is sensitive to mutational changes in the HA1 domain affecting its binding behavior. Therefore, the ratio of Vn04-9/Vn04-16 reactivity was calculated and plotted as a function of pH**.** The pH of conformational change was determined as the point at which 50 % change in Vn04-9/Vn04-16 ratio was observed (Figure 3.6).

Mutation to alanine and asparagine resulted in a shift in the pH of conformational change of +0.5 and +0.2 units, respectively, similar to the RBC assay. Also for the H184D we observed a decrease of the ratio with lowering of the pH. The data implicate an increase in the pH threshold of conformational change of +0.5 units, similar to the H184A mutant. However, it could be remarked that the change of ratio of antibody binding activity is rather smooth compared to the wild type HA and mutants H184N and H184A. For H184R we did not

observe a pH dependence of binding demonstrating that this mutant does not undergo a conformational change. This is supported by the failure to trigger fusion.

As observed in the RBC fusion assay the R216E mutant caused a shift in the pH of conformational change of +0.2 units compared to the H5 HP wild type, from pH 5.7 to 5.9. Mutation E216R in the H5 LP protein led to a decrease in the pH of conformational change of 0.4 units whereas in the RBC fusion assay only a decrease of 0.2 units was detected. An anti-fusion peptide antiserum from rabbit which binds to the fusion peptide of H3 HA was kindly provided from Dr. Judith White. The fusion peptide is only exposed upon structural rearrangement of HA at low pH which allows distinguishing the neutral from the low pH conformation of H3 HA. However, using this antibody we could not detect a difference in antibody binding after incubation at low pH. Thus, we could not determine the pH of conformational change of H3 wild type and the T212E-216R mutant.

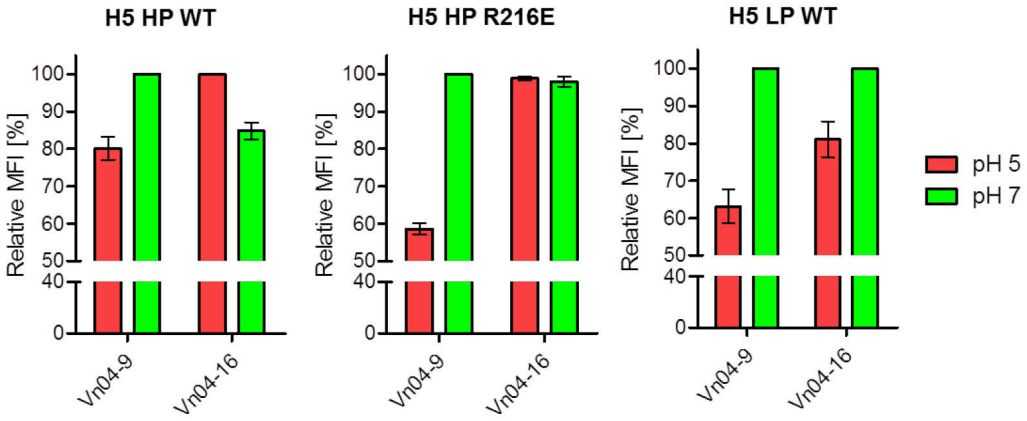

Figure 3.5: Binding of conformation specific antibodies to highly and low pathogenic H5 HA.
After incubating HA expressing cells at neutral (green) or low pH (red) at 37°C for 15 min and re-neutralization cells were stained against H5 using antibody Vn04-9 or -16, respectively. Secondary anti-mouse Alexa568 antibody was used to obtain a fluorescent signal which was measured by flow cytometry. Mean fluorescence intensities (MFI) of fluorescent positive cells were normalized to the higher MFI obtained after incubation at pH 5 or pH 7, respectively.

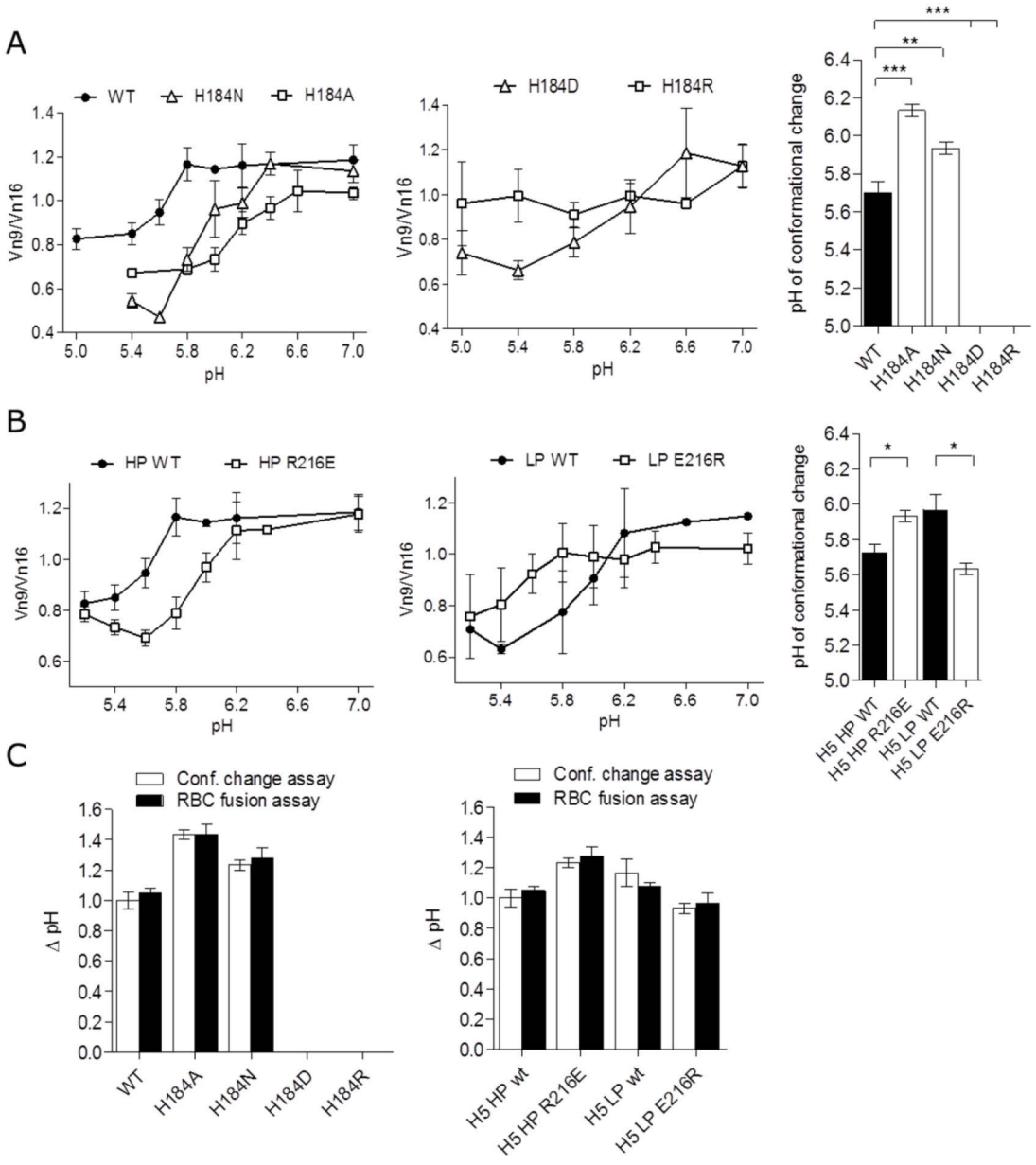

Figure 3.6: pH dependence of conformational change for His184 mutants (A) and for H5 HP and LP wild type and mutant proteins (B).
The conformational change was assessed by plotting the obtained Vn04-9/Vn04-16 ratios of median fluorescence intensities as a function of pH. The pH of conformational change which corresponds to the pH of 50 % change in the Vn04-9/Vn04-16 ratios obtained from Vn04-9/Vn04-16 ratios of wild type and mutant proteins are compared in the right panels (n ≥ 3). (C) The differences of the pH shift of fusion and conformational change of His184 mutants relative to the wild type are shown. Error bars represent the standard error of the mean, asterisks denote a statistical difference based on one-way ANOVA and Dunnett's multiple comparison post-test with P<0.05 denoted by '*', P <0.01 by '**' and P <0.001 by '***', respectively.

3.4 Summary of 3.1 to 3.3

The conformational change of the influenza virus HA was suggested to be triggered by the sequential protonation of specific histidines upon acidification [162,163]. However, evidence is still missing about the residues involved in this process. In this section different substitutes were used to study His184 and His110 as potential pH sensors in the highly pathogenic H5 HA. The mutational effect was assessed by using the RBC fusion and a conformational change assay. The obtained results revealed that substitution of His184 has a significant effect on the pH dependence of conformational change and of membrane fusion of H5 HP, whereas mutation of His110 does not affect the ability of the protein to induce membrane fusion. The only exception was mutation to tyrosine (H110Y) which significantly decreased the pH of membrane fusion of the protein.

Furthermore, by mutating Glu to Arg at position 216 in H5 HP and Arg to Glu in H5 LP we found that the exchange of charge at that position alters the pH dependence of conformational change and of fusion of both, H5 HP and H5 LP. Apart from the charged amino acid at position 216 an additional charge (arginine) was shown to be present at position 212 at the HA1-HA1 interface of H2 and H5 HA but not in the H3 subtype [295]. By introducing these two charges into H3 HA we found that the pH dependence of conformational change of this protein was even more significantly affected.

These mutant HA proteins with significantly altered fusion pH provided the basis to study host-specific virus infection in dependence of the acid stability of HA. To this end we used reverse genetics to produce recombinant WSN H3 virus particles containing the pH modulating mutation T212E-N216R. The effect of the altered acid stability of H3 on pH dependent fusion and on infectivity in living cells was assessed. The results of these studies are described in the following section.

3.5 Production of recombinant influenza viruses in MDCK cells

Recombinant WSN H1N1 viruses were produced by simultaneous transfection of HEK-293T cells with the eight pHW master strain plasmids encoding all viral proteins of the A/WSN/1933 virus (WSN H1 wt). However, to obtain recombinant viruses with H3 instead of H1 in the background of the WSN virus, the plasmid encoding H1 HA was exchanged against the newly constructed pHW plasmids containing the gene sequence of H3 wt or H3 T212E-N216R, respectively. The virus-containing supernatant was harvested 48h post-transfection and viruses were amplified by infection of MDCK cells in 6 well plates (see 2.2.4.1). Purified virus concentrates were obtained by infection of MDCK cells growing in

T175 flasks or in roller bottles with respective viruses at an MOI 0.01. Harvested viruses were concentrated by ultra-centrifugation and purified over a sucrose gradient (20-60 %) (see 2.2.4.3). The content of recombinant virus in each sample was quantified using the BCA protein assay kit. Infection of 8 T175 flasks or 1 roller bottle typically yielded 300 µl of about 6 mg/ml of concentrated and purified recombinant H3 viruses. Transmission electron microscopy (TEM) images[4] of recombinant wild type and mutant H3 viruses are shown in Figure 3.7. All viruses produced had a spherical shape and were well decorated with HA molecules as revealed by the high density of spike molecules at the viral surface as well as by SDS PAGE analysis of purified virus samples. Also the presence of M1, NP and NA proteins could be confirmed.

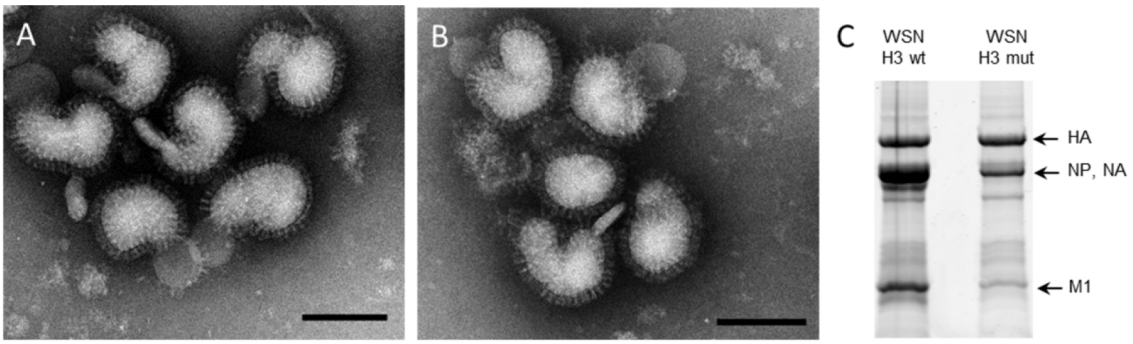

Figure 3.7: Purification of recombinant WSN H3 viruses.
(A and B) Transmission EM micrographs of purified WSN H3 wild type (wt) (A) and T212E-N216R mutant (mut) (B) viruses after concentration and purification over a 20-60 % sucrose gradient. Scale bar 100 µm. (C) 5 µl of purified WSN H3 viruses were run on a 10 % SDS PAGE under non-reducing conditions and viral proteins were detected by coomassie blue staining.

Recombinant viruses containing H5 LP in the WSN background were also produced. However, the yield obtained for these viruses was much lower than that of recombinant H3 viruses limiting further characterization of the former. Efficient packaging of the viral RNP segments was reported to depend not only on the conserved packaging signals but also on other signals present in the coding and non-coding region (NCR) of each segment [6,327]. A lower compatibility of the H5 gene segment with the other vRNPs of the WSN H1N1 strain might thus explain the lower yields obtained for recombinant H5 viruses.
The production of recombinant viruses containing a highly pathogenic avian HA such as H5 HP was in general not allowed since this would require a biosafety level (BSL) 3 containment which was not present in the laboratory where the study was conducted.

[4] Sample preparation and image acquisition was conducted by Dr. Kai Ludwig, Research Center of Electron Microscopy, Free University Berlin

3.6 pH dependent fusion of recombinant viruses

The introduction of two charges at the HA1-HA1 interface of H3 HA (mutation T212E-N216R) had the greatest effect on the pH dependence of fusion of HA (see 3.3.1). H3 T212E-N216R resulted in a shift in the pH of fusion of +0.4 units and thus in the destabilization of H3 HA. To assess how this mutation affects the pH dependent fusion efficiency of recombinant viruses the pH threshold of fusion was measured using the R18 fluorescence dequenching assay. Concentrated and purified recombinant WSN H3 wt and T212E-N216R mutant viruses were labeled with 20 µM R18 and fusion of labeled viruses with RBC ghosts was assessed by the increase of R18 fluorescent signal upon acidification in the spectrophotometer (see 2.2.3.4).
The fusion efficiencies measured in the pH range from 4.9 to 6.5 were plotted as a function of pH and the pH threshold was obtained by fitting the data to the Hill equation

$$y(x) = a^* \frac{x^n}{x^n + k_{H+}{}^n}$$

where a is the scaling factor, x the proton concentration $[H^+]$, n the Hill coefficient and k the proton concentration at half-maximal fusion efficiency. Parameters a, n and k were estimated from obtained data [328] and the pH threshold was calculated according to $k_{pH} = -\log10(k_{H+})$[5]. The pH threshold of fusion was also assessed for WSN H1 wt and for influenza virus X-31 (H3N2) which carries the identical H3 HA as the recombinant WSN H3 wild type virus but differs in all other viral proteins. For both, recombinant WSN H3 wt as well as the A/X-31 strain, we obtained a similar pH threshold of 5.5-5.6 confirming that pH dependent fusion induced by HA is independent from other viral proteins (Figure 3.8). The mutation T212E-N216R in H3 resulted in an increase of the pH threshold of fusion as it was observed in the RBC fusion assay. However, the increase was less pronounced with a shift of around +0.2 units from 5.6 to 5.8. Remarkably, whereas the fusion efficiency of the WSN H3 wild type reached its maximum at pH of 5.2 and decreased constantly with increasing pH (Hill coefficient n=1.8), the maximal fusion efficiency of the WSN H3 mutant virus remained rather constant until a pH of 5.6 and then dropped dramatically with increasing pH (n=3.6). For the recombinant WSN H1 wild type virus a pH threshold of 6.2 was obtained suggesting that the H1 subtype has a much lower acid stability than H3 HA. Similar to the WSN H3 T212E-N216R mutant virus the fusion efficiency of WSN H1N1 virus remained rather constant until a pH of 6.0 followed by a steep decrease with increasing pH (n=3.2).

[5] Data were fit by Max Schelker, Group of Theoretical Biophysics, Institute of Biology, Humboldt University Berlin

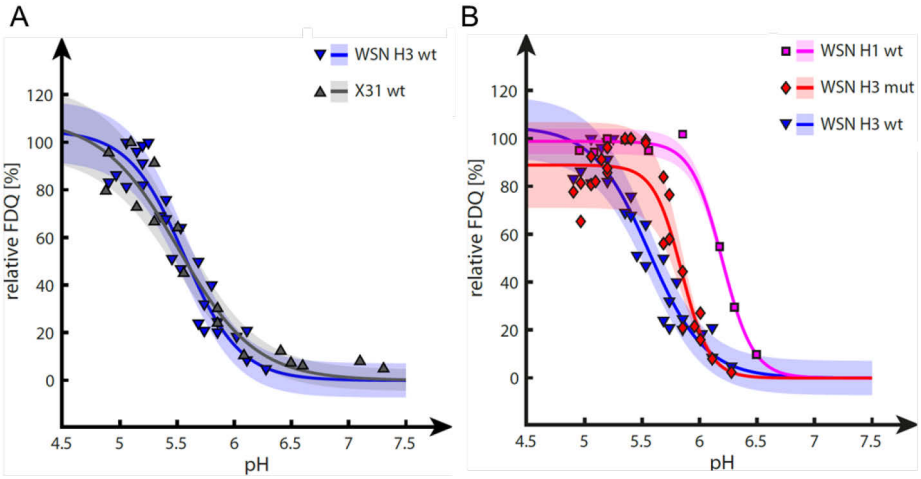

C

Virus strain	pH threshold	Hill coeffcient
X-31 (H3N2)	5.51 ± 1.09	1.30 ± 0.86
WSN H3 wt	5.56 ± 0.02	1.78 ± 0.70
WSN H3 T212E-N216R	5.84 ± 0.05	3.55 ± 1.20
WSN H1 wt	6.20 ± 0.03	3.20 ± 0.88

Figure 3.8: pH dependent fusion efficiency of recombinant WSN viruses.
(A and B) Relative fusion efficiencies measured for A/X-31 and recombinant WSN viruses were plotted as a function of pH. (C) The pH thresholds corresponding to the pH at half-maximal fusion efficiency were obtained by fitting the data to a Hill equation.

3.7 Infection studies of recombinant viruses in MDCK and A549 cells

Following fusion of the viral with the endosomal membrane the released vRNPs are transported into the nucleus were RNA synthesis and assembly of newly produced vRNPs takes place. MDCK and A549 cells were shown to exhibit different endosomal acidification kinetics which might affect the time-point of vRNP release and thus of infection efficiency [329]. To observe a potential difference in the infectivity of recombinant viruses with an altered pH threshold of fusion infection studies in MDCK and A549 cells were performed using virus-containing supernatants from MDCK cells[6]. Cells were infected with the respective virus at the MOI of 0.1 and stained against influenza virus NP 20 h post-infection. Images were acquired at the confocal microscope. The number of infected cells in percent of total cells in each image was analyzed using the cell image analysis software Cell Profiler (Broad Institute, Cambridge, USA).

Clear differences in the infection efficiencies of the recombinant WSN viruses were observed between viruses and cell lines (Figure 3.9). The WSN H3 wild type virus with the lowest pH threshold of fusion (pH 5.6) exhibited a much higher infection efficiency in MDCK cells than

[6] Infection and replication studies were performed by Katjana Schneider in the course of her study project under my supervision.

the WSN H3 mutant and the WSN H1 wild type virus whereas in A549 cells it was similar to that of WSN H1 wt and the H3 mutant viruses. In contrast, the infection efficiencies of the WSN H3 mutant virus were similar in both cell lines. Interestingly, the WSN H1 wild type, which had the highest pH threshold (6.2), infected only a number of MDCK cells but in A549 cells it displayed higher infection efficiency than the WSN H3 viruses.

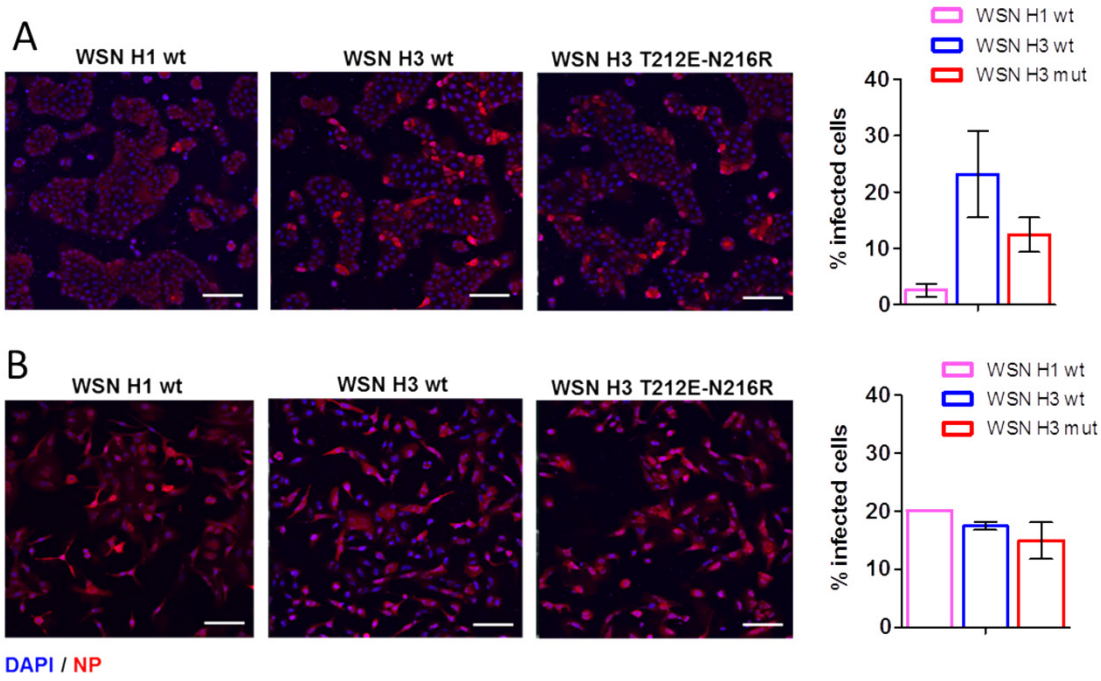

Figure 3.9: Representative images of MDCK and A549 cells infected with recombinant WSN viruses. MDCK (A) and A549 (B) cells were infected with WSN H1 wt, WSN H3 wt and the WSN H3 T212E-N216R mutant viruses at an MOI of 0.1 and stained against the nucleoprotein (NP) 20h post-infection. Nuclei were stained with DAPI. Images were acquired with an Olympus FV1000 microscope. Scale bar 100 µm. (C) The percent of positively infected cells was evaluated using the software Cell Profiler. The plotted values are the mean of three independent experiments with error bars representing the standard error of the mean.

3.8 Replication efficiency of recombinant viruses in MDCK cells

By growing the recombinant H3 viruses in MDCK cells we could observe major differences in viral titers between the wild type and the T212E-N216R mutant. Viral titers obtained for the mutant were 0.2 to 1.0 order of magnitude lower than that of the WSN H3 wt virus as assessed by TCID50 (Figure 3.10 A). Thus, the replication efficiency of recombinant viruses was assessed by infection of MDCK cells for 10, 24, 36, 48 and 72 hours at an MOI of 0.001 and titration of virus-containing supernatants by using the $TCID_{50}$ assay. Log $TCID_{50}$ values were normalized to the initial viral titers used for infection and plotted against time post-infection. As shown in Figure 3.10 B, replication of the mutant virus was less efficient in MDCK cells than for the WSN H3 wild type explaining the higher viral titers that we obtained

for the wild type in these cells. However, the growth kinetics of WSN H3 wild type and mutant viruses were only measured once and thus need further characterization.

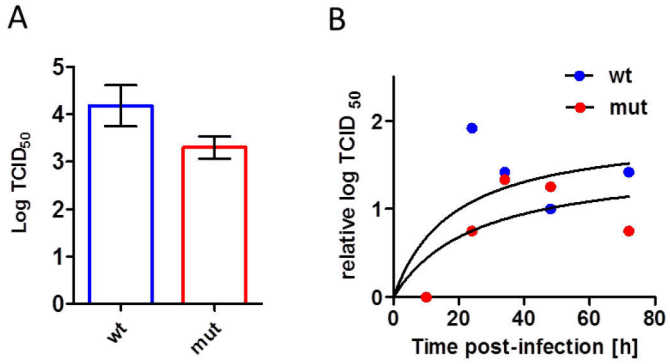

Figure 3.10: Replication efficiency of WSN H3 recombinant viruses.
(A) Viral titers obtained for WSN H3 wild type (wt) and the T212E-N216R mutant (mut) viruses as determined by TCID50 in MDCK cells. Plotted values are the mean of four independent experiments with error bars representing the standard error of the mean. (B) Growth kinetics of wild type and mutant H3 virus in MDCK cells (n=1).

3.9 Intracellular fusion kinetics of recombinant viruses

The infection pathway of influenza A viruses is a complex, multistep process including binding, receptor-mediated endocytosis and movement from endocytic vesicles to early endosomes and finally to late endosomes where the viruses fuse with the endosomal membrane. The time-point of fusion as well as the fusion kinetics of virus-endosome fusion might strongly depend on the type of cell and host specific factors, such as endocytic transport, endosomal acidification kinetics and other host signaling factors [70,245].

To visualize pH dependent fusion kinetics of single recombinant virus particles inside living cells we used the dual wavelength imaging technique adapted from Sakai *et al*. [322]. This approach makes use of two fluorophores (DiO and R18) with overlapping fluorescence emission spectra allowing Foerster Resonance Energy Transfer (FRET) to occur from DiO (green) to R18 (red) due to their high proximity within the viral membrane. Fusion of the viral with the endosomal membrane leads to the dilution of fluorophores in the membrane reducing self-quenching and FRET which is expressed by an increase in the green fluorescence (DiO) (see 2.2.4.7). We applied this method to resolve a possible difference in the fusion kinetics of WSN H3 wild type and mutant viruses inside cells. However, instead of R18 we used DiI which has similar fluorescence excitation and emission spectra as R18. MDCK cells were infected with double-labeled recombinant H3 viruses and fluorescent signals of DiO and DiI upon excitation at 488 nm were recorded every 2-5 min for 40 min at 37°C and 5 % CO_2. At every time point image stacks of the whole cell were acquired,

summed and fluorescent intensities of DiI and DiO of each virion were analyzed using Cell Profiler.

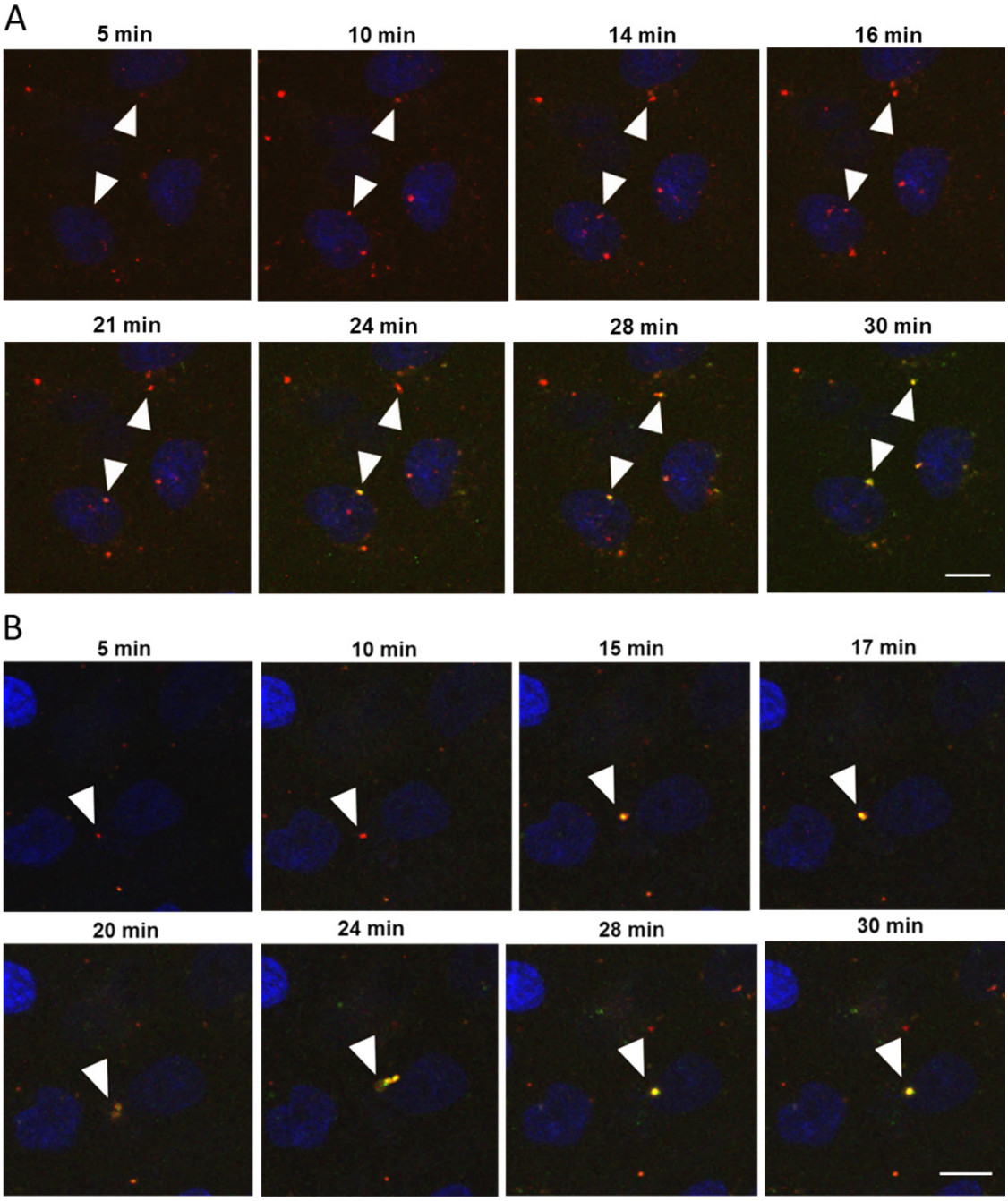

Figure 3.11: Single virus-endosome fusion events in living cells.
MDCK cells were infected with double-labeled recombinant WSN H3 wt (A) or T212E-N216R mutant (B), respectively and DiI and DiO fluorescent signals upon excitation at 488 nm were recorded for 40min at 37°C and 5 % CO_2. Images were taken every 2-5 min. In the first image (5 min post-infection) viruses appear red due to self-quenching of DiO and FRET to DiI. Upon fusion with the endosomal membrane FRET and self-quenching of DiO is reduced resulting in an increase of the green fluorescence (marked by arrows). Nuclei are stained with Hoechst (blue). Scale bar 10 µm.

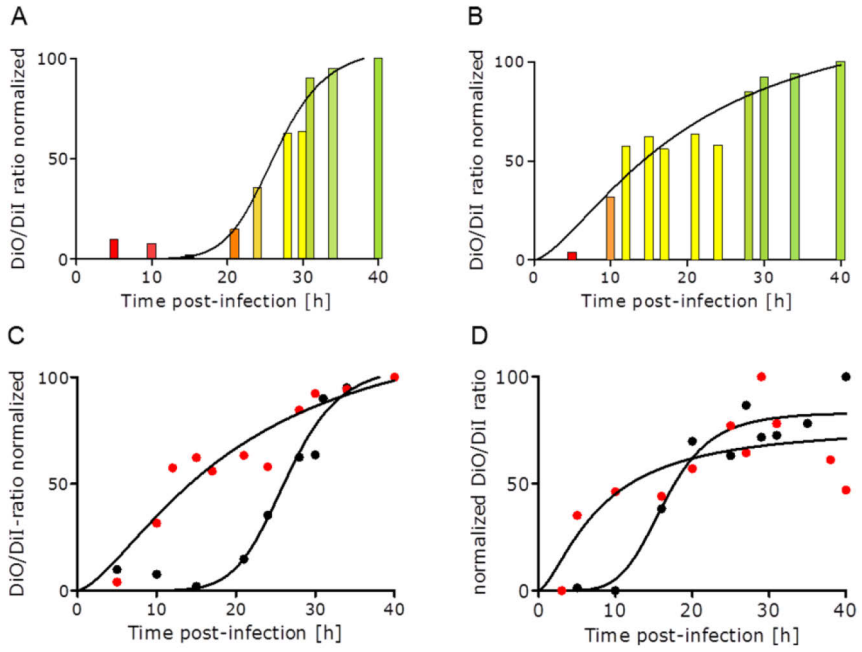

Figure 3.12: Intracellular fusion kinetics of recombinant H3 viruses.
MDCK cells were infected with double-labeled H3 wild type (A) or H3 T212E-N216R mutant (B) viruses and DiO/DiI intensity-ratios (red: 0.2-0.3, orange:0.4- 0.5, yellow: 0.6-0.7, green: 0.8-1.0) of detected virions were acquired from one position in the sample between 0 and 40 min at 37°C and 5 % CO_2 after initial binding for 10 min at 4°C. (C and D) The fusion kinetics of recombinant H3 wt (—●—) and H3 T212E-N216R mutant viruses (—●—) obtained from one (C) or from random positions in the sample are compared. Data were fit using Hill equation.

Image sections recorded at different time-points are shown in Figure 3.11 and the results of averaging the DiO/DiI-ratios obtained from detected virions are displayed in Figure 3.12 A and B. Early post-infection (5-10 min) viruses appear red due to FRET and self-quenching of DiO. Upon fusion an increasing green fluorescence first results in a yellow spot representing virus-endosome fusion whereas higher green fluorescence late post-infection corresponds to endosome-endosome and virus-endosome fusion [322].

For the wild type an accumulating number of fusion events represented by an increasing number of yellow spots in the sample was only observed 20 min post-infection which turned green 30-40 min post-infection. In contrast, WSN T212E-N216R mutant viruses already started to fuse 10-15 min post-infection. The increase in green fluorescence was moderate and also saturated only 30-40 min post-infection. However, it is possible that the addition of pre-warmed DMEM after 10 min of binding at 4°C did not immediately yield 37°C in the sample resulting in the delayed onset of fusion. Furthermore, the number of fusion events observed for both viruses was low resulting in an overall weak increase of the DiO signal. Another problem of recording fusion events in one spot of the sample for long time-periods is the bleaching of fluorescent signals. Therefore, in a second analysis image stacks were acquired from random positions of the sample and DiO/DiI-ratios were obtained as described above (Figure 3.12 C).

Using this approach we found an earlier increase in green fluorescence for both, WSN H3 wt and T212E-N216R mutant viruses with half-maximal fusion reached at 16.4 and 7.6 min, respectively. Furthermore, movement of the viral particles to the nucleus could be observed with the fusion events primarily taking place in the perinuclear region of the cell.

3.10 Summary of 3.5 to 3.9

In the second part of the thesis the effect of an altered acid stability of HA on host-specific virus infection was assessed. Therefore, recombinant viruses were produced containing the H1 or the H3 subtype, respectively or the destabilized H3 mutant protein (H3 T212E-N216R). Similar to the results obtained in the RBC fusion assay the pH threshold of fusion was also increased for WSN H3 viruses containing the T212E-N216R mutation within HA compared to the respective wild type. However, the pH shift was less pronounced with an increase of only 0.2 units compared to 0.4 units determined for HA-mediated RBC fusion. For the WSN H1 wild type an even higher fusion pH threshold was measured. Studying viral infectivity in MDCK and A549 cells we found that the fusion pH threshold affected the infectivity of WSN H3 and H1 viruses in MDCK but not in A549 cells. These two cell lines were reported to exhibit different endosomal acidification kinetics [330] which might affect the kinetics of virus-endosome fusion and as a result the efficiency of vRNP release. To resolve a potential difference in the intracellular fusion kinetics of WSN H3 wild type and T212E-N216R mutant virus in MDCK cells we applied a dual-wavelength-imaging technique adapted from Sakai et al. [322]. Our results revealed that the timing of virus-endosome fusion in MDCK cells was indeed altered for the WSN H3 mutant virus which provides a possible explanation for its reduced infection efficiency in these cells.

4 Discussion

The influenza virus HA mediates cell entry of influenza viruses, which after binding to sialic acid cell receptors includes membrane fusion between the viral and the endosomal bilayer. This process is strictly pH dependent since the conformational change of HA initiating the fusion of membranes only occurs upon protonation of yet unknown relevant residues within HA at low pH (~5.0-6.0). Due to the high abundance of protonable residues within HA subtypes and the difficulty to predict their protonation states the identification of such critical residues remains challenging.

In the first part of the present study a comprehensive mutational analysis of His184 and His110 was performed including characterization of the pH dependence of conformational change and of fusion of wild type and mutant H5 HA. The results suggest that His184, but not His110 is an important regulator of HA conformational change at low pH.

Another aim was to assess the effect of a Glu-to-Arg mutation at position 216 of H5 HP on the acid stability of the protein. This mutation evolved in 2003-2004 and thus, as we reason, might have contributed to adaptation of the virus to the human host. By mutating Glu to Arg at position 216 in H5 HP and Arg to Glu in H5 LP we found that the exchange of charge at that position indeed alters the pH dependence of conformational change and of fusion of both, H5 HP and H5 LP. The introduction of two additional charges into the H3 subtype (T212E-N216R) also resulted in a shift of the pH of fusion proposing that charges might play an essential role for the pH dependent stability of HA.

However, little is known about the role of an altered acid stability in the context of host adaptation. Hence, in the second part of this study we used reverse genetics to assess the effect of an altered acid stability of HA on the fusion and infection efficiency of recombinant viruses in two different cell lines. We found that an alteration in the pH threshold of fusion affects the infection efficiency in MDCK, but not in A549 cells. Studying virus-endosome fusion kinetics in MDCK cells we could resolve a significant difference in the timing of fusion induction. These results suggest that the time-point of vRNP release is another critical determinant of viral infection efficiency which seems to depend on the endosomal acidification in different cell lines and the acid stability of the virus itself.

4.1 His184 - a determinant of the pH dependence of conformational change?

Stevens et al. [288,331] were the first to describe pH-sensitive histidine patches in the influenza virus HA that might play a role in triggering the dissociation of subunit and domain interactions. Later on histidine residues were also suggested to act as “pH sensors” in other class I and class II fusion proteins since their pH of protonation (pK_a) matches the pH range of endosomes where the proteins are activated (pH 5.0-6.5) [156–159,163]. It was further proposed that sequential protonation of histidines at positions 18 and 38 in HA1 and at positions 106/111 and 142 of HA2 controls the structural transitions of HA [162,163,331]. Indeed, Kalani et al. demonstrated that protonation of His106/111 induces the bending of peptides of H3 and H1 subtypes [157]. However, mutational analysis of these histidines in H3 and H2 HA [162,290] as well as H5 HA [297] barely had any effect on membrane fusion and its pH threshold.

In this study we focused on His184 at the HA1-HA1 interface and His110 at the HA1-HA2 interface of the influenza virus H5 HA as potential molecular switches. Both histidines were replaced by a set of different amino acids in the highly pathogenic H5 HA and analyzed the mutational effect on pH dependent conformational change and fusion. In our model system using labeled RBCs as target membrane for binding and fusion, the pH of membrane fusion was completely unaffected by mutation of His110 to most selected residues (Table 4.1). Only mutation to tyrosine shifted the pH of fusion to a lower value (-0.3 units). This mutation (H110Y) was already previously shown to stabilize HA at this position owing to an additional hydrogen bond [260,324]. Apparently, the altered pH of fusion was not due to the absence of histidine but due to the interaction of tyrosine with Asn413 of the adjacent monomer. Therefore, we do not consider His110 as trigger of conformational change. In support of these findings a recent continuous constant pH molecular dynamics simulation (CPHMD) of H2 HA indicated that, in contrast to the significantly increased net charge of the HA1 globular heads and the fusion peptide region at low pH, the net charge in the B loop region does not change upon acidification. Thus, the B-loop is likely trapped in a meta-stable conformation in the pre-fusion state and acidification may be simply required for other steps of HA conformational change releasing the clamp [332]. In contrast to His110, we found a significant impact of mutating His184 on the pH dependence of conformational change and fusion. Mutation of His184 either abrogated the ability of HA to undergo a fusion triggering conformational change (H184R, H184D), or shifted the pH dependence of conformational change and fusion to a higher pH (H184A, H184N).

Table 4.1: Summary of data obtained for histidine mutants.

Protein	Surface expression Mean ± SD[a]	ΔpH[b]		
		RBC fusion assay	conf. change assay	Average
H5 HP wt	100 ± 5	5.9	5.7	5.8
H5 HP H184A	109 ± 2	+0.5	+0.5	+0.5
H5 HP H184N	111 ± 27	+0.3	+0.2	+0.3
H5 HP H184D	73 ± 13	-	+0.5[c]	+0.5[c]
H5 HP H184R	140 ± 14	-	-	-
H5 HP H110Y	87 ± 2	-0.3	ND	-0.3
H5 HP H110R	123 ± 22	0.0	ND	0.0
H5 HP H110E	95 ± 1	0.0	ND	0.0
H5 HP H110G	99 ± 10	0.0	ND	0.0

[a] Relative MFI [%]

[b] The values represent the average from a minimum of three experiments. In all cases the difference between the three measurements did not exceed 0.1 pH units. ND, not determined; - no fusion or conformational change detected at any pH

[c] Data only indicate a conformational change. See Results and Discussion.

In general, the pH of conformational change measured by antibody binding and flow cytometry was lower than the pH of fusion. The difference could be explained by the assumption that the number of activated HA molecules required to induce fusion is lower than that corresponding to the midpoint of change in Vn04-9/Vn04-16 ratio, which was defined as the pH of conformational change. However, the shifts in the pH of fusion and in the pH of conformational change caused by the individual mutation were mostly identical for both assays. Only for the H184D mutant the results obtained did not coincide. Although we observed a decrease of the ratio of antibody binding by lowering the pH, fusion was not observed for H184D. This might be related to the significantly lower expression of the mutant on the plasma membrane of CHO cells. Another explanation could be a conformational change not able to mediate fusion or even no conformational change at all. Indeed, the decrease of the Vn04-9/Vn04-16 ratio was moderate missing a sharp decline as observed, for example, the wild type.

4.1.1 Protonation of His184 destabilizes the HA1-HA1 interface

To gain insight into the structural basis for an altered pH of conformational change and fusion due to mutation of His184, we performed computational modeling of the neutral pH crystal structure of the highly pathogenic wild type H5 HA (PDB ID: 2IBX) containing the neutral or doubly protonated His184[7]. We addressed the influence of the protonation state of

[7] Molecular modeling and pK_a calculations of His184 were performed by Tim Meyer, Institute of Chemistry and Biochemistry, Free University Berlin

His184 on interactions with neighboring residues and, in turn, possible consequences for the pH dependent stability of the HA ectodomain.

In the wild type H5 HA His184 forms an intra-monomeric salt bridge with glutamate at position 231 (Figure 4.1 A and D). Interestingly, a pair of positively charged arginine residues (Arg220 and Arg229) is located close to His184 at the interface of HA1 monomers. Being shielded from water the two charged amino acids need to be stabilized by a defined number of hydrogen bonds inside the protein which are mostly formed with the backbone amides of neighboring residues of the same monomer (Figure 4.1 B and C). Arg220 thereby interacts with the backbone of His184 and with the side chain oxygen of Asn210 from the adjacent monomer. These hydrogen bonds are at the same time the only inter-monomeric interactions in this region. HA, especially the association of HA1 monomers clamping the HA2 subunit at neutral pH is meta-stable so that small alterations at the HA1-HA1 interface could affect the stabilization of the complex leading to the fusion inducing conformational change. We surmise that at low pH His184 becomes doubly protonated and thus competes with Arg220 for hydrogen bonding resulting in the destabilization of the structure and thus in the HA conformational change. By modeling of the doubly protonated His184 into the H5 HP crystal structure we could indeed confirm that protonation may cause His184 to interact with Asn210 thereby weakening the hydrogen bond network of Arg220 (Figure 4.1 E).

To obtain the protonation state of His184 at neutral pH we performed an electrostatic energy calculation using Karlsberg+ [319] based on the crystal structure of H5 HP HA (PDB ID: 2IBX, resolved at pH 6.5). We obtained a pK_a value for His184, which is below -10. Since the HA structure with charged histidines is not known, the real pK_a of His184 cannot be predicted accurately using this approach and the obtained value very likely does not correspond to the actual pK_a of this residue. However, the result clearly indicates that (i) His184 is deprotonated in the crystal structure at pH 6.5 as shown in Fig. 4D, (ii) therefore very likely also at neutral pH and (iii) that its pK_a is below 6.5. Due to the complexity of the structural changes, that are expected to follow the protonation, the accurate prediction of the pK_a of His184 is a challenging task that we leave open for future investigation.

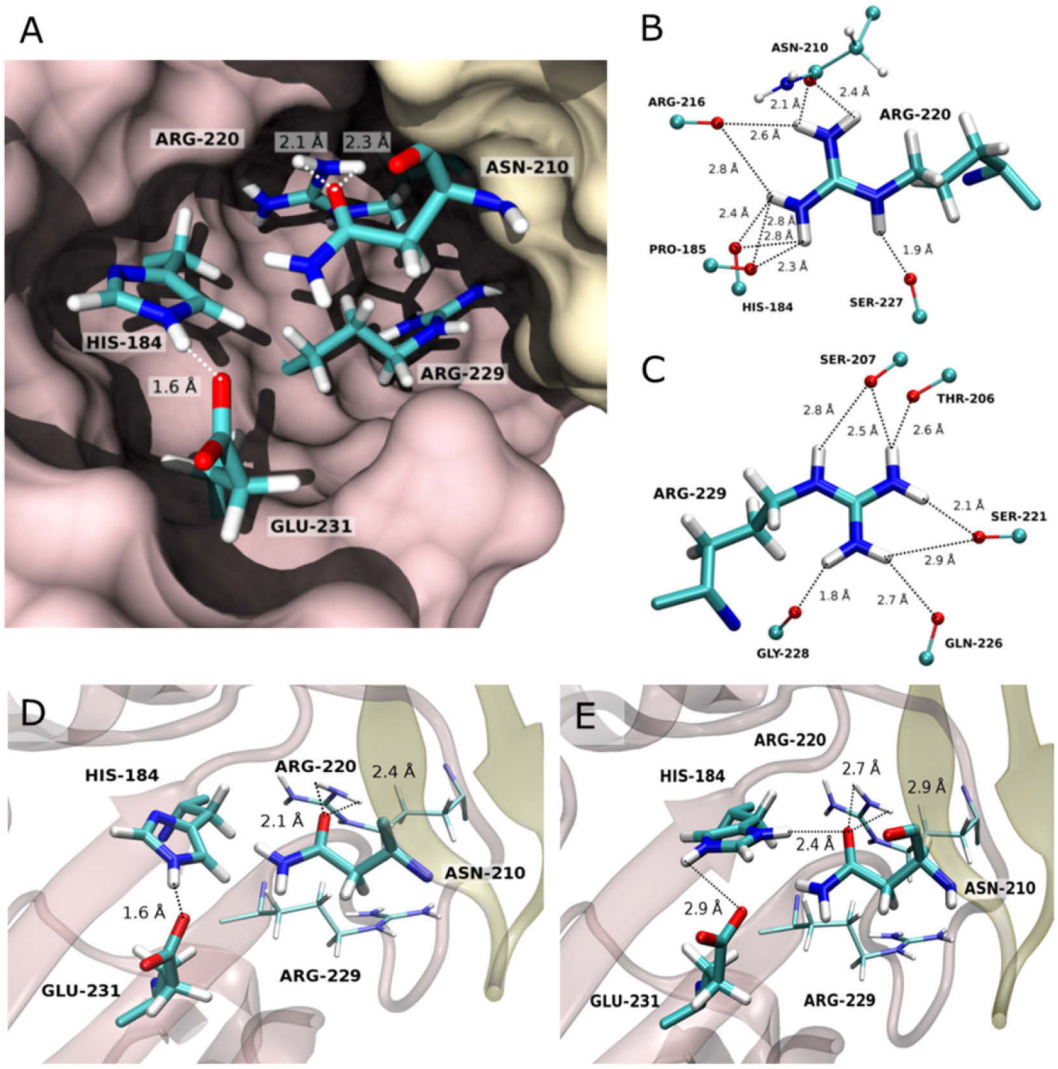

Figure 4.1: Interactions of His184 and of neighboring residues at the HA1-HA1 interface in its neutral and doubly protonated state.
(A) Interactions at the HA1-HA1 interface (PDB ID: 2IBX). Monomers (chain A in brown and chain E in yellow) are depicted in surface representation and residues which might be crucial for the regulation of HA1 monomer dissociation are shown in stick model. (B, C) Hydrogen bond network of residues Arg220 and Arg229. Interactions are formed between the polar atoms of residues Arg220 (B) and Arg229 (C) with those of the backbone amides, except from Asn210, where the hydrogen bond is formed with the side chain carbonyl-oxygen. The hydrogens were modeled as described in Material and Methods. (D, E) Crystal structure of the HA1-HA1 interface at neutral pH (PDB ID: 2IBX) (D) and its modeled conformation upon protonation of His184 at a pH below 5 (E). Secondary structures of chain A (brown) and E (yellow) are displayed in cartoon representation with residues His184, Arg216, Glu231 and Asn210 in stick model. For the modeling, the side chain of His184 has been rotated by 180 degrees and the structure has been subsequently energy minimized. We suggest that a strong hydrogen bond is formed between His184 and Asn210, while the interaction between Asn210 and Arg220 is significantly weakened.

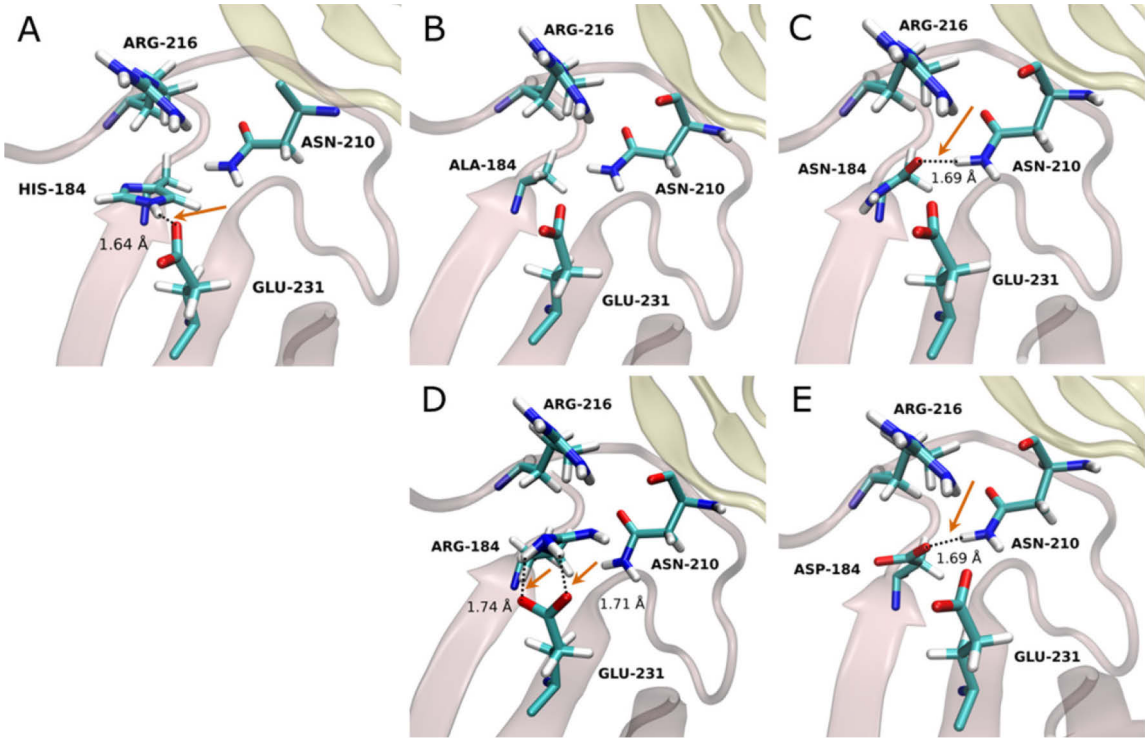

Figure 4.2: Structural representation of the HA1-HA1 interface of H5 HP wild type and of modeled mutations at position 184.
Secondary structures of chain A (brown) and E (yellow) are shown in cartoon representation with central residues of the interface represented in stick model. Interactions of the respective residue at position 184 are displayed (marked by arrows). For modeling the residue His184 in chains A, C and E was replaced by alanine (H184A) (B), asparagine (H184N) (C), arginine (H184R) (D) or aspartate (H184D) (E).

4.1.2 Structural effect of mutations at position 184

Modeling of the different amino acids at position 184 in the H5 HP structure at neutral pH (PDB ID: 2IBX) supports the hypothesis of His184 controlling the pH dependence of the conformational change at low pH (Figure 4.2). In the case of alanine at position 184 no interaction of this amino acid with surrounding residues occurs. However, being the smallest amino acid it leaves enough space for water to enter the hydrophobic cavity which possibly weakens the interfacial interactions in general. Asparagine as well as aspartate at this position forms a hydrogen bond with Asn210 in the neutral pH structure. As a result these residues have a strong influence on the hydrogen bond network of Arg220 and Arg229 near the inter-monomeric interface suggesting a destabilizing effect of these mutations. While for asparagine this is in line with our experimental results, for aspartate we could not observe fusion and only an indication for a conformational change, though with moderate pH dependence. This result illustrates and supports the high sensitivity of this region to the character of the amino acid which is present at position 184. Aspartate and asparagine are structurally very similar and thus both are able to form a hydrogen bond with Asn210 as

shown by computational modeling. However, due to its negative polarity aspartate might have a diverse effect on the stability of the complex than asparagine which we are not able to predict.

According to our experimental studies arginine at position 184 prevents a conformational change of HA which is – at a first glance – an unexpected observation. Arginine is positively charged like a protonated histidine and the latter one is thought to support the dissociation of the monomers due to ionization. As revealed by modeling of the H184R mutation into the crystal structure of H5 HP, arginine at position 184 forms a double salt bridge with Glu231 which is very stable. Furthermore, the polar atoms of the long residue are most distant to Asn210 and Arg220 and closer to the surrounding water what may result in a much weaker influence on the hydrogen bond network of Arg220 and Arg229 residues compared to the residues discussed before. Taken together, except for H184D, our modeling approach allows to rationalize the molecular basis for the influence of His184 mutations on the respective pH shift of the conformational change of HA and fusion.

4.1.3 His184 is part of a conserved interaction network at the HA1-HA1 interface

Crystal structure analysis of H5 HP and modeling of His184 mutants revealed that a pair of positively charged arginine residues (Arg220 and Arg229) and their hydrogen network formed with neighboring residues and Asn210 of the adjacent monomer may play an essential role for triggering the HA1-HA1 monomer dissociation at low pH. By aligning the protein sequences of subtypes from H1 to H18 we found that apart from His184 also both arginine residues (R220 and R229) are highly conserved (Table 4.2). Residue 210 is also partly conserved being an asparagine, a glutamine, a threonine or a serine in most subtypes. These amino acids are all structurally similar and polar enabling their interaction with Arg220. Interestingly, residue 231 directly interacting with His184 at neutral pH is also conserved to some degree, meaning that in most cases it is an amino acid which is able to form a hydrogen bond with His184. Only the degree of polarity of the participating side chain varies which could influence the pK_a of His184 and thereby also contribute to the variances observed in the fusion pH of different HA subtypes [273]. However, there are remarkable differences in sequence and structure between subtypes which might conceal the effect of this single amino acid difference.

Table 4.2: Sequence alignment of subtypes H1 to H18[a].

Strain	PDB ID	Accession number	HA1 sequence in H3 numbering												
			180	181	182	183[b]	**184**	195	**210**	215	**216[c]**	**220**	221	**229**	**231[b]**
H1N1	4JTV	C3W5S1	W	G	I	H	**H**	Y	**S**	P	**E**	**R**	P	**R**	**N**
H2N2	2WR0	D0VWP8	W	G	I	H	**H**	Y	**N**	P	**E**	**R**	P	**R**	**E**
H3N2	1HGD	P03438	W	G	I	H	**H**	Y	**Q**	P	**N**	**R**	P	**R**	**S**
H4N6		M1UPL4	W	G	V	H	**H**	Y	**Q**	P	**N**	**R**	P	**R**	**S**
H5N3	1JSM	A5Z226	W	G	I	H	**H**	Y	**N**	P	**E**	**R**	P	**R**	**E**
H5N1	2IBX	Q45ZQ3	W	G	I	H	**H**	Y	**N**	P	**R**	**R**	S	**R**	**E**
H6N5		F2P1Y8	W	G	V	H	**H**	Y	**N**	P	**E**	**R**	P	**R**	**D**
H7N9		D0FI67	W	G	I	H	**H**	Y	**Q**	P	**S**	**R**	P	**R**	**D**
H7N3	4BSG	Q6GYW3	W	G	I	H	**H**	Y	**Q**	P	**S**	**R**	P	**R**	**D**
H8N4		G2TWE4	W	G	I	H	**H**	Y	**N**	P	**N**	**R**	P	**R**	**D**
H9N2	1JSD	Q91CD4	W	G	I	H	**H**	Y	**N**	P	V	**R**	P	**R**	**D**
H10N7		M1UTF6	W	G	I	H	**H**	Y	**Q**	P	V	**R**	P	**R**	**D**
H11N6		P04661	W	G	I	H	**H**	Y	**N**	P	**E**	**R**	P	**R**	**T**
H12N5		P03446	W	A	I	H	**H**	Y	**N**	P	**N**	**R**	P	**R**	**D**
H13N6	4KPQ	P13103	W	G	I	H	**H**	Y	**S**	L	**E**	**R**	P	W	**K**
H14N5		P26136	W	G	V	H	**H**	Y	**Q**	P	**N**	**R**	P	**R**	**S**
H15N8		Q82565	W	G	V	H	**H**	Y	**Q**	P	**S**	**R**	P	**R**	**D**
H16N3	4F23	Q5DL24	W	G	I	H	**H**	Y	**S**	L	**E**	**R**	I	W	**K**
H17N10	4H32	H6QM93	W	G	I	H	N	Y	**S**	P	**D**	**R**	D	**R**	**D**
H18N11	4MC5	U5N1D3	W	G	V	H	Q	Y	**S**	L	V	**S**	S	**R**	**N**

[a] HA subtypes are listed in alphabetical order. Important residues at the HA1-HA1 interface are marked in bold. Residues forming the conserved interactions at the HA1-HA1 interface are highlighted in cyan (His184), orange (residue 210) and green (Arg220 and Arg229/Lys231), respectively.

[b] highly conserved His183 is involved in receptor binding

[c] Residues 216 and 231 potentially influence the pKa of His184.

The only exception of the consensus interactions at the HA1-HA1 interface are the four subtypes of the newly defined group 3 HAs (H13, H16, H17 and H18) [240,333,334]. H13 and H16 carry tryptophan at position 229. However, both have a lysine at position 231 which might compensate for the “lost” Arg229. In bat-derived H17 and H18 position 184 is an asparagine and a glutamine, respectively. These two subtypes were suggested to have a different mechanism of fusion activation and might not necessitate a pH dependent conformational change of HA [240,334,335]. Thus, the absence of histidine at position 184 in H17 and H18 subtypes in contrast to its high degree of conservation not only between but also within all other subtypes reinforces the requirement of a histidine at position 184 for the pH dependent conformational change of histidine. Furthermore, the fact that the interactions of Arg229 (or Lys231), Arg220, His184 and residues 210 (and 231) are also conserved indicates that these residues as well play a crucial role for the pH dependent stability of HA.

4.1.4 Models of the pH induced conformational change of HA

According to our results histidine is the only amino acid at position 184 which is able to stabilize or destabilize the HA1 monomers depending on its pH of protonation explaining its high degree of conservation in all subtypes (except H17 and H18). Other residues at position 184 were shown to destabilize (Ala, Asn, and perhaps Asp) the associated HA1 monomers already at a higher sub acidic pH (>6.0) or to completely stabilize the HA1-HA1 interface (Arg) abrogating a conformational change and fusion even at rather low pH. Thus, we suggest that His184 is not the sole trigger of fusion but one determinant regulating the HA conformational change at low pH. Studying the requirement of histidine protonation in the E protein of West Nile virus Nelson et al. also found that the substitution of key histidines did not abolish the formation of reporter virus particles and the pH dependency of fusion but remarkably reduced viral titers [336]. These results indicate that individual histidines are dispensable for triggering fusion but might be required for the regulation of the pH of conformational change and thus of fusion. Also for the E1 protein of SFV the absence of a critical histidine (His230) did not affect the pH dependence of conformational change of E1 but viral particles carrying the H230A mutation were completely non-infectious [156]. Thus, by regulating the dissociation of HA1 monomers, His184 is possibly required as one of several pH sensors controlling the time-point of the fusion inducing conformational change of HA which might be essential for viral infectivity.

Zhou et al. suggested that the dissociation of the HA1 monomers is caused by an overall increase of the positive net charge of the HA1 subunits whereas fusion peptide release and the structural reorganization of the helical loop domain are triggered by step-wise protonation of critical pH sensors such as His18 and Glu89 of HA1 and Glu103 of HA2 [332]. The dissociation of HA1 monomers was also previously proposed to be triggered by the repulsion of the positively charged monomers [235] and subsequent interaction of HA2 with the incoming water was proposed to trigger the subsequent spring-loaded conformational of HA [236,337]. This model of HA conformational change is supported by a time-resolved study on single-virion fusion where the rate-limiting step of membrane fusion was assigned to the release of the fusion peptide from its pocket [219]. However, this step requires prior or simultaneous dissociation of the HA1 domains which was not considered in this study.

Li et al. provided direct evidence that efficient genome release and infection requires sequential exposure to the pH of both, early and late endosomes which involves conformational changes in both, the M1 and the HA protein [71]. Furthermore, Zhou et al. identified His184 as a possible late stage pH sensor [332] which correlates with our proposed model described above. In summary, we believe that protonation of several residues in the HA1 as well as the HA2 domain simultaneously might be required for a controlled sequence of structural rearrangements resulting in the fusion inducing conformational change. However, in which order the identified residues are protonated and

which other residues participate in the complex rearrangement of HA still needs to be clarified.

4.2 Identification of mutations modulating the pH stability of H5 HP

The adaptation of avian influenza A viruses to humans has been shown to require mutations in several viral genes, which enable the virus to cross the species barrier. These genetic traits are often associated with increased host range and virulence in the mammalian host [338]. Low and highly pathogenic avian H5N1 strains have been differentiated by the presence of a mono- or polybasic cleavage site, which was found to determine the virulence of these strains in infected chicken. However, in 2003-2004 a more aggressive form of the highly pathogenic H5N1 virus evolved which did not only result in a massive bird-die off but also in an accumulating number of human spill-over infections. Apart from mutations in the RBS of HA resulting in increased α-2,6-SA binding adaptation to the mammalian host has been suggested to require additional mutations preserving the stability of the HA protein and thus of the whole virus. We identified a glutamate-to-arginine mutation at position 216 in the highly pathogenic H5 HA which has evolved in the period of the so-called “bird flu” and thus might have contributed to the emergence of the highly aggressive H5N1 virus.

Table 4.3: Summary of data obtained for the highly and low pathogenic H5 HA as well as for H3 HA carrying mutations at positions 212 and/or 216.

Protein	Surface expression Mean ± SD[a]	ΔpH[b]		
		RBC fusion assay	conf. change assay	Average
H5 HP wt	100 ± 5	5.9	5.7	5.8
H5 HP R216E	127 ± 13	+0.3	+0.2	+0.3
H5 LP wt	158 ± 73	6.0	6.0	6.0
H5 LP E216R	113 ± 13	-0.2	-0.4	-0.3
H3 wt	ND	5.4	ND	5.4
H3 T212E-N216R	ND	+0.4	ND	+0.4

[a] Relative MFI [%]

[b] The values represent the average from a minimum of three experiments. In all cases the difference between the three measurements did not exceed 0.1 pH units. ND, not determined; - no fusion or conformational change detected at any pH

By exchanging the charge in H5 HP and LP we found that glutamate at position 216 increases the pH threshold of the conformational change and fusion in H5 HP whereas exchanging glutamate by arginine in the low pathogenic subtype resulted in a decrease of the pH threshold (Table 4.3). In support of our study, an increase of the pH of fusion when exchanging residue 216 from a lysine, which is positively charged like arginine, to a glutamic acid (K216E) was reported for a highly pathogenic H5 subtype [284]. The authors argued that the effect of this K216E mutation on the pH of fusion was due to a change in hydrogen bonding with the adjacent monomer (from K216-N210 to E216-R212) [284]. However, analyzing the known crystal structures (PDB ID: 3S11 and 3S13) we could not identify any of the mentioned hydrogen bonds.

4.2.1 Fine-tuning of the pK_a of His184 - Implications for host adaptation

Structural analysis revealed that residue 216 is located at the HA1-HA1 interface in vicinity to His184 (see Figure 4.2) suggesting that it may affect the acid stability of HA by a pK_a-modulating effect on His184. Histidine at position 184 is partially buried in the protein and thus its pK_a depends on the residues in its local environment, i.e. it can be strongly affected and, by that, precisely adjusted by those residues and mutations thereof [339,340]. Although our experimental data do not provide direct evidence, they support this hypothesis. The obtained data correlate with the previously described pK_a dependency of histidines on neighboring residues [163,339–342]. An additional negative charge is known to support protonation of histidine resulting in an increased pK_a whereas in the environment of a positively charged residue the protonated and thus positively charged form is less favored shifting its pK_a to lower values. Thus, we suppose that the exchange of charge at position 216 causes an alteration in the pH of conformational change and of fusion via its effect on the pK_a of His184. The exchange of residues in proximity to histidines was also reported in other studies to significantly affect the fusion pH proposing that some mutations exhibit a pK_a-modulating effect on neighboring histidines [162]. However, what is the consequence for a shifted fusion-pH and how can it contribute to host adaptation?

Several studies have provided evidence that the pH of fusion is crucial for influenza virus infection in distinct organisms [298,329,330]. It was further shown that viral adaptation to different host cells and species often necessitates mutations in the HA protein which alter the fusion pH to account for host specific variations in the endosomal pH and/or for different transmission modes [260,261,343–345]. In particular, there has been evidence that a high pH of fusion increases the pathogenicity of the virus in infected chicken and ducks [284,298] whereas it is not favorable for the infection of a mammalian host [329,330,343,344]. Sequence alignment of H5 HAs of isolated H5N1 strains revealed that the glutamate-to-arginine (or –lysine) mutation is present in all highly pathogenic virus strains not only isolated

from birds and humans in 2003-2004 but also in subsequent years suggesting that the charge-charge mutation and the altered pH of fusion involved contributed to a highly pathogenic phenotype. We propose that this E216R/K mutation stabilizes the HA ectodomain of H5 HP shifting the fusion triggering conformational change to a more acidic pH. The mutation might also have compensated for other destabilizing mutations, preventing conformational change of H5 HP HA at elevated pH [284]. Also in previous studies the substitution of charged residues were suggested to play a dominant role in the course of virus adaptation [292,295]. In line with this, the introduction of two additional charges at the HA1-HA1 interface of the H3 subtype the pH of fusion was even more significantly affected, however the structural effect of the double-mutation was not characterized in detail.

4.3 The acid stability of HA–a new determinant of host range and pandemicity?

4.3.1 Reviewing host adaptation of influenza A viruses

Successful adaptation of avian influenza A viruses to humans was shown to require mutations in several viral genes, which enable the virus to efficiently infect and replicate in the human host, as well as to spread via the airborne route between humans. Several influenza viruses from the avian reservoir already have the ability to infect the human host (H5N1, H7N9, H9N2), but are not further transmitted via aerosols or respiratory droplets (RD) between humans. To avoid the emergence of a new pandemic it is of substantial importance to understand the mechanisms of host adaptation resulting in the acquisition of airborne transmissibility and increased virulence in the mammalian host.

One of the best characterized mammalian adaptations is the E627K mutation in the polymerase subunit PB2, which enhances replication efficiency of the virus at lower temperature in the human lung (33°C versus 41°C in avian intestines) [346,347]. This substitution was reported to confer increased virulence and transmissibility in the mammalian host [348] and was also found in the highly pathogenic H5N1 strains isolated from humans in 2004 [243]. In addition, most human H7N9 virus isolates carried the E627K mutation and/or the alternative adaptive substitution D701N [348,349]. The latter causes enhanced binding to mammalian importin-α1 resulting in increased transport of PB2 to the nucleus [350]. The presence of one of the two mutations, D701N or E627K, was shown to be required for transmission of influenza viruses suggesting that they are critical determinants for mammalian infection and transmissibility [348]. Adaptation to the mammalian host is also known to necessitate mutations in the RBS of HA which result in a switch in the receptor binding specificity from α-2,3- to α-2,6-SA. Recent studies reported that a Q226L mutation

conferred increased α-2,6-SA binding to many avian viruses such as H5N1, the natural occurring H9N2 [351] and the recent H7N9 strains [352,353]. The latter was even found to weakly transmit between ferrets via the airborne route [354–357] which was ascribed to the higher affinity of H7N9 to α2,6-SA than other H7 and H5 subtypes [352,358,359]. Also transmission of the H9 subtype in combination with human adapted genes was promoted by the presence of the Q226L mutation suggesting that this amino acid change in the RBS might be sufficient to confer human type receptor binding.

While in several studies α-2,6-SA binding was clearly shown to be a pre-requisite for infection of the human host and transmissibility between ferrets [360–362], changing the receptor specificity of natural or recombinant H5N1 viruses from α-2,3- to α-2,6-SA was insufficient to confer airborne transmissibility [259–261]. Even with the proper HA-NA balance, a mutated H5 virus with α-2,6-receptor binding specificity supported only partial transmission via respiratory droplets [363]. Moreover mutations in the RBS were associated with reduced replication and virulence [259,364] suggesting that there are other mutations needed that retain viral fitness. In line with this hypothesis, two independent studies demonstrated that mutations additionally to human type receptor binding were required to confer efficient respiratory droplet transmission of H5N1 viruses between ferrets [260,261]. In both cases these additional mutations were associated with higher stability of the HA protein [261,262,324]. Also for the 2013 H7N9 virus the pH threshold of membrane fusion was found to be relatively high (pH 5.6-5.8) and might thus in part be responsible for the limited airborne transmissibility of this virus (Figure 4.3).

The requirement of a stable HA for mammalian adaptation can be explained by the fact that transmission via respiratory droplets, which is also the primary transmission mode in humans, requires passage of the virus through the nasal airway epithelium which presents a significant extracellular barrier to influenza infection [344]. The mucociliary clearance system, viscous fluids, and macrophages interfere with the virus access to the cell surface. At the same time the nasal cavity is mildly acidic promoting a conformational change of HA resulting in viral inactivation. Indeed, the replication efficiency of an avian influenza H5N1 virus in mice was reported to be enhanced by a stabilizing mutation in the stalk domain of HA ($K58_2I$). Due to a lower pH of activation it retained infectivity in the nasal cavity of mice whereas the infectivity of the wild type was reduced [344]. The $K58_2I$ mutation was also reported in another study to support increased growth of the virus in mice and the upper respiratory tract of ferrets whereas in infected mallards no physiological symptoms were detected [298,329,330]. Hence, an increased acid stability of HA might not only be required for efficient viral transmission but also for increased infectivity in a specific host.

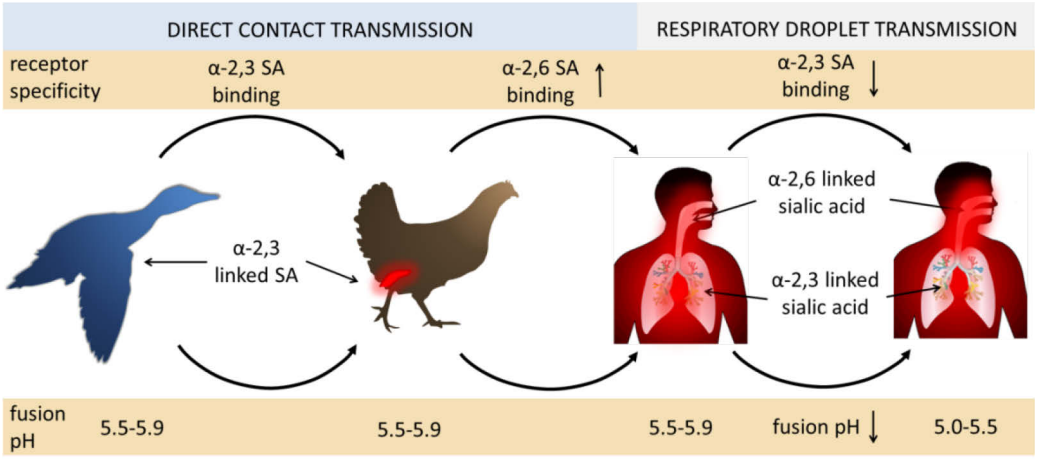

Figure 4.3: Requirements for adaptation of avian influenza virus HA to the human host.
Apart from a change in the receptor binding specificity from avian (α-2,3-SA) to human (α-2,6-SA) type receptors, an increase of the acid stability of HA is mandatory. Higher acid stability of HA is thought to promote spreading of the virus via respiratory droplets, a pre-condition for pandemicitiy.

Replication of influenza viruses in different cell lines or hosts was also linked to a change in acid stability of HA [298,329,330,343,345,364]. In particular, a lower acid stability of HA (pH 5.5-6.0) was shown to increase the pathogenicity of H5N1 viruses in the avian host [284] as well as replication of influenza viruses in ducks [298] whereas viral growth in mice and in the URT of ferrets was favored by mutant viruses containing an acid-stable HA protein (pH 5.0-5.5) [329,330]. A recent characterization of avian and human-adapted HA subtypes further revealed that the fusion pH of HA of avian isolates was in general higher than that of human isolates [15]. These results suggest that infection and replication of avian viruses in the human host requires an increased acid stability of HA. In support of this hypothesis all human influenza viruses, including the recently appeared pandemic H1N1 virus were capable of infecting cells at acidic conditions while two highly pathogenic H5N1 viruses infected human nasal epithelial cells only at a neutral pH [344].

4.3.2 The acid stability of HA determines the pH threshold of fusion

Knowledge of the molecular properties that govern efficient infection and growth of an influenza virus strain in one cell type, tissue, or host species versus another may help to understand the requirements for successful host adaptation. This is important in conducting surveillance and risk assessment of currently circulating viruses. Furthermore, it may help to optimize vaccine yield and efficacy and suggest novel ways to treat infection [329]. Thus, the aim in the second part of my study was to determine how a single destabilizing mutation in the HA protein influences pH dependent fusion when introduced into the background of the

WSN H1N1 influenza virus. Furthermore, the effect of an altered acid stability on host-specific virus infection and intracellular fusion was assessed.

Introduction of the destabilizing double mutation T212E-N216R into the H3 subtype of recombinant WSN viruses resulted in higher pH threshold of membrane fusion. However, the increase was less pronounced with a shift of only +0.2 units (see 3.6) compared to an increase of 0.4 units determined in the RBC fusion assay (see 3.3.1). The disparity in the delta pH is likely due to the fact that the RBC fusion assay was only measured in steps of 0.2 pH unit increments and quantitative data about the number of HA molecules undergoing a conformational change were not obtained. Furthermore, the pH threshold of WSN H3 viruses was determined at half-maximal fusion efficiency of the respective virus, whereas in the RBC assay the pH of fusion is determined as the pH where more than 50 % of HA molecules undergo a fusion inducing conformational change. The pH dependent fusion efficiency of the WSN H3 wild type virus is maximal at pH 5.2 and decreases steadily reaching half-maximal fusion efficiency at pH 5.6. The maximal pH dependent fusion efficiency of the WSN H3 mutant virus is at pH 5.6 and is thus 0.4 units higher than that of the wild type corresponding to the delta pH obtained in the RBC fusion assay. In contrast, due to a faster decrease in fusion efficiency with augmenting pH the half-maximal fusion efficiency is already reached at pH 5.8 and thus only 0.2 units higher than that of the wild type.

Other sources possibly being responsible for the disparity in the obtained delta pHs are the HA protein itself, the curvature of the membrane where it is inserted and the curvature of the target membrane. All of these parameters can affect the pH dependent fusion efficiency of HA and therefore, the delta pH of fusion between wild type and mutant WSN H3 viruses strongly depends on the experimental system used and ranges from 0.2-0.4 units.

4.3.3 The acid stability of HA affects cell-specific infectivity

The human epithelial cell line A549 and Madin Darby canine kidney (MDCK) cells were recently shown to differ in their endosomal acidification using dextran-conjugated pH sensitive dyes. A pH of 5.4 was measured for MDCK and a pH of 5.9 for A549 cells after incubation for 15 min [329]. According to our results the lower acid stability of the mutant resulted in lower infection efficiency in MDCK cells whereas in A549 cells the infection efficiency was similar to that obtained for the wild type (see 3.7). Also the replication efficiency of the WSN H3 T212E-N216R mutant virus was reduced compared to the wild type (see 3.8). This means that the lower endosomal pH of MDCK cells might not be suitable for infection with a virus of a high fusion pH threshold. In line with this the WSN H1 wild type virus, for which an even higher pH threshold of fusion of 6.21 was determined, also exhibited reduced infection efficiency in MDCK but not in A549 cells. However, H1 HA is a different subtype and thus might differ from H3 HA in other factors additional to its modulated acid

stability, such as the receptor binding specificity and the associated uptake of the virus by the host cell. Therefore, the infection efficiency of this virus cannot be directly compared to that of the WSN H3 viruses.

Zaraket et al. reported that recombinant viruses with a stabilizing mutation in the H5 subtype (fusion pH of 5.4 compared to 5.9 for the wild type) replicated equally well in MDCK cells as the wild type but less efficiently in A549 cells [329], which indirectly supports our result that a lower acid stability is favored for the infection in MDCK but not in A549 cells. Similarly, VSV which induces fusion at higher pH (6.0-6.5) than influenza virus (5.0-6.0) exhibits greater infectivity in Vero than in MDCK cells. In contrast to these findings indicating that the acid stability of HA affects host-specific virus infection, the replication efficiency of a highly pathogenic H5N1 virus was similar in all of these cell lines [365]. Also the acid-stable $K58_2I$ mutant was reported to replicate equally well in MDCK, A549 and Vero cells [344]. Though, in that study a delta NS1 mutant strain was used and therefore does not represent the natural situation of an influenza virus infection. Nevertheless, several other studies on the adaptation of influenza viruses to a different host provided evidence for an existing link between acid stability of HA and host specificity. Passage of an egg-grown virus in mammalian cells resulted in an altered pH of membrane fusion of HA [294] as well as passage of a human-derived virus in mice [366]. In particular, adaptation of influenza virus H1N1 and H3N2 to the higher endosomal pH of Vero cells caused destabilizing mutations in the HA protein [343,345], which promoted its replication in these cells [33]. Also influenza viruses growing in the presence of amantadine hydrochloride, which blocks the M2 ion channel were reported to acquire mutations in the HA protein shifting the pH of fusion to higher values [289,292,293] which indicates a link between M1 and HA conformational changes during acidification. To conclude, an adjustment of the acid stability of HA seems to be required due to varying endosomal pHs among cell lines or hosts.

4.3.4 The acid stability of HA regulates the time-point of membrane fusion

By tracking virus-endosome fusion in MDCK cells we found a significant difference in the fusion kinetics of WSN H3 wild type and the T212E-N216R mutant viruses (see 3.9). For the mutant fusion of the viral with the endosomal membrane was already detected after 5 min whereas for the wild type an increased green fluorescence due to DiO dequenching and removal of FRET was only exhibited 10 to 15 min post-infection. Lakadamyali et al. using live cell imaging in combination with single particle tracking reported that influenza virus particles reached Rab5-positive early endosomes after 5 min and co-localized with Rab5 and Rab7 on maturing endosomes (multivesicular bodies), where most of the fusion events were detected [367]. Fusion for influenza virus A/X-31 which contains the identical HA protein as the recombinant H3 viruses used in the present study was reported to occur already 10 min

post-infection in CHO cells [70]. A half-time of 10 min for A/X-31 virus-endosome fusion in HeLa cells was also reported by Sakai et al. whereas we found a half-time of virus-endosome fusion of 16 min for the recombinant wild type H3 virus in MDCK cells using the same approach. However, my experiment was only conducted twice and thus might need some optimization.

The determination of the exact timing of virus-endosome fusion is challenging due to a relatively "long" acquisition time of around 0.5 min between the first and the last points of a Z-stack and movement of the virus inside the cell which can lead to less precise observations. This limitation can be overcome by spinning disc confocal laser microscopy, a more powerful tool for rapid spatial and temporal imaging of living cells. Nevertheless, using the dual-wavelength imaging approach in combination with confocal microscopy we could show that the green fluorescence increased between 5 to 20 min for both, wild type and mutant virus which corresponds to virus-endosome fusion in MDCK cells. Fusion events were clearly detected in the perinuclear region after movement of the particle towards the center of the cell. This suggests the localization of major fusion events in the late endosomal compartment as also described by Lakadamyali [70] and Sakai et al. [322]. Furthermore, fusion of the WSN mutant viruses containing a destabilized HA protein was detected 7-9 min earlier compared to the wild type which correlates with the higher pH threshold of the virus measured *in vitro.* Thus, the stability of HA controls the pH threshold of the conformational change and thereby seems to affect intracellular fusion of the virus.

A possible explanation how the pH of membrane fusion and the associated modulated intracellular fusion kinetics translate into altered infection efficiency is provided in Figure 4.4. (1) The earlier the viral genome is released from the endosome, the higher the probability that the cellular immune response is stimulated. For example, the released viral RNA is recognized by the RNA helicase RIG-I [44,45] which leads to the activation of transcription factors IRF3 and/or IRF7 and subsequent induction of type I interferon (IFN) and IFN inducible genes [60]. Other viral proteins including NP, M1 and HA within the cytoplasm activate nuclear factor κB (NF-κB) via activation of IκB kinase 2 (IKK2), which also results in interferon induction [368]. (2) At the same time, fusion has to occur before the endosome has matured into a lysosome where recognition of the viral RNA by Toll like receptors (TLR) 3 and/or 7 would also result in the induction of immune signaling pathways leading to the expression of type I interferon as well as NF-κB [60]. Thus, the endosomal acidification as well as the acid stability of HA determine time and localization of virus-endosome fusion and thereby the fate of the virus after endocytic uptake providing a model for the requirement of an adapted pH of membrane fusion to a different endosomal pH.

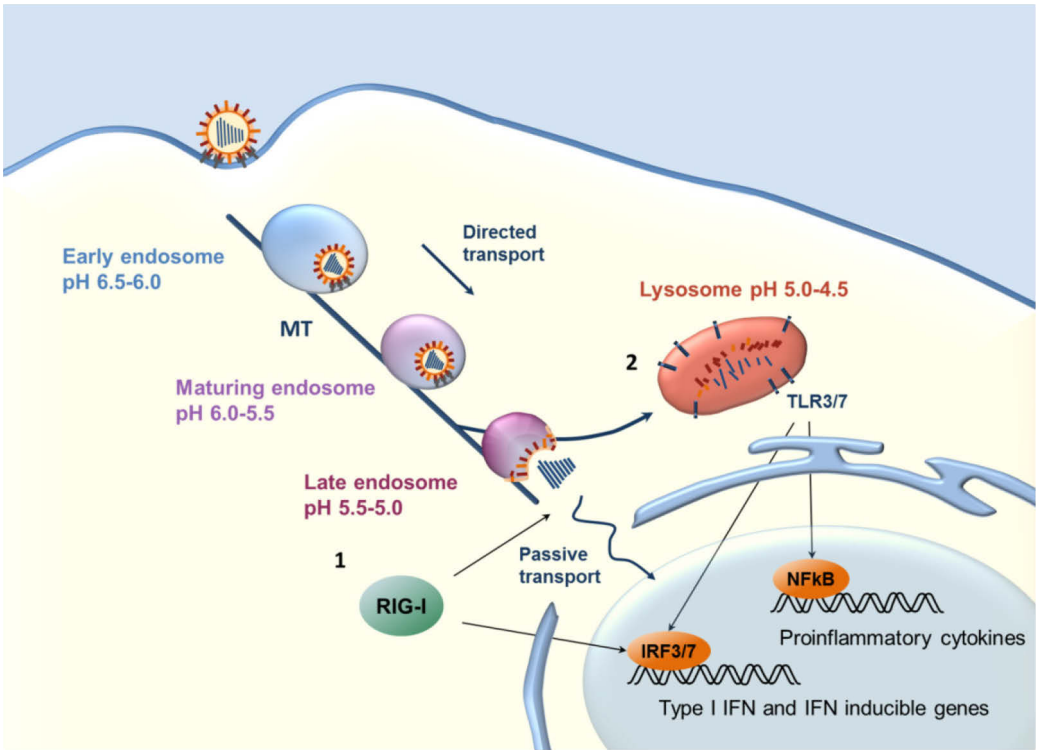

Figure 4.4: Relevance of acid stability of HA for viral entry.
After endocytosis of the viral particle, it is transported along microtubules (MT) towards the center of the cell. (1) The earlier the viral genome is released from the endosome, the higher the probability that the released vRNPs can be recognized by the RNA helicase RIG-I. Upon RIG-I binding transcription factors IRF3 and/or IRF7 are activated, which induce type I interferon (IFN) and IFN inducible genes. (2) At the same time, fusion has to occur before the endosome has matured into a lysosome where detection of the viral RNA by Toll like receptors (TLR) 3 and/or 7 would also result in the induction of immune signaling pathways leading to the expression of type I IFN as well as NF-κB. Thus, the acid stability of HA has to be optimized to control time and localization of fusion.

The lower acid stability of the T212E-N216R mutant virus was shown to result in an earlier time-point of viral fusion in the maturing endosome, possibly in higher distance to the nucleus. This in turn increases the probability of vRNA recognition by the cellular innate immune response resulting in the reduced infection observed in MDCK cells. Indirect evidence for this hypothesis was achieved by studies reporting that the induction of influenza virus fusion at the plasma membrane and resulting bypass of endocytic trafficking results in a more than 80 % lower infection efficiency of the virus [71,72]. While this effect was ascribed to inefficient uncoating of the viral genome, another reason might be the longer distance between plasma membrane and nucleus that the released vRNPs have to overcome by diffusion. This in turn increases the probability that the vRNA is recognized by cellular immune factors resulting in lower infection efficiency. In summary, we propose that the HA stability is an essential determinant which must be optimized to allow viral transmission between humans and to control time and localization of intracellular fusion for efficient infection and replication in the mammalian host.

4.4 Conclusion and Outlook

Influenza A viruses are still one of the major health problems worldwide. Especially avian influenza viruses pose a great risk since they have already crossed the species barrier and infected humans. The currently available vaccine against flu is a tri- or quadrivalent formulation composed of the seasonally changing influenza A H1N1 and H3N2 virus strains and one or two influenza B virus strains, respectively (Centers for Disease Control and Prevention, CDC). Drawbacks of this strategy are the requirement of an annually changing formulation necessitating constant surveillance of circulating strains and a time-consuming production of these vaccines. To date only a limited number of therapeutic drugs are available, which include inhibitors of the M2 ion channel (amantadine and rimantadine) and of neuraminidase (oseltamivir and zanamivir). However, single amino acid substitutions in the M2, NA and HA protein resulted in increasing resistance among circulating influenza viruses (e.g. H7N9) which makes these drugs useless and emphasize the need to develop alternative approaches for the prevention and/or treatment of an influenza virus infection [303].

The entry of influenza virus into host cells is established by HA and thus represents a promising target for novel antiviral drug development. Several synthetic receptor mimics, which inhibit HA-SA binding and peptides blocking the fusion inducing conformational change of HA have been tested for their antiviral efficacy. However, these exhibited mostly subtype-dependent activities and low barriers against mutational drift of HA [369–371]. As a consequence, new antiviral strategies target conserved regions of HA such as the RBS or highly conserved structures of the HA2 domain which are involved in fusion. Also small molecules that perturb the membrane thereby inhibiting fusion have been sought [304–306]. To inhibit influenza virus infection at the stage of membrane fusion it is essential to understand the exact mechanism of conformational change and of fusion. The fusion inhibitor T20 which targets the fusion protein gp41 is already employed against HIV (Fuzeon, Roche) proving the therapeutic potential of such drugs. Thus, the elucidation of conserved protonable residues and their role in the fusion process might facilitate the identification of drugable domains of the influenza virus HA and the development of antivirals.

In the first part of the study His184 was demonstrated to be a crucial molecular switch at the HA1-HA1 interface regulating the pH dependence of the conformational change of HA. His184 is highly conserved among all subtypes (except H17 and H18) as well as its neighboring residues including Arg220 and Arg229 and residues 210 and 231 which make the region a useful target for inhibitory peptides. At the same time, the residues are mostly buried at the HA1-HA1 interface and thus only become accessible upon protonation and

dissociation of the HA1 domains making it difficult to design a suitable inhibitor. In contrast, the His18 pH sensor group (His18, His38 of HA1 and His111 of HA2), which was described to facilitate fusion peptide release upon protonation, was recently demonstrated as suitable drug target. Protonation of this group could be successfully blocked by binding of the antibody CR6261 [332]. However, the existence of the pH sensor group and its fusion inhibition were only predicted by computational methods and experimental evidence such as provided in the current study for His184, is missing. Nevertheless, it demonstrates that the identification of conserved protonable residues might indeed be useful for the development of new viral inhibitors.

In the present study His184 and its local environment are suggested to be important determinants for the pH of HA conformational change and membrane fusion, an essential step of the infection cascade. In support of this hypothesis mutation of residue 216, which is located in vicinity to His184, was shown to alter the pH threshold of conformational change and of fusion in H5 HP and LP in correlation to the known pK_a dependence of histidines on the local environment. Therefore, the Glu-to-Arg mutation was suggested to modulate the pH dependence of H5 HA by its effect on the pK_a of His184. Furthermore, the exchange of charge in H5 HP and associated fine-tuning of the pK_a of His184 may have facilitated the adaptation of the fusion pH to the mammalian host which was shown to be required for efficient infection and spread of the virus [260,261]. Another example of such a mechanism of adaptation is provided by the experimental adaptation of a recombinant H5N1 virus to ferrets model. Apart from mutations conferring human type receptor binding the passage of the virus in ferrets resulted in the stabilizing mutation T318I in the fusion domain of HA1 [262]. This residue was reported to increase the thermal stability of HA due to packing with hydrophobic residues Trp21 and two valine residues in proximity thereby stabilizing the fusion peptide and helix C. In combination with mutations increasing human type receptor specificity of H5 HA the T318I mutation was shown to confer respiratory droplet transmission to ferrets. However, Thr318 is located close to the His18 pH sensor group mentioned above and interacts with His111 in the H5 subtype. The exchange of Thr318 to isoleucine was shown to alter the conformation of His38 in the structure [262] and thus might as well abrogate the triggering function of the His18 pH sensor group at low pH (Figure 4.5). In contrast, the stabilizing mutation H110Y, which also enabled airborne transmissibility of a natural H5N1 strain between ferrets [260], is not associated with the loss of a protonable residue as initially believed, but with a loss of a hydrogen bond at the HA1-HA2 interface.

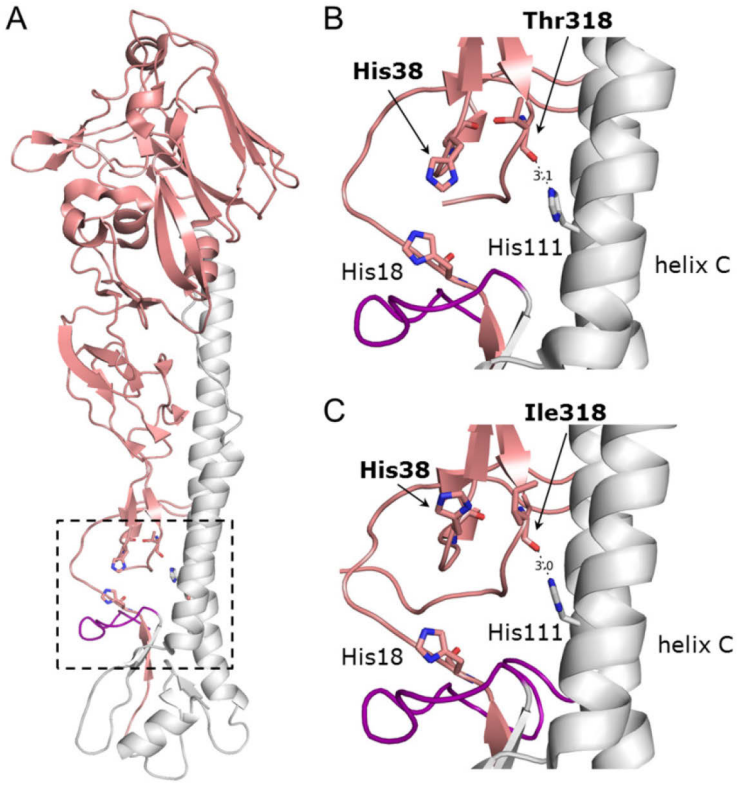

Figure 4.5: Crystal structure of the natural and the ferret-transmissible mutant H5 HA.
(A) Cartoon representation of the monomer of H5 HA with the HA1 subunit shown in salmon and the HA2 subunit in gray (PDB ID: 4BH1). The fusion peptide is colored in purple. (B and C) In the magnification the His18 pH sensor of the natural (PDB ID: 4BH1) and the ferret-transmissible mutant (PDB-ID: 4BH3) H5 HA is shown with histidines residues His18 and His38 of HA1 and His111 of HA2 as well as residue 318 of HA1 depicted in stick representation.

The two described studies [260,261] present the first evidence for the requirement of an increased acid stability for viral transmission between mammals. Studying the effect of a modulated pH threshold of fusion on virus infectivity revealed that the acid stability of HA also affects the infection and replication efficiency depending on the endosomal acidification in the respective cell line. This is in line with other studies reporting that the adaptation of influenza viruses to a given cell line or host containing a different endosomal pH caused mutations within HA altering the pH of fusion. However, the reason for this observation has long been unknown. Here, it is suggested that the pH of fusion controls the time and localization of vRNP release and thereby the infection efficiency of the virus. Following ejection of the viral genome into the cell cytoplasm the vRNPs are thought to be transported to the cell nucleus by diffusion [76]. Thus, if fusion occurs in greater distance to the nucleus the probability of detection by cellular immune factors such as RIG-I and resulting RNA degradation and induction of interferon signaling might be increased. Indirect evidence was provided that an earlier release of the viral genome reduces the efficacy of infection in MDCK cells suggesting that an optimal pH of fusion is required which allows the release of

the viral genome in close vicinity to the nucleus. However, this is only one possibility which still needs to be verified.

It is likely that also other viral proteins additional to HA are involved in controlling the release of the viral genome. For example, Lee et al. [372] suggested a different model of membrane fusion where the dissolution of the matrix layer M1 controls fusion pore opening at pH 5.0 and thus also the release of the viral RNPs. However, two recent studies provided evidence that efficient uncoating of the viral genome requires sequential acid exposure as well as the presence of K+ ions resulting in the irreversible disassembly of M1 at a higher pH (pH 5.5-6.0) than that of HA conformational change [71,72]. This also explains that HA conformational change at pH < 6.0 is favored for efficient viral infection in the mammalian as well as the avian host [298,330]. Thus, an ensemble of events in the M1 and HA proteins seem to trigger the release of the viral genome. Detecting the release of vRNPs by the split-GFP method published by Avilov et al. [373] and/or measuring the vRNP accumulation in the nucleus following fusion might shed more light on the role of HA acid stability for viral entry and infection.

Bibliography

[1] R. Shope, Swine influenza III. Filtration experiments and etiology, J. Exp. Med. (1931) 373–385.

[2] J.K. Taubenberger, D.M. Morens, Influenza: the once and future pandemic., Public Health Rep. 125 Suppl (2010) 16–26.

[3] G. Neumann, T. Noda, Y. Kawaoka, Emergence and pandemic potential of swine-origin H1N1 influenza virus., Nature. 459 (2009) 931–9.

[4] T. Horimoto, Y. Kawaoka, Influenza: lessons from past pandemics, warnings from current incidents, Nat. Rev. Microbiol. 3 (2005) 591–600.

[5] N. Ferguson, A. Galvani, R. Bush, Ecological and immunological determinants of influenza evolution, Nature. 422 (2003).

[6] M. Gerber, C. Isel, V. Moules, R. Marquet, Selective packaging of the influenza A genome and consequences for genetic reassortment., Trends Microbiol. (2014) 1–10.

[7] D. Tscherne, A. García-Sastre, Virulence determinants of pandemic influenza viruses, J. Clin. Invest. 121 (2011).

[8] J. Taubenberger, J. Kash, Influenza virus evolution, host adaptation, and pandemic formation, Cell Host Microbe. 7 (2010) 440–451.

[9] W.H. Organization, Overview of the emergence and characteristics of the avian influenza A (H7N9) virus, World Heal. Organ. (2013) 1–38.

[10] S.L. Noton, E. Medcalf, D. Fisher, A.E. Mullin, D. Elton, P. Digard, Identification of the domains of the influenza A virus M1 matrix protein required for NP binding, oligomerization and incorporation into virions., J. Gen. Virol. 88 (2007) 2280–90.

[11] A. Harris, F. Forouhar, S. Qiu, B. Sha, M. Luo, The crystal structure of the influenza matrix protein M1 at neutral pH: M1-M1 protein interfaces can rotate in the oligomeric structures of M1., Virology. 289 (2001) 34–44.

[12] A. V Vasin, O.A. Temkina, V. V Egorov, S.A. Klotchenko, M.A. Plotnikova, O.I. Kiselev, Molecular mechanisms enhancing the proteome of influenza A viruses: An overview of recently discovered proteins., Virus Res. 185 (2014) 53–63.

[13] R. Coloma, J.M. Valpuesta, R. Arranz, J.L. Carrascosa, J. Ortín, J. Martín-Benito, The structure of a biologically active influenza virus ribonucleoprotein complex., PLoS Pathog. 5 (2009) e1000491.

[14] T. Noda, H. Sagara, A. Yen, A. Takada, H. Kida, R.H. Cheng, et al., Architecture of ribonucleoprotein complexes in influenza A virus particles, Nature. 439 (2006) 490–492.

[15] L. Turrell, J.W. Lyall, L.S. Tiley, E. Fodor, F.T. Vreede, The role and assembly mechanism of nucleoprotein in influenza A virus ribonucleoprotein complexes, Nat Commun. 4 (2013) 1591.

[16] Q. Ye, R.M. Krug, Y.J. Tao, The mechanism by which influenza A virus nucleoprotein forms oligomers and binds RNA, Nature. 444 (2006) 1078–1082.

[17] G. Neumann, T. Watanabe, Generation of influenza A viruses entirely from cloned cDNAs, Proc. Natl. Acad. Sci. 96 (1999) 9345–9350.

[18] E. Fodor, L. Devenish, O.G. Engelhardt, P. Palese, G.G. Brownlee, A. García-Sastre, Rescue of influenza A virus from recombinant DNA., J. Virol. 73 (1999) 9679–82.

[19] E. Hoffmann, G. Neumann, Y. Kawaoka, G. Hobom, R.G. Webster, A DNA transfection system for generation of influenza A virus from eight plasmids., Proc. Natl. Acad. Sci. U. S. A. 97 (2000) 6108–13.

[20] E. de Wit, M.I.J. Spronken, G. Vervaet, G.F. Rimmelzwaan, A.D.M.E. Osterhaus, R.A.M. Fouchier, A reverse-genetics system for Influenza A virus using T7 RNA polymerase., J. Gen. Virol. 88 (2007) 1281–7.

[21] E.C. Hutchinson, E. Fodor, Transport of the influenza virus genome from nucleus to nucleus., Viruses. 5 (2013) 2424–46.

[22] S. V. Bourmakina, Reverse genetics studies on the filamentous morphology of influenza A virus, J. Gen. Virol. 84 (2003) 517–527.

[23] C.J. Elleman, W.S. Barclay, The M1 matrix protein controls the filamentous phenotype of influenza A virus., Virology. 321 (2004) 144–53.

[24] L.J. Calder, S. Wasilewski, J. a Berriman, P.B. Rosenthal, Structural organization of a filamentous influenza A virus., Proc. Natl. Acad. Sci. U. S. A. 107 (2010) 10685–90.

[25] D. Blaas, E. Patzelt, E. Kuechler, Identification of the cap binding protein of influenza virus, Nucleic Acids Res. 10 (1982).

[26] J. Stech, Influenza A virus polymerase: A determinant of host range and pathogenicity, 27 (2008) 187–194.

[27] W. Chen, P. Calvo, D. Malide, J. Gibbs, A novel influenza A virus mitochondrial protein that induces cell death, Nat. Med. 7 (2001) 1306–12.

[28] H.M. Wise, A. Foeglein, J. Sun, R.M. Dalton, S. Patel, W. Howard, et al., A complicated message: Identification of a novel PB1-related protein translated from influenza A virus segment 2 mRNA., J. Virol. 83 (2009) 8021–31.

[29] A. Dias, D. Bouvier, T. Crépin, A.A. McCarthy, D.J. Hart, F. Baudin, et al., The cap-snatching endonuclease of influenza virus polymerase resides in the PA subunit., Nature. 458 (2009) 914–8.

[30] B. Jagger, H. Wise, J. Kash, K. Walters, An overlapping protein-coding region in influenza A virus segment 3 modulates the host response, Science (80-.). 337 (2012) 199–204.

[31] Y. Muramoto, T. Noda, E. Kawakami, R. Akkina, Y. Kawaoka, Identification of novel influenza A virus proteins translated from PA mRNA., J. Virol. 87 (2013) 2455–62.

[32] J. Skehel, D. Wiley, Receptor binding and membrane fusion in virus entry: The influenza hemagglutinin, Annu. Rev. Biochem. 69 (2000) 531–569.

[33] K. Martin, A. Helenius, Transport of incoming influenza virus nucleocapsids into the nucleus., J. Virol. 65 (1991) 232–44.

[34] A. Portela, P. Digard, The influenza virus nucleoprotein: a multifunctional RNA-binding protein pivotal to virus replication., J. Gen. Virol. 83 (2002) 723–34.

[35] M. Bui, E.G. Wills, a Helenius, G.R. Whittaker, Role of the influenza virus M1 protein in nuclear export of viral ribonucleoproteins., J. Virol. 74 (2000) 1781–6.

[36] K. Shimbo, D.L. Brassard, R. a Lamb, L.H. Pinto, Ion selectivity and activation of the M2 ion channel of influenza virus., Biophys. J. 70 (1996) 1335–46.

[37] J. Rossman, X. Jing, G. Leser, R. Lamb, Influenza virus M2 protein mediates ESCRT-independent membrane scission, Cell. 142 (2010) 902–913.

[38] H.M. Wise, E.C. Hutchinson, B.W. Jagger, A.D. Stuart, Z.H. Kang, N. Robb, et al., Identification of a novel splice variant form of the influenza A virus M2 ion channel with an antigenically distinct ectodomain., PLoS Pathog. 8 (2012) e1002998.

[39] W. Wang, R.M. Krug, The RNA-binding and effector domains of the viral NS1 protein are conserved to different extents among influenza A and B viruses., Virology. 223 (1996) 41–50.

[40] B.G. Hale, R.E. Randall, J. Ortín, D. Jackson, The multifunctional NS1 protein of influenza A viruses., J. Gen. Virol. 89 (2008) 2359–76.

[41] D. Paterson, E. Fodor, Emerging roles for the influenza A virus nuclear export protein (NEP)., PLoS Pathog. 8 (2012) e1003019.

[42] L. Brunotte, J. Flies, H. Bolte, P. Reuther, F. Vreede, M. Schwemmle, The nuclear export protein of H5N1 influenza A viruses recruits M1 to the viral ribonucleoprotein to mediate nuclear export., J. Biol. Chem. (2014).

[43] M. Selman, S.K. Dankar, N.E. Forbes, J.-J. Jia, E.G. Brown, Adaptive mutation in influenza A virus non-structural gene is linked to host switching and induces a novel protein by alternative splicing, Emerg. Microbes Infect. 1 (2012) e42.

[44] J. Rehwinkel, C.P. Tan, D. Goubau, O. Schulz, A. Pichlmair, K. Bier, et al., RIG-I detects viral genomic RNA during negative-strand RNA virus infection., Cell. 140 (2010) 397–408.

[45] M. Yoneyama, T. Fujita, RNA recognition and signal transduction by RIG-I-like receptors, Immunol. Rev. 227 (2009) 54–65.

[46] F.T. Vreede, A.Y. Chan, J. Sharps, E. Fodor, Mechanisms and functional implications of the degradation of host RNA polymerase II in influenza virus infected cells., Virology. 396 (2010) 125–34.

[47] F. Vreede, E. Fodor, The role of the influenza virus RNA polymerase in host shut-off, Virulence. 1 (2010) 436–439.

[48] J. Mercer, M. Schelhaas, A. Helenius, Virus entry by endocytosis., Annu. Rev. Biochem. 79 (2010) 803–33.

[49] A.E. Smith, A. Helenius, How viruses enter animal cells., Science. 304 (2004) 237–42.

[50] P.-Y. Lozach, J. Huotari, A. Helenius, Late-penetrating viruses., Curr. Opin. Virol. 1 (2011) 35–43.

[51] M. Lakadamyali, Endocytosis of influenza viruses, Microbes Infect. 6 (2004) 929–936.

[52] K.S. Matlin, H. Reggio, a Helenius, K. Simons, Infectious entry pathway of influenza virus in a canine kidney cell line., J. Cell Biol. 91 (1981) 601–13.

[53] M.J. Rust, M. Lakadamyali, F. Zhang, X. Zhuang, Assembly of endocytic machinery around individual influenza viruses during viral entry., Nat. Struct. Mol. Biol. 11 (2004) 567–73.

[54] E. de Vries, D.M. Tscherne, M.J. Wienholts, V. Cobos-Jiménez, F. Scholte, A. García-Sastre, et al., Dissection of the influenza A virus endocytic routes reveals macropinocytosis as an alternative entry pathway., PLoS Pathog. 7 (2011) e1001329.

[55] J.S. Rossman, G.P. Leser, R.A. Lamb, Filamentous influenza virus enters cells via macropinocytosis., J. Virol. 86 (2012) 10950–60.

[56] V.C. Chu, G.R. Whittaker, Influenza virus entry and infection require host cell N-linked glycoprotein., Proc. Natl. Acad. Sci. U. S. A. 101 (2004) 18153–8.

[57] J. Grove, M. Marsh, The cell biology of receptor-mediated virus entry., J. Cell Biol. 195 (2011) 1071–82.

[58] H.S.Y. Leung, O.T.W. Li, R.W.Y. Chan, M.C.W. Chan, J.M. Nicholls, L.L.M. Poon, Entry of influenza A Virus with a α2,6-linked sialic acid binding preference requires host fibronectin., J. Virol. 86 (2012) 10704–13.

[59] T. Eierhoff, E.R. Hrincius, U. Rescher, S. Ludwig, C. Ehrhardt, The epidermal growth factor receptor (EGFR) promotes uptake of influenza A viruses (IAV) into host cells., PLoS Pathog. 6 (2010).

[60] C. Ehrhardt, R. Seyer, E.R. Hrincius, T. Eierhoff, T. Wolff, S. Ludwig, Interplay between influenza A virus and the innate immune signaling, Microbes Infect. 12 (2010) 81–87.

[61] S.J. Stray, R.D. Cummings, G.M. Air, Influenza virus infection of desialylated cells., Glycobiology. 10 (2000) 649–58.

[62] E. de Vries, R.P. de Vries, M.J. Wienholts, C.E. Floris, M.-S. Jacobs, A. van den Heuvel, et al., Influenza A virus entry into cells lacking sialylated N-glycans., Proc. Natl. Acad. Sci. U. S. A. 109 (2012) 7457–62.

[63] T. Betakova, M2 protein-a proton channel of influenza A virus., Curr. Pharm. Des. 13 (2007) 3231–5.

[64] J. Fontana, G. Cardone, J.B. Heymann, D.C. Winkler, A.C. Steven, Structural changes in Influenza virus at low pH characterized by cryo-electron tomography., J. Virol. 86 (2012) 2919–29.

[65] K. Zhang, Z. Wang, X. Liu, C. Yin, Z. Basit, B. Xia, et al., Dissection of influenza A virus M1 protein: pH-dependent oligomerization of N-terminal domain and dimerization of C-terminal domain., PLoS One. 7 (2012) e37786.

[66] J.M. White, I.A. Wilson, Anti-peptide antibodies detect steps in a protein conformational change: low-pH activation of the influenza virus hemagglutinin., J. Cell Biol. 105 (1987) 2887–96.

[67] S.B. Sieczkarski, G.R. Whittaker, Differential requirements of Rab5 and Rab7 for endocytosis of influenza and other enveloped viruses., Traffic. 4 (2003) 333–43.

[68] S.R. Pfeffer, Rab GTPases: specifying and deciphering organelle identity and function, Trends Cell Biol. 11 (2001) 487–491.

[69] J. Rink, E. Ghigo, Y. Kalaidzidis, M. Zerial, Rab Conversion as a Mechanism of Progression from Early to Late Endosomes, Cell. 122 (2005) 735–749.

[70] M. Lakadamyali, M.J. Rust, H.P. Babcock, X. Zhuang, Visualizing infection of individual influenza viruses., Proc. Natl. Acad. Sci. U. S. A. 100 (2003) 9280–5.

[71] S. Li, C. Sieben, K. Ludwig, C. Höfer, pH-Controlled Two-Step Uncoating of Influenza Virus, Biophys. J. 106 (2014) 1447–1456.

[72] S. Stauffer, Y. Feng, F. Nebioglu, R. Heilig, P. Picotti, A. Helenius, Stepwise priming by acidic pH and high K+ is required for efficient uncoating of influenza A virus cores after penetration., J. Virol. (2014).

[73] G. Whittaker, M. Bui, A. Helenius, Nuclear trafficking of influenza virus ribonuleoproteins in heterokaryons., J. Virol. 70 (1996).

[74] R.E. O'Neill, R. Jaskunas, G. Blobel, P. Palese, M. Junona, Nuclear Import of Influenza Virus RNA Can Be Mediated by Viral Nucleoprotein and Transport Factors Required for Protein Import, J. Biol. Chem. 270 (1995) 22701–22704.

[75] W.W.H. Wu, Y.-H.B. Sun, N. Panté, Nuclear import of influenza A viral ribonucleoprotein complexes is mediated by two nuclear localization sequences on viral nucleoprotein., Virol. J. 4 (2007) 49.

[76] H.P. Babcock, C. Chen, X. Zhuang, Using single-particle tracking to study nuclear trafficking of viral genes., Biophys. J. 87 (2004) 2749–58.

[77] A. Hay, B. Lomniczi, A. Bellamy, J. Skehel, Transcription of the influenza virus genome, Virology. 355 (1977) 337–355.

[78] J.T. Perez, A. Varble, R. Sachidanandam, I. Zlatev, M. Manoharan, A. García-Sastre, et al., Influenza A virus-generated small RNAs regulate the switch from transcription to replication., Proc. Natl. Acad. Sci. U. S. A. 107 (2010) 11525–30.

[79] G.I. Shapiro, T. Gurney, R.M. Krug, Influenza virus gene expression: control mechanisms at early and late times of infection and nuclear-cytoplasmic transport of virus-specific RNAs., J. Virol. 61 (1987) 764–73.

[80] M. Chua, S. Schmid, J. Perez, Influenza A virus utilizes suboptimal splicing to coordinate the timing of infection, Cell Rep. 3 (2013) 23–29.

[81] I. Mohr, Phosphorylation and dephosphorylation events that regulate viral mRNA translation, Virus Res. 119 (2006) 89–99.

[82] W.J. Wurzer, O. Planz, C. Ehrhardt, M. Giner, T. Silberzahn, S. Pleschka, et al., Caspase 3 activation is essential for efficient influenza virus propagation., EMBO J. 22 (2003) 2717–28.

[83] S. V Avilov, D. Moisy, N. Naffakh, S. Cusack, Influenza A virus progeny vRNP trafficking in live infected cells studied with the virus-encoded fluorescently tagged PB2 protein., Vaccine. 30 (2012) 7411–7.

[84] E.A. Bruce, P. Digard, A.D. Stuart, The Rab11 pathway is required for influenza A virus budding and filament formation., J. Virol. 84 (2010) 5848–59.

[85] A.J. Eisfeld, E. Kawakami, T. Watanabe, G. Neumann, Y. Kawaoka, RAB11A is essential for transport of the influenza virus genome to the plasma membrane., J. Virol. 85 (2011) 6117–26.

[86] Y. Chou, N.S. Heaton, Q. Gao, P. Palese, R.H. Singer, R. Singer, et al., Colocalization of different influenza viral RNA segments in the cytoplasm before viral budding as shown by single-molecule sensitivity FISH analysis., PLoS Pathog. 9 (2013) e1003358.

[87] M. Veit, B. Thaa, Association of influenza virus proteins with membrane rafts., Adv. Virol. 2011 (2011) 370606.

[88] J.S. Rossman, R.A. Lamb, Influenza virus assembly and budding., Virology. 411 (2011) 229–36.

[89] B.J. Chen, M. Takeda, R.A. Lamb, Influenza virus hemagglutinin (H3 subtype) requires palmitoylation of its cytoplasmic tail for assembly: M1 proteins of two subtypes differ in their ability to support assembly, J. Virol. 79 (2005) 13673–13684.

[90] P. Gómez-Puertas, C. Albo, E. Pérez-Pastrana, A. Vivo, A. Portela, Influenza virus matrix protein is the major driving force in virus budding., J. Virol. 74 (2000) 11538–47.

[91] R. Ruigrok, F. Baudin, I. Petit, W. Weissenhorn, Role of influenza virus M1 protein in the viral budding process, Int. Congr. Ser. 1219 (2001) 397–404.

[92] M. Hilsch, B. Goldenbogen, C. Sieben, C.T. Höfer, J.P. Rabe, E. Klipp, et al., Influenza A Matrix Protein M1 Multimerizes upon Binding to Lipid Membranes., Biophys. J. 107 (2014) 912–23.

[93] L. Mitnaul, M. Matrosovich, M. Castrucci, A. Tuzikov, N. Bovin, D. Kobasa, et al., Balanced hemagglutinin and neuraminidase activities are critical for efficient replication of influenza A virus, J. Virol. 74 (2000) 6015–6020.

[94] Y. Chou, R. Vafabakhsh, S. Doğanay, Q. Gao, T. Ha, P. Palese, One influenza virus particle packages eight unique viral RNAs as shown by FISH analysis., Proc. Natl. Acad. Sci. U. S. A. 109 (2012) 9101–6.

[95] Y. Liang, Y. Hong, T. Parslow, cis-Acting packaging signals in the influenza virus PB1, PB2, and PA genomic RNA segments, J. Virol. 79 (2005) 10348–10355.

[96] G.A. Marsh, R. Rabadán, A.J. Levine, P. Palese, Highly conserved regions of influenza a virus polymerase gene segments are critical for efficient viral RNA packaging., J. Virol. 82 (2008) 2295–304.

[97] E. Fournier, V. Moules, B. Essere, J.-C. Paillart, J.-D. Sirbat, C. Isel, et al., A supramolecular assembly formed by influenza A virus genomic RNA segments., Nucleic Acids Res. 40 (2012) 2197–209.

[98] C. Gavazzi, C. Isel, E. Fournier, V. Moules, A. Cavalier, D. Thomas, et al., An in vitro network of intermolecular interactions between viral RNA segments of an avian H5N2 influenza A virus: comparison with a human H3N2 virus., Nucleic Acids Res. 41 (2013) 1241–54.

[99] T. Noda, Y. Kawaoka, Packaging of influenza virus genome: robustness of selection., Proc. Natl. Acad. Sci. U. S. A. 109 (2012) 8797–8.

[100] T.H. Söllner, Intracellular and viral membrane fusion: a uniting mechanism., Curr. Opin. Cell Biol. 16 (2004) 429–35.

[101] R. Jahn, T. Lang, T. Südhof, Membrane fusion, Cell. 112 (2003) 519–533.

[102] A. Sapir, O. Avinoam, B. Podbilewicz, L. Chernomordik, Viral and developmental cell fusion mechanisms: conservation and divergence, Dev. Cell. 14 (2008) 11–21.

[103] W. Weissenhorn, A. Hinz, Y. Gaudin, Virus membrane fusion., FEBS Lett. 581 (2007) 2150–5.

[104] L. Hernandez, L. Hoffmann, T. Wolfsberg, J. White, Virus-cell and cell-cell fusion, Annu. Rev. Cell Dev. Biol. (1996) 627–61.

[105] J.M. White, S.E. Delos, M. Brecher, K. Schornberg, Structure and mechanisms of viral membrane fusion proteins: Multiple variations on a common theme, 43 (2008) 189–219.

[106] S.C. Harrison, Viral membrane fusion, Nat Struct Mol Biol. 15 (2008) 690–698.

[107] M. Shmulevitz, R. Duncan, A new class of fusion-associated small transmembrane (FAST) proteins encoded by the non-enveloped fusogenic reoviruses., EMBO J. 19 (2000) 902–12.

[108] C.G. Giraudo, C. Hu, D. You, A.M. Slovic, E. V Mosharov, D. Sulzer, et al., SNAREs can promote complete fusion and hemifusion as alternative outcomes., J. Cell Biol. 170 (2005) 249–60.

[109] L. V Chernomordik, M.M. Kozlov, Membrane hemifusion: crossing a chasm in two leaps., Cell. 123 (2005) 375–82.

[110] C. Reese, F. Heise, A. Mayer, Trans-SNARE pairing can precede a hemifusion intermediate in intracellular membrane fusion., Nature. 436 (2005) 410–4.

[111] G. Melikyan, L. Chernomordik, Membrane rearrangements in fusion mediated by viral proteins, Trends Microbiol. (1997) 349–355.

[112] J. Nikolaus, M. Stöckl, D. Langosch, R. Volkmer, A. Herrmann, Direct visualization of large and protein-free hemifusion diaphragms., Biophys. J. 98 (2010) 1192–9.

[113] Y. Kozlovsky, L. V Chernomordik, M.M. Kozlov, Lipid intermediates in membrane fusion: formation, structure, and decay of hemifusion diaphragm., Biophys. J. 83 (2002) 2634–51.

[114] L. V Chernomordik, M.M. Kozlov, Protein-lipid interplay in fusion and fission of biological membranes., Annu. Rev. Biochem. 72 (2003) 175–207.

[115] V. Knecht, S.-J. Marrink, Molecular dynamics simulations of lipid vesicle fusion in atomic detail., Biophys. J. 92 (2007) 4254–61.

[116] P.I. Kuzmin, J. Zimmerberg, Y.A. Chizmadzhev, F.S. Cohen, A quantitative model for membrane fusion based on low-energy intermediates., Proc. Natl. Acad. Sci. U. S. A. 98 (2001) 7235–40.

[117] D.P. Siegel, Energetics of intermediates in membrane fusion: comparison of stalk and inverted micellar intermediate mechanisms., Biophys. J. 65 (1993) 2124–40.

[118] M. Müller, K. Katsov, M. Schick, A new mechanism of model membrane fusion determined from Monte Carlo simulation., Biophys. J. 85 (2003) 1611–23.

[119] L. V Chernomordik, M.M. Kozlov, Mechanics of membrane fusion., Nat. Struct. Mol. Biol. 15 (2008) 675–83.

[120] A. Chanturiya, L. V Chernomordik, J. Zimmerberg, Flickering fusion pores comparable with initial exocytotic pores occur in protein-free phospholipid bilayers., Proc. Natl. Acad. Sci. U. S. A. 94 (1997) 14423–8.

[121] R.M. Markosyan, F.S. Cohen, G.B. Melikyan, The lipid-anchored ectodomain of influenza virus hemagglutinin (GPI-HA) is capable of inducing nonenlarging fusion pores., Mol. Biol. Cell. 11 (2000) 1143–52.

[122] M. Lindau, E. Neher, Patch-clamp techniques for time-resolved capacitance measurements in single cells., Pflugers Arch. 411 (1988) 137–46.

[123] F.S. Cohen, G.B. Melikyan, Methodologies in the study of cell-cell fusion., Methods. 16 (1998) 215–26.

[124] G.W. Kemble, T. Danieli, J.M. White, Lipid-anchored influenza hemagglutinin promotes hemifusion, not complete fusion., Cell. 76 (1994) 383–91.

[125] G.B. Melikyan, S.A. Brener, D.C. Ok, F.S. Cohen, Inner but not outer membrane leaflets control the transition from glycosylphosphatidylinositol-anchored influenza hemagglutinin-induced hemifusion to full fusion., J. Cell Biol. 136 (1997) 995–1005.

[126] G.B. Melikyan, J.M. White, F.S. Cohen, GPI-anchored influenza hemagglutinin induces hemifusion to both red blood cell and planar bilayer membranes., J. Cell Biol. 131 (1995) 679–91.

[127] L. V Chernomordik, V.A. Frolov, E. Leikina, P. Bronk, J. Zimmerberg, The pathway of membrane fusion catalyzed by influenza hemagglutinin: restriction of lipids, hemifusion, and lipidic fusion pore formation., J. Cell Biol. 140 (1998) 1369–82.

[128] L. V Chernomordik, G.B. Melikyan, Y.A. Chizmadzhev, Biomembrane fusion: a new concept derived from model studies using two interacting planar lipid bilayers., Biochim. Biophys. Acta. 906 (1987) 309–52.

[129] L. V Chernomordik, E. Leikina, V. Frolov, P. Bronk, J. Zimmerberg, An early stage of membrane fusion mediated by the low pH conformation of influenza hemagglutinin depends upon membrane lipids., J. Cell Biol. 136 (1997) 81–93.

[130] G.B. Melikyan, R.M. Markosyan, H. Hemmati, M.K. Delmedico, D.M. Lambert, F.S. Cohen, Evidence that the transition of HIV-1 gp41 into a six-helix bundle, not the bundle configuration, induces membrane fusion., J. Cell Biol. 151 (2000) 413–23.

[131] Y. Gaudin, Rabies virus-induced membrane fusion pathway., J. Cell Biol. 150 (2000) 601–12.

[132] E. Grote, M. Baba, Y. Ohsumi, P.J. Novick, Geranylgeranylated SNAREs are dominant inhibitors of membrane fusion., J. Cell Biol. 151 (2000) 453–66.

[133] C. Amatore, S. Arbault, Y. Bouret, M. Guille, F. Lemaître, Y. Verchier, Regulation of exocytosis in chromaffin cells by trans-insertion of lysophosphatidylcholine and arachidonic acid into the outer leaflet of the cell membrane., Chembiochem. 7 (2006) 1998–2003.

[134] R.P. Rand, V.A. Parsegian, Physical force considerations in model and biological membranes, Can. J. Biochem. Cell Biol. 62 (1984) 752–759.

[135] Y. Kozlovsky, A. Efrat, D.P. Siegel, D.A. Siegel, M.M. Kozlov, Stalk phase formation: effects of dehydration and saddle splay modulus., Biophys. J. 87 (2004) 2508–21.

[136] Y. Kozlovsky, M.M. Kozlov, Stalk model of membrane fusion: solution of energy crisis., Biophys. J. 82 (2002) 882–95.

[137] L. Yang, H.W. Huang, Observation of a membrane fusion intermediate structure., Science. 297 (2002) 1877–9.

[138] V.S. Malinin, P. Frederik, B.R. Lentz, Osmotic and curvature stress affect PEG-induced fusion of lipid vesicles but not mixing of their lipids., Biophys. J. 82 (2002) 2090–100.

[139] F.S. Cohen, J. Zimmerberg, A. Finkelstein, Fusion of phospholipid vesicles with planar phospholipid bilayer membranes. II. Incorporation of a vesicular membrane marker into the planar membrane., J. Gen. Physiol. 75 (1980) 251–70.

[140] S. Ohki, Surface Tension, Hydration Energy and Membrane Fusion, in: S. Ohki, D. Doyle, T. Flanagan, S. Hui, E. Mayhew (Eds.), Mol. Mech. Membr. Fusion SE - 10, Springer US, 1988: pp. 123–138.

[141] V.S. Malinin, B.R. Lentz, Energetics of vesicle fusion intermediates: comparison of calculations with observed effects of osmotic and curvature stresses., Biophys. J. 86 (2004) 2951–64.

[142] A. Chanturiya, P. Scaria, M. Woodle, The role of membrane lateral tension in calcium-induced membrane fusion, J. Membr. Biol. 75 (2000) 67–75.

[143] J.Y. Lee, M. Schick, Calculation of free energy barriers to the fusion of small vesicles., Biophys. J. 94 (2008) 1699–706.

[144] L. Gao, R. Lipowsky, J. Shillcock, Tension-induced vesicle fusion: pathways and pore dynamics, Soft Matter. 4 (2008) 1208.

[145] K. Katsov, M. Müller, M. Schick, Field theoretic study of bilayer membrane fusion. I. Hemifusion mechanism., Biophys. J. 87 (2004) 3277–90.

[146] J.C. Shillcock, R. Lipowsky, Tension-induced fusion of bilayer membranes and vesicles., Nat. Mater. 4 (2005) 225–8.

[147] J. Lee, B.R. Lentz, Secretory and viral fusion may share mechanistic events with fusion between curved lipid bilayers., Proc. Natl. Acad. Sci. U. S. A. 95 (1998) 9274–9.

[148] M.J. Clague, C. Schoch, L. Zech, R. Blumenthal, Gating kinetics of pH-activated membrane fusion of vesicular stomatitis virus with cells: stopped-flow measurements by dequenching of octadecylrhodamine fluorescence., Biochemistry. 29 (1990) 1303–8.

[149] F.S. Cohen, G.B. Melikyan, The Energetics of Membrane Fusion from Binding, through Hemifusion, Pore Formation, and Pore Enlargement, J. Membr. Biol. 199 (2004) 1–14.

[150] X. Yang, S. Kurteva, X. Ren, S. Lee, J. Sodroski, Stoichiometry of envelope glycoprotein trimers in the entry of human immunodeficiency virus type 1, J. Virol. 79 (2005) 12132–47.

[151] E. Zaitseva, A. Mittal, D.E. Griffin, L. V Chernomordik, Class II fusion protein of alphaviruses drives fusion through the same pathway as class I proteins, J. Cell Biol. 169 (2005) 167–77.

[152] S. Roche, A.A. V Albertini, J. Lepault, S. Bressanelli, Y. Gaudin, Structures of vesicular stomatitis virus glycoprotein: membrane fusion revisited., Cell. Mol. Life Sci. 65 (2008) 1716–28.

[153] R.M. Markosyan, M.Y. Leung, F.S. Cohen, The six-helix bundle of human immunodeficiency virus Env controls pore formation and enlargement and is initiated at residues proximal to the hairpin turn., J. Virol. 83 (2009) 10048–57.

[154] M.M. Kozlov, L. V Chernomordik, A mechanism of protein-mediated fusion: coupling between refolding of the influenza hemagglutinin and lipid rearrangements., Biophys. J. 75 (1998) 1384–96.

[155] J. Pérez-Vargas, T. Krey, C. Valansi, O. Avinoam, A. Haouz, M. Jamin, et al., Structural basis of eukaryotic cell-cell fusion., Cell. 157 (2014) 407–19.

[156] C. Chanel-Vos, M. Kielian, A conserved histidine in the ij loop of the Semliki Forest virus E1 protein plays an important role in membrane fusion, J. Virol. 78 (2004) 13543–13552.

[157] M.R. Kalani, A. Moradi, M. Moradi, E. Tajkhorshid, Characterizing a Histidine Switch Controlling pH-Dependent Conformational Changes of the Influenza Virus Hemagglutinin, Biophys. J. 105 (2013) 993–1003.

[158] R. Fritz, K. Stiasny, F.X. Heinz, Identification of specific histidines as pH sensors in flavivirus membrane fusion., J. Cell Biol. 183 (2008) 353–61.

[159] Z.-L. Qin, Y. Zheng, M. Kielian, Role of conserved histidine residues in the low-pH dependence of the Semliki Forest virus fusion protein., J. Virol. 83 (2009) 4670–7.

[160] S.M. de Boer, J. Kortekaas, L. Spel, P.J.M. Rottier, R.J.M. Moormann, B.J. Bosch, Acid-activated structural reorganization of the Rift Valley fever virus Gc fusion protein., J. Virol. 86 (2012) 13642–52.

[161] V. Nayak, M. Dessau, K. Kucera, K. Anthony, M. Ledizet, Y. Modis, Crystal structure of dengue virus type 1 envelope protein in the postfusion conformation and its implications for membrane fusion., J. Virol. 83 (2009) 4338–44.

[162] S. Thoennes, Z.-N. Li, B.-J. Lee, W.A. Langley, J.J. Skehel, R.J. Russell, et al., Analysis of residues near the fusion peptide in the influenza hemagglutinin structure for roles in triggering membrane fusion., Virology. 370 (2008) 403–14.

[163] T. Kampmann, D.S. Mueller, A.E. Mark, P.R. Young, B. Kobe, The Role of histidine residues in low-pH-mediated viral membrane fusion., Structure. 14 (2006) 1481–7.

[164] M. Brecher, K.L. Schornberg, S.E. Delos, M.L. Fusco, E.O. Saphire, J.M. White, Cathepsin cleavage potentiates the Ebola virus glycoprotein to undergo a subsequent fusion-relevant conformational change., J. Virol. 86 (2012) 364–72.

[165] G. Simmons, P. Zmora, S. Gierer, A. Heurich, S. Pöhlmann, Proteolytic activation of the SARS-coronavirus spike protein: Cutting enzymes at the cutting edge of antiviral research, Antiviral Res. 100 (2013) 605–614.

[166] M. Côté, J. Misasi, T. Ren, A. Bruchez, K. Lee, M. Claire, et al., Small molecule inhibitors reveal Niemann-Pick C1 is essential for Ebola virus infection, Nature. 477 (2011) 344–348.

[167] R.K. Plemper, G.B. Melikyan, Membrane fusion, Elsevier. 2 (2004) 36–43.

[168] E. Baquero, A.A. Albertini, P. Vachette, J. Lepault, S. Bressanelli, Y. Gaudin, Intermediate conformations during viral fusion glycoprotein structural transition., Curr. Opin. Virol. 3 (2013) 143–50.

[169] R. Rand, V. Parsegian, Hydration forces between phospholipid bilayers, Biochim. Biophys. Acta. 988 (1989).

[170] S. Roche, S. Bressanelli, F.A. Rey, Y. Gaudin, Crystal structure of the low-pH form of the vesicular stomatitis virus glycoprotein G., Science. 313 (2006) 187–91.

[171] S. Martens, M.M. Kozlov, H.T. McMahon, How synaptotagmin promotes membrane fusion., Science. 316 (2007) 1205–8.

[172] D.L. Gibbons, M.-C. Vaney, A. Roussel, A. Vigouroux, B. Reilly, J. Lepault, et al., Conformational change and protein-protein interactions of the fusion protein of Semliki Forest virus., Nature. 427 (2004) 320–5.

[173] T. Korte, R.F. Epand, R.M. Epand, R. Blumenthal, Role of the Glu residues of the influenza hemagglutinin fusion peptide in the pH dependence of fusion activity., Virology. 289 (2001) 353–61.

[174] X. Han, J.H. Bushweller, D.S. Cafiso, L.K. Tamm, Membrane structure and fusion-triggering conformational change of the fusion domain from influenza hemagglutinin., Nat. Struct. Biol. 8 (2001) 715–20.

[175] Y. Li, X. Han, A. Lai, J. Bushweller, Membrane structures of the hemifusion-inducing fusion peptide mutant G1S and the fusion-blocking mutant G1V of influenza virus hemagglutinin suggest a mechanism for pore opening in membrane fusion, J. Virol. 79 (2005) 12065–12076.

[176] J.A. McNew, T. Weber, F. Parlati, R.J. Johnston, T.J. Melia, T.H. Söllner, et al., Close is not enough: SNARE-dependent membrane fusion requires an active mechanism that transduces force to membrane anchors., J. Cell Biol. 150 (2000) 105–17.

[177] D. Langosch, J.M. Crane, B. Brosig, A. Hellwig, L.K. Tamm, J. Reed, Peptide mimics of SNARE transmembrane segments drive membrane fusion depending on their conformational plasticity., J. Mol. Biol. 311 (2001) 709–21.

[178] D. Cleverley, J. Lenard, The transmembrane domain in viral fusion: Essential role for a conserved glycine residue in vesicular stomatitis virus G protein, Proc. Natl. Acad. Sci. U. S. A. 95 (1998) 3425–3430.

[179] R.T. Armstrong, A.S. Kushnir, J.M. White, The transmembrane domain of influenza hemagglutinin exhibits a stringent length requirement to support the hemifusion to fusion transition., J. Cell Biol. 151 (2000) 425–37.

[180] G.B. Melikyan, S. Lin, M.G. Roth, F.S. Cohen, Amino acid sequence requirements of the transmembrane and cytoplasmic domains of influenza virus hemagglutinin for viable membrane fusion., Mol. Biol. Cell. 10 (1999) 1821–36.

[181] L. Yue, L. Shang, E. Hunter, Truncation of the membrane-spanning domain of human immunodeficiency virus type 1 envelope glycoprotein defines elements required for fusion, incorporation, and infectivity., J. Virol. 83 (2009) 11588–98.

[182] L. Shang, L. Yue, E. Hunter, Role of the membrane-spanning domain of human immunodeficiency virus type 1 envelope glycoprotein in cell-cell fusion and virus infection., J. Virol. 82 (2008) 5417–28.

[183] G.W. Kemble, D.L. Bodian, J. Rosé, I.A. Wilson, J.M. White, Intermonomer disulfide bonds impair the fusion activity of influenza virus hemagglutinin., J. Virol. 66 (1992) 4940–50.

[184] D. Odell, E. Wanas, J. Yan, H.P. Ghosh, Influence of membrane anchoring and cytoplasmic domains on the fusogenic activity of vesicular stomatitis virus glycoprotein G., J. Virol. 71 (1997) 7996–8000.

[185] K. Salzwedel, P.B. Johnston, S.J. Roberts, J.W. Dubay, E. Hunter, Expression and characterization of glycophospholipid-anchored human immunodeficiency virus type 1 envelope glycoproteins., J. Virol. 67 (1993) 5279–88.

[186] C.D. Weiss, J.M. White, Characterization of Stable Chinese Hamster Ovary Cells Expressing Anchored Human Immunodeficiency Virus Type 1 Envelope Glycoprotein, J. Virol. 67 (1993) 7060–7066.

[187] D. Langosch, M. Hofmann, C. Ungermann, The role of transmembrane domains in membrane fusion, Cell. Mol. Life Sci. 64 (2007) 850–864.

[188] T. Danieli, S.L. Pelletier, Y.I. Henis, J.M. White, Membrane fusion mediated by the influenza virus hemagglutinin requires the concerted action of at least three hemagglutinin trimers., J. Cell Biol. 133 (1996) 559–69.

[189] J. Bentz, Minimal aggregate size and minimal fusion unit for the first fusion pore of influenza hemagglutinin-mediated membrane fusion., Biophys. J. 78 (2000) 227–45.

[190] R. Blumenthal, D.P. Sarkar, S. Durell, D.E. Howard, S.J. Morris, Dilation of the influenza hemagglutinin fusion pore revealed by the kinetics of individual cell-cell fusion events., J. Cell Biol. 135 (1996) 63–71.

[191] L.J. Earp, S.E. Delos, H.E. Park, J.M. White, The Many Mechanisms of Viral Membrane Fusion Proteins, in: M. Marsh (Ed.), Membr. Traffick. Viral Replication, Springer Berlin Heidelberg, 2005: pp. 25–66.

[192] B. Welch, Y. Liu, C. Kors, G. Leser, T. Jardetzky, R. Lamb, Structure of the cleavage-activated prefusion form of the parainfluenza virus 5 fusion protein, Proc. Natl. Acad. Sci. 109 (2012) 1–6.

[193] C. Carr, C. Chaudhry, P. Kim, Influenza hemagglutinin is spring-loaded by a metastable native conformation, Proc. Natl. Acad. Sci. U. S. A. 94 (1997) 14306–14313.

[194] M. Lobigs, Flavivirus premembrane protein cleavage and spike heterodimer secretion require the function of the viral proteinase NS3., Proc. Natl. Acad. Sci. U. S. A. 90 (1993) 6218–22.

[195] J. Chen, S.A. Wharton, W. Weissenhorn, L.J. Calder, F.M. Hughson, J.J. Skehel, et al., A soluble domain of the membrane-anchoring chain of influenza virus hemagglutinin (HA2) folds in Escherichia coli into the low-pH-induced conformation., Proc. Natl. Acad. Sci. U. S. A. 92 (1995) 12205–9.

[196] H.-S. Yin, R.G. Paterson, X. Wen, R. a Lamb, T.S. Jardetzky, Structure of the uncleaved ectodomain of the paramyxovirus (hPIV3) fusion protein, Proc. Natl. Acad. Sci. U. S. A. 102 (2005) 9288–93.

[197] L. Chen, J.J. Gorman, J. McKimm-Breschkin, L.J. Lawrence, P. a Tulloch, B.J. Smith, et al., The structure of the fusion glycoprotein of Newcastle disease virus suggests a novel paradigm for the molecular mechanism of membrane fusion., Structure. 9 (2001) 255–66.

[198] P. Bullough, F. Hughson, J. Skehel, D. Wiley, Structure of influenza haemagglutinin at the pH of membrane fusion, Nature. 371 (1994) 37–43.

[199] I. Wilson, J. Skehel, Structure of the haemagglutinin membrane glycoprotein of influenza virus at 3 A resolution, Nature. 289 (1981) 366–373.

[200] H.-S. Yin, X. Wen, R.G. Paterson, R. a Lamb, T.S. Jardetzky, Structure of the parainfluenza virus 5 F protein in its metastable, prefusion conformation., Nature. 439 (2006) 38–44.

[201] R.A. Lamb, T.S. Jardetzky, Structural basis of viral invasion: lessons from paramyxovirus F., Curr. Opin. Struct. Biol. 17 (2007) 427–36.

[202] Y. Modis, Relating structure to evolution in class II viral membrane fusion proteins., Curr. Opin. Virol. 5C (2014) 34–41.

[203] S.K. Jain, S. DeCandido, M. Kielian, Processing of the p62 envelope precursor protein of Semliki Forest virus., J. Biol. Chem. 266 (1991) 5756–61.

[204] M. Kielian, F.A. Rey, Virus membrane-fusion proteins: More than one way to make a hairpin, Nat Rev Micro. 4 (2006) 67–76.

[205] K. Stiasny, S. Bressanelli, J. Lepault, Characterization of a membrane-associated trimeric low-pH-induced form of the class II viral fusion protein E from tick-borne encephalitis virus and its crystallization, J. Virol. 78 (2004) 3178–3183.

[206] R.M. DuBois, M.-C. Vaney, M.A. Tortorici, R. Al Kurdi, G. Barba-Spaeth, T. Krey, et al., Functional and evolutionary insight from the crystal structure of rubella virus protein E1., Nature. 493 (2013) 552–6.

[207] M. Dessau, Y. Modis, Crystal structure of glycoprotein C from Rift Valley fever virus, Proc. Natl. Acad. Sci. 110 (2013) 1696–1701.

[208] Y. Li, Y. Modis, A novel membrane fusion protein family in Flaviviridae?, Trends Microbiol. (2014) 1–7.

[209] E.E. Heldwein, H. Lou, F.C. Bender, G.H. Cohen, R.J. Eisenberg, S.C. Harrison, Crystal structure of glycoprotein B from herpes simplex virus 1., Science. 313 (2006) 217–20.

[210] S. Roche, F.A. Rey, Y. Gaudin, S. Bressanelli, Structure of the prefusion form of the vesicular stomatitis virus glycoprotein G., Science. 315 (2007) 843–8.

[211] Y. Gaudin, C. Tuffereau, P. Durrer, Biological function of the low-pH, fusion-inactive conformation of rabies virus glycoprotein (G): G is transported in a fusion-inactive state-like conformation., J. Virol. 69 (1995) 5528–34.

[212] Y. Gaudin, Reversibility in Fusion Protein Conformational Changes The Intriguing Case of Rhabdovirus-Induced Membrane Fusion, in: H. Hilderson, S. Fuller (Eds.), Fusion Biol. Membr. Relat. Probl., Springer US, 2002: pp. 379–408.

[213] F.A. Rey, F.X. Heinz, C. Mandl, C. Kunz, S.C. Harrison, The envelope glycoprotein from tick-borne encephalitis virus at 2 Å resolution, Nature. 375 (1995) 291–8.

[214] M.M. Kozlov, L. V Chernomordik, The protein coat in membrane fusion: lessons from fission., Traffic. 3 (2002) 256–67.

[215] E. Leikina, A. Mittal, M.-S. Cho, K. Melikov, M.M. Kozlov, L. V Chernomordik, Influenza hemagglutinins outside of the contact zone are necessary for fusion pore expansion., J. Biol. Chem. 279 (2004) 26526–32.

[216] S. Roche, Y. Gaudin, Characterization of the Equilibrium between the Native and Fusion-Inactive Conformation of Rabies Virus Glycoprotein Indicates That the Fusion Complex Is Made of Several Trimers, Virology. 297 (2002) 128–135.

[217] D.L. Floyd, J.R. Ragains, J.J. Skehel, S.C. Harrison, A.M. van Oijen, Single-particle kinetics of influenza virus membrane fusion., Proc. Natl. Acad. Sci. U. S. A. 105 (2008) 15382–7.

[218] M.P. Dobay, A. Dobay, J. Bantang, E. Mendoza, How many trimers? Modeling influenza virus fusion yields a minimum aggregate size of six trimers, three of which are fusogenic., Mol. Biosyst. 7 (2011) 2741–9.

[219] T. Ivanovic, J.L. Choi, S.P. Whelan, A.M. van Oijen, S.C. Harrison, Influenza-virus membrane fusion by cooperative fold-back of stochastically induced hemagglutinin intermediates., Elife. 2 (2013) e00333.

[220] D. Wiley, I. Wilson, J. Skehel, Structural identification of the antibody-binding sites of Hong Kong influenza haemagglutinin and their involvement in antigenic variation., Nature. (1981).

[221] D.C. Wiley, J.J. Skehel, The structure and function of the hemagglutinin membrane glycoprotein of influenza virus, Annu. Rev. Biochem. 56 (1987) 365–394.

[222] R.W. Ruigrok, A. Aitken, L.J. Calder, S.R. Martin, J.J. Skehel, S.A. Wharton, et al., Studies on the structure of the influenza virus haemagglutinin at the pH of membrane fusion., J. Gen. Virol. 69 (Pt 11 (1988) 2785–95.

[223] C.S. Copeland, R.W. Doms, E.M. Bolzau, R.G. Webster, A. Helenius, Assembly of influenza hemagglutinin trimers and its role in intracellular transport., J. Cell Biol. 103 (1986) 1179–91.

[224] C.S. Copeland, K.P. Zimmer, K.R. Wagner, G.A. Healey, I. Mellman, A. Helenius, Folding, trimerization, and transport are sequential events in the biogenesis of influenza virus hemagglutinin., Cell. 53 (1988) 197–209.

[225] M. Veit, E. Kretzschmar, K. Kuroda, W. Garten, M.F. Schmidt, H.D. Klenk, et al., Site-specific mutagenesis identifies three cysteine residues in the cytoplasmic tail as acylation sites of influenza virus hemagglutinin., J. Virol. 65 (1991) 2491–500.

[226] S. Mir-Shekari, D. Ashford, The Glycosylation of the Influenza A Virus Hemagglutinin by Mammalian Cells-A site specific study, J. Biol. …. 272 (1997) 4027–4036.

[227] W. Keil, R. Geyer, J. Dabrowski, U. Dabrowski, H. Niemann, S. Stirm, et al., Carbohydrates of influenza virus. Structural elucidation of the individual glycans of the FPV hemagglutinin by two-dimensional 1H n.m.r. and methylation analysis., EMBO J. 4 (1985) 2711–20.

[228] M.S. Segal, J.M. Bye, J.F. Sambrook, M.J. Gething, Disulfide bond formation during the folding of influenza virus hemagglutinin., J. Cell Biol. 118 (1992) 227–44.

[229] H. Klenk, R. Rott, M. Orlich, J. Blödorn, Activation of influenza A viruses by trypsin treatment, Virology. 439 (1975) 426–439.

[230] H.D. Klenk, R. Rott, M. Orlich, Further studies on the activation of influenza virus by proteolytic cleavage of the haemagglutinin., J. Gen. Virol. 36 (1977) 151–61.

[231] F.X. Bosch, M. Orlich, H.D. Klenk, R. Rott, The structure of the hemagglutinin, a determinant for the pathogenicity of influenza viruses., Virology. 95 (1979) 197–207.

[232] J. Chen, K.H. Lee, D.A. Steinhauer, D.J. Stevens, J.J. Skehel, D.C. Wiley, Structure of the hemagglutinin precursor cleavage site, a determinant of influenza pathogenicity and the origin of the labile conformation., Cell. 95 (1998) 409–17.

[233] C.M. Carr, P.S. Kim, A spring-loaded mechanism for the conformational change of influenza hemagglutinin., Cell. 73 (1993) 823–32.

[234] C. Böttcher, K. Ludwig, A. Herrmann, M. Van Heel, H. Stark, Structure of influenza haemagglutinin at neutral and at fusogenic pH by electron cryo-microscopy, FEBS Lett. 463 (1999) 255–259.

[235] Q. Huang, R. Opitz, E.-W. Knapp, A. Herrmann, Protonation and stability of the globular domain of influenza virus hemagglutinin., Biophys. J. 82 (2002) 1050–8.

[236] Q. Huang, Early steps of the conformational change of influenza virus hemagglutinin to a fusion active state Stability and energetics of the hemagglutinin, Biochim. Biophys. Acta - Biomembr. 1614 (2003) 3–13.

[237] J.A. Gruenke, R.T. Armstrong, W.W. Newcomb, J.C. Brown, J.M. White, New Insights into the Spring-Loaded Conformational Change of Influenza Virus Hemagglutinin †, 76 (2002) 4456–4466.

[238] W. Weis, J.H. Brown, S. Cusack, J.C. Paulson, J.J. Skehel, D.C. Wiley, Structure of the influenza virus haemagglutinin complexed with its receptor, sialic acid, Nature. 333 (1988) 426–431.

[239] M.B. Eisen, S. Sabesan, J.J. Skehel, D.C. Wiley, Binding of the influenza A virus to cell-surface receptors: structures of five hemagglutinin-sialyloligosaccharide complexes determined by X-ray crystallography., Virology. 232 (1997) 19–31.

[240] Y. Wu, Y. Wu, B. Tefsen, Y. Shi, G.F. Gao, Bat-derived influenza-like viruses H17N10 and H18N11., Trends Microbiol. (2014) 1–9.

[241] G.N. Rogers, T.J. Pritchett, J.L. Lane, J.C. Paulson, Differential sensitivity of human, avian, and equine influenza A viruses to a glycoprotein inhibitor of infection: selection of receptor specific variants., Virology. 131 (1983) 394–408.

[242] S. Wilks, M. de Graaf, D.J. Smith, D.F. Burke, A review of influenza haemagglutinin receptor binding as it relates to pandemic properties., Vaccine. 30 (2012) 4369–76.

[243] M. de Graaf, R.A.M. Fouchier, Role of receptor binding specificity in influenza A virus transmission and pathogenesis., EMBO J. (2014) 1–19.

[244] M. Imai, Y. Kawaoka, The role of receptor binding specificity in interspecies transmission of influenza viruses., Curr. Opin. Virol. 2 (2012) 160–7.

[245] C.M. Mair, K. Ludwig, A. Herrmann, C. Sieben, Receptor binding and pH stability - How influenza A virus hemagglutinin affects host-specific virus infection., Biochim. Biophys. Acta. 1838 (2013) 1153–1168.

[246] A. García-Sastre, Influenza virus receptor specificity - Disease and transmission., Am. J. Pathol. 176 (2010) 1584–5.

[247] J.M. Nicholls, M.C.W. Chan, W.Y. Chan, H.K. Wong, C.Y. Cheung, D.L.W. Kwong, et al., Tropism of avian influenza A (H5N1) in the upper and lower respiratory tract., Nat. Med. 13 (2007) 147–9.

[248] K. Shinya, M. Ebina, S. Yamada, M. Ono, N. Kasai, Y. Kawaoka, Avian flu: Influenza virus receptors in the human airway., Nature. 440 (2006) 435–6.

[249] D. van Riel, V. Munster, E. De Wit, H5N1 virus attachment to lower respiratory tract, Science (80-.). (2006) 5.

[250] J.M. Nicholls, A.J. Bourne, H. Chen, Y. Guan, J.S.M. Peiris, Sialic acid receptor detection in the human respiratory tract: evidence for widespread distribution of potential binding sites for human and avian influenza viruses., Respir. Res. 8 (2007) 73.

[251] A. Vines, K. Wells, M. Matrosovich, M.R. Castrucci, T. Ito, Y. Kawaoka, The role of influenza A virus hemagglutinin residues 226 and 228 in receptor specificity and host range restriction., J. Virol. 72 (1998) 7626–31.

[252] G.N. Rogers, R.S. Daniels, J.J. Skehelt, D.C. Wileyl, X. Wangs, H.H. Higas, et al., Host-mediated Selection of Influenza Virus Receptor Variants, (1985) 7362–7367.

[253] M. Matrosovich, A. Tuzikow, Early alterations of the receptor-binding properties of H1, H2, and H3 avian influenza virus hemagglutinins after their introduction into mammals, J. Virol. 74 (2000) 8502–8512.

[254] S.J. Gamblin, L.F. Haire, R.J. Russell, D.J. Stevens, B. Xiao, Y. Ha, et al., The Structure and Receptor Binding Properties of the 1918 Influenza Hemagglutinin, Sci. . 303 (2004) 1838–1842.

[255] L. Glaser, J. Stevens, D. Zamarin, A. Ian, A. García-sastre, T.M. Tumpey, et al., A single amino acid substitution in 1918 influenza virus hemagglutinin changes receptor binding specificity, J. Virol. 79 (2005) 11533–11536.

[256] T.M. Tumpey, T.R. Maines, N. Van Hoeven, L. Glaser, A. Solórzano, C. Pappas, et al., A two-amino acid change in the hemagglutinin of the 1918 influenza virus abolishes transmission., Science. 315 (2007) 655–9.

[257] C. Pappas, K. Viswanathan, A. Chandrasekaran, R. Raman, J.M. Katz, R. Sasisekharan, et al., Receptor specificity and transmission of H2N2 subtype viruses isolated from the pandemic of 1957., PLoS One. 5 (2010) e11158.

[258] K. Tharakaraman, A. Jayaraman, R. Raman, K. Viswanathan, N.W. Stebbins, D. Johnson, et al., Glycan Receptor Binding of the Influenza A Virus H7N9 Hemagglutinin, Cell. 153 (2013) 1486–1493.

[259] T.R. Maines, L.-M. Chen, N. Van Hoeven, T.M. Tumpey, O. Blixt, J.A. Belser, et al., Effect of receptor binding domain mutations on receptor binding and transmissibility of avian influenza H5N1 viruses., Virology. 413 (2011) 139–47.

[260] S. Herfst, E.J.A. Schrauwen, M. Linster, S. Chutinimitkul, E. de Wit, V.J. Munster, et al., Airborne transmission of influenza A/H5N1 virus between ferrets., Science. 336 (2012) 1534–41.

[261] M. Imai, T. Watanabe, M. Hatta, S.C. Das, M. Ozawa, K. Shinya, et al., Experimental adaptation of an influenza H5 HA confers respiratory droplet transmission to a reassortant H5 HA/H1N1 virus in ferrets., Nature. 486 (2012) 420–8.

[262] X. Xiong, P.J. Coombs, S.R. Martin, J. Liu, H. Xiao, J.W. McCauley, et al., Receptor binding by a ferret-transmissible H5 avian influenza virus, Nature. (2013) 1–6.

[263] R. Rott, The pathogenic determinant of influenza virus., Vet. Microbiol. 33 (1992) 303–10.

[264] H.-D. Klenk, W. Garten, Host cell proteases controlling virus pathogenicity, Trends Microbiol. 2 (1994) 39–43.

[265] D.A. Steinhauer, Role of Hemagglutinin Cleavage for the Pathogenicity of Influenza Virus, Virology. 20 (1999) 1–20.

[266] B.S. Hamilton, G.R. Whittaker, S. Daniel, Influenza virus-mediated membrane fusion: determinants of hemagglutinin fusogenic activity and experimental approaches for assessing virus fusion., Viruses. 4 (2012) 1144–68.

[267] W. Garten, H. Klenk, Cleavage activation of the influenza virus hemagglutinin and its role in pathogenesis, in: Avian Influ., 2008: pp. 156–167.

[268] W. Garten, F. Bosch, D. Linder, R. Rott, H. Klenk, Proteolytic activation of the influenza virus hemagglutinin: The structure of the cleavage site and the enzymes involved in cleavage, Virology. 115 (1981) 361–374.

[269] Y. Kawaoka, R.G. Webster, Sequence requirements for cleavage activation of influenza virus hemagglutinin expressed in mammalian cells., Proc. Natl. Acad. Sci. U. S. A. 85 (1988) 324–8.

[270] A. Stieneke-Gröber, M. Vey, H. Angliker, E. Shaw, G. Thomas, C. Roberts, et al., Influenza virus hemagglutinin with multibasic cleavage site is activated by furin, a subtilisin-like endoprotease., EMBO J. 11 (1992) 2407–14.

[271] T. Horimoto, K. Nakayama, S.P. Smeekens, Y. Kawaoka, Proprotein-processing endoproteases PC6 and furin both activate hemagglutinin of virulent avian influenza viruses., J. Virol. 68 (1994) 6074–8.

[272] X. Sun, L. V Tse, A.D. Ferguson, G.R. Whittaker, Modifications to the hemagglutinin cleavage site control the virulence of a neurotropic H1N1 influenza virus., J. Virol. 84 (2010) 8683–90.

[273] S.E. Galloway, M.L. Reed, C.J. Russell, D.A. Steinhauer, Influenza HA Subtypes Demonstrate Divergent Phenotypes for Cleavage Activation and pH of Fusion: Implications for Host Range and Adaptation, PLoS Pathog. 9 (2013) e1003151.

[274] J.A. McCullers, Insights into the interaction between influenza virus and pneumococcus., Clin. Microbiol. Rev. 19 (2006) 571–82.

[275] M. Tashiro, P. Ciborowski, M. Reinacher, Synergistic role of staphylococcal proteases in the induction of influenza virus pathogenicity, Virology. 157 (1987) 421–430.

[276] H. Kido, Y. Okumura, E. Takahashi, H.-Y. Pan, S. Wang, D. Yao, et al., Role of host cellular proteases in the pathogenesis of influenza and influenza-induced multiple organ failure., Biochim. Biophys. Acta. 1824 (2012) 186–94.

[277] E. Böttcher, T. Matrosovich, M. Beyerle, H.-D. Klenk, W. Garten, M. Matrosovich, Proteolytic activation of influenza viruses by serine proteases TMPRSS2 and HAT from human airway epithelium., J. Virol. 80 (2006) 9896–8.

[278] E. Böttcher-Friebertshäuser, C. Freuer, F. Sielaff, S. Schmidt, M. Eickmann, J. Uhlendorff, et al., Cleavage of influenza virus hemagglutinin by airway proteases TMPRSS2 and HAT differs in subcellular localization and susceptibility to protease inhibitors., J. Virol. 84 (2010) 5605–14.

[279] Y. Okumura, E. Takahashi, M. Yano, M. Ohuchi, T. Daidoji, T. Nakaya, et al., Novel type II transmembrane serine proteases, MSPL and TMPRSS13, Proteolytically activate membrane fusion activity of the hemagglutinin of highly pathogenic avian influenza viruses and induce their multicycle replication., J. Virol. 84 (2010) 5089–96.

[280] T. Korte, K. Ludwig, F.P. Booy, R. Blumenthal, A. Herrmann, Conformational intermediates and fusion activity of influenza virus hemagglutinin., J. Virol. 73 (1999) 4567–74.

[281] T. Korte, K. Ludwig, Q. Huang, P.S. Rachakonda, A. Herrmann, Conformational change of influenza virus hemagglutinin is sensitive to ionic concentration., Eur. Biophys. J. 36 (2007) 327–35.

[282] A. Puri, F.P. Booy, R.W. Doms, J.M. White, R. Blumenthal, Conformational changes and fusion activity of influenza virus hemagglutinin of the H2 and H3 subtypes: Effects of acid pretreatment., J. Virol. 64 (1990) 3824–32.

[283] J.D. Brown, D.E. Swayne, R.J. Cooper, R.E. Burns, D.E. Stallknecht, Persistence of H5 and H7 avian influenza viruses in water., Avian Dis. 51 (2007) 285–9.

[284] R. DuBois, H. Zaraket, M. Reddivari, R. Heath, S. White, C. Russell, Acid stability of the hemagglutinin protein regulates H5N1 influenza virus pathogenicity, PLoS Pathog. 7 (2011) e1002398.

[285] R.W. Doms, M.J. Gething, J. Henneberry, J. White, A. Helenius, Variant influenza virus hemagglutinin that induces fusion at elevated pH., J. Virol. 57 (1986) 603–13.

[286] R.J. Russell, S.J. Gamblin, L.F. Haire, D.J. Stevens, B. Xiao, Y. Ha, et al., H1 and H7 influenza haemagglutinin structures extend a structural classification of haemagglutinin subtypes., Virology. 325 (2004) 287–96.

[287] Y. Ha, D.J. Stevens, J.J. Skehel, D.C. Wiley, H5 avian and H9 swine influenza virus haemagglutinin structures: Possible origin of influenza subtypes., EMBO J. 21 (2002) 865–75.

[288] J. Stevens, A.L. Corper, C.F. Basler, J.K. Taubenberger, P. Palese, I.A. Wilson, Structure of the uncleaved human H1 hemagglutinin from the extinct 1918 influenza virus., Science. 303 (2004) 1866–70.

[289] W.I. Weis, S.C. Cusack, J.H. Brown, R.S. Daniels, J.J. Skehel, D.C. Wiley, The structure of a membrane fusion mutant of the influenza virus haemagglutinin., EMBO J. 9 (1990) 17–24.

[290] R. Xu, I.A. Wilson, Structural characterization of an early fusion intermediate of influenza virus hemagglutinin., J. Virol. 85 (2011) 5172–82.

[291] W.A. Langley, S. Thoennes, K.C. Bradley, S.E. Galloway, G.R. Talekar, S.F. Cummings, et al., Single residue deletions along the length of the influenza HA fusion peptide lead to inhibition of membrane fusion function., Virology. 394 (2009) 321–30.

[292] R.S. Daniels, J.C. Downie, A.J. Hay, M. Knossow, J.J. Skehel, M.L. Wang, et al., Fusion mutants of the influenza virus hemagglutinin glycoprotein, Cell. 40 (1985) 431–439.

[293] D.A. Steinhauer, S.A. Wharton, J.J. Skehel, D.C. Wiley, A.J. Hay, Amantadine selection of a mutant influenza virus containing an acid-stable hemagglutinin glycoprotein: Evidence for virus-specific regulation of the pH of glycoprotein transport vesicles., Proc. Natl. Acad. Sci. U. S. A. 88 (1991) 11525–9.

[294] Y.P. Lin, S.A. Wharton, J. Martín, J.J. Skehel, D.C. Wiley, D.A. Steinhauer, Adaptation of egg-grown and transfectant influenza viruses for growth in mammalian cells: Selection of hemagglutinin mutants with elevated pH of membrane fusion., Virology. 233 (1997) 402–10.

[295] P.S. Rachakonda, M. Veit, T. Korte, K. Ludwig, C. Böttcher, Q. Huang, et al., The relevance of salt bridges for the stability of the influenza virus hemagglutinin., FASEB J. 21 (2007) 995–1002.

[296] N.A. Ilyushina, E.A. Govorkova, C.J. Russell, E. Hoffmann, R.G. Webster, Contribution of H7 haemagglutinin to amantadine resistance and infectivity of influenza virus., J. Gen. Virol. 88 (2007) 1266–74.

[297] M.L. Reed, H.-L. Yen, R.M. DuBois, O.A. Bridges, R. Salomon, R.G. Webster, et al., Amino acid residues in the fusion peptide pocket regulate the pH of activation of the H5N1 influenza virus hemagglutinin protein., J. Virol. 83 (2009) 3568–80.

[298] M.L. Reed, O.A. Bridges, P. Seiler, J.-K. Kim, H.-L. Yen, R. Salomon, et al., The pH of activation of the hemagglutinin protein regulates H5N1 influenza virus pathogenicity and transmissibility in ducks., J. Virol. 84 (2010) 1527–35.

[299] L. Godley, J. Pfeifer, D. Steinhauer, B. Ely, G. Shaw, R. Kaufmann, et al., Introduction of intersubunit disulfide bonds in the membrane-distal region of the influenza hemagglutinin abolishes membrane fusion activity., Cell. 68 (1992) 635–45.

[300] D. Hulse, R. Webster, R. Russell, D. Perez, Molecular determinants within the surface proteins involved in the pathogenicity of H5N1 influenza viruses in chickens, J. Virol. 78 (2004) 9954–9964.

[301] Y. Watanabe, M.S. Ibrahim, K. Ikuta, Evolution and control of H5N1. A better understanding of the evolution and diversity of H5N1 flu virus and its host species in endemic areas could inform more efficient vaccination and control strategies., EMBO Rep. (2013) 1–6.

[302] H.D. Klenk, Influenza Viruses En Route from Birds to Man., Cell Host Microbe. 15 (2014) 653–654.

[303] D.Y. Oh, A.C. Hurt, A Review of the Antiviral Susceptibility of Human and Avian Influenza Viruses over the Last Decade., Scientifica (Cairo). 2014 (2014) 430629.

[304] S. Liu, R. Li, R. Zhang, C.C.S. Chan, B. Xi, Z. Zhu, et al., CL-385319 inhibits H5N1 avian influenza A virus infection by blocking viral entry., Eur. J. Pharmacol. 660 (2011) 460–7.

[305] Y. Si, J. Li, Y. Niu, X. Liu, L. Ren, L. Guo, et al., Entry Properties and Entry Inhibitors of a Human H7N9 Influenza Virus., PLoS One. 9 (2014) e107235.

[306] F. Vigant, J. Lee, A. Hollmann, L.B. Tanner, Z. Akyol Ataman, T. Yun, et al., A mechanistic paradigm for broad-spectrum antivirals that target virus-cell fusion., PLoS Pathog. 9 (2013) e1003297.

[307] V. Czudai-Matwich, M. Schnare, O. Pinkenburg, A simple and fast system for cloning influenza A virus gene segments into pHW2000- and pCAGGS-based vectors., Arch. Virol. 158 (2013) 2049–58.

[308] E. Hoffmann, J. Stech, Y. Guan, R.G. Webster, D.R. Perez, Universal primer set for the full-length amplification of all influenza A viruses., Arch. Virol. 146 (2001) 2275–89.

[309] J. Stech, O. Stech, A. Herwig, H. Altmeppen, J. Hundt, S. Gohrbandt, et al., Rapid and reliable universal cloning of influenza A virus genes by target-primed plasmid amplification., Nucleic Acids Res. 36 (2008) e139.

[310] A. Bryksin, I. Matsumura, Overlap extension PCR cloning: a simple and reliable way to create recombinant plasmids, Biotechniques. 48 (2010) 463–465.

[311] H. Erlich, Polymerase chain reaction, J. Clin. Immunol. 9 (1989) 437–447.

[312] E. Hoffmann, R.G. Webster, Unidirectional RNA polymerase I-polymerase II transcription system for the generation of influenza A virus from eight plasmids., J. Gen. Virol. 81 (2000) 2843–7.

[313] E. Hoffmann, S. Krauss, D. Perez, R. Webby, R.G. Webster, Eight-plasmid system for rapid generation of influenza virus vaccines., Vaccine. 20 (2002) 3165–70.

[314] M. Geiser, R. Cèbe, D. Drewello, R. Schmitz, Integration of PCR fragments at any specific site within cloning vectors without the use of restriction enzymes and DNA ligase., Biotechniques. (2001).

[315] S.N. Ho, H.D. Hunt, R.M. Horton, J.K. Pullen, L.R. Pease, Site-directed mutagenesis by overlap extension using the polymerase chain reaction, Gene. 77 (1989) 51–59.

[316] N. V Kaverin, I.A. Rudneva, E.A. Govorkova, T.A. Timofeeva, A.A. Shilov, K.S. Kochergin-Nikitsky, et al., Epitope mapping of the hemagglutinin molecule of a highly pathogenic H5N1 influenza virus by using monoclonal antibodies., J. Virol. 81 (2007) 12911–7.

[317] A.D. MacKerell, D. Bashford, M. Bellott, R.L. Dunbrack, D. Evanseck, M. Field, et al., All-atom empirical potential for molecular modeling and dynamics studies of proteins, J. Phys. Chem. 5647 (1998) 3586–3616.

[318] W. Im, M.S. Lee, C.L. Brooks, Generalized born model with a simple smoothing function., J. Comput. Chem. 24 (2003) 1691–702.

[319] G. Kieseritzky, E.-W. Knapp, Optimizing pKa computation in proteins with pH adapted conformations., Proteins. 71 (2008) 1335–48.

[320] G. Neumann, Y. Kawaoka, Influenza virus - Methods and Protocols, n.d.

[321] L. Reed, H. Muench, A simple method of estimating fifty per cent endpoints, Am. J. Epidemiol. 27 (1938) 493–497.

[322] T. Sakai, M. Ohuchi, M. Imai, Dual wavelength imaging allows analysis of membrane fusion of influenza virus inside cells, J. Virol. 80 (2006) 2013–2018.

[323] R. Daniels, J. Downie, A. Hay, Fusion mutants of the influenza virus hemagglutinin glycoprotein, Cell. 40 (1985) 431–439.

[324] W. Zhang, Y. Shi, X. Lu, Y. Shu, An Airborne Transmissible Avian Influenza H5 Hemagglutinin Seen at the Atomic Level., Science (80-.). 9 (2013) 590–603.

[325] A.P.C. Lim, S.K.K. Wong, A.H.Y. Chan, C.E.Z. Chan, E.E. Ooi, B.J. Hanson, Epitope characterization of the protective monoclonal antibody VN04-2 shows broadly neutralizing activity against highly pathogenic H5N1., Virol. J. 5 (2008) 80.

[326] C. Kozerski, E. Ponimaskin, B. Schroth-Diez, M.F. Schmidt, A. Herrmann, Modification of the cytoplasmic domain of influenza virus hemagglutinin affects enlargement of the fusion pore., J. Virol. 74 (2000) 7529–37.

[327] H. Goto, Y. Muramoto, T. Noda, Y. Kawaoka, The genome-packaging signal of the influenza A virus genome comprises a genome incorporation signal and a genome-bundling signal., J. Virol. 87 (2013) 11316–22.

[328] A. Raue, M. Schilling, J. Bachmann, A. Matteson, M. Schelker, M. Schelke, et al., Lessons learned from quantitative dynamical modeling in systems biology., PLoS One. 8 (2013) e74335.

[329] H. Zaraket, O. a Bridges, S. Duan, T. Baranovich, S.-W. Yoon, M.L. Reed, et al., Increased Acid Stability of the Hemagglutinin Protein Enhances H5N1 Influenza Virus Growth in the Upper Respiratory Tract but Is Insufficient for Transmission in Ferrets., J. Virol. 87 (2013) 9911–22.

[330] H. Zaraket, O.A. Bridges, C.J. Russell, The pH of Activation of the Hemagglutinin Protein Regulates H5N1 Influenza Virus Replication and Pathogenesis in Mice., J. Virol. 87 (2013) 4826–34.

[331] J. Stevens, O. Blixt, T.M. Tumpey, J.K. Taubenberger, J.C. Paulson, I.A. Wilson, Structure and receptor specificity of the hemagglutinin from an H5N1 influenza virus., Science. 312 (2006) 404–10.

[332] Y. Zhou, C. Wu, L. Zhao, N. Huang, Exploring the early stages of the pH-induced conformational change of influenza hemagglutinin., Proteins. 82 (2014) 2412–28.

[333] X. Sun, Y. Shi, X. Lu, J. He, F. Gao, J. Yan, et al., Bat-derived influenza hemagglutinin H17 does not bind canonical avian or human receptors and most likely uses a unique entry mechanism., Cell Rep. 3 (2013) 769–78.

[334] X. Lu, J. Qi, Y. Shi, M. Wang, D.F. Smith, J. Heimburg-Molinaro, et al., Structure and receptor binding specificity of hemagglutinin H13 from avian influenza A virus H13N6., J. Virol. 87 (2013) 9077–85.

[335] X. Zhu, W. Yu, R. McBride, Y. Li, L.-M. Chen, R.O. Donis, et al., Hemagglutinin homologue from H17N10 bat influenza virus exhibits divergent receptor-binding and pH-dependent fusion activities., Proc. Natl. Acad. Sci. U. S. A. 110 (2013) 1458–63.

[336] S. Nelson, S. Poddar, T.-Y. Lin, T.C. Pierson, Protonation of individual histidine residues is not required for the pH-dependent entry of west nile virus: Evaluation of the “histidine switch” hypothesis., J. Virol. 83 (2009) 12631–5.

[337] Q. Chen, S. Huang, J. Chen, S. Zhang, Z. Chen, NA proteins of influenza A viruses H1N1/2009, H5N1, and H9N2 show differential effects on infection initiation, virus release, and cell-cell fusion., PLoS One. 8 (2013) e54334.

[338] E.J. Schrauwen, R.A. Fouchier, Host adaptation and transmission of influenza A viruses in mammals, Emerg. Microbes Infect. 3 (2014) e9.

[339] G.R. Grimsley, J.M. Scholtz, C.N. Pace, A summary of the measured pK values of the ionizable groups in folded proteins., Protein Sci. 18 (2009) 247–51.

[340] C.N. Pace, G.R. Grimsley, J.M. Scholtz, Protein ionizable groups: pK values and their contribution to protein stability and solubility., J. Biol. Chem. 284 (2009) 13285–9.

[341] J. Warwicker, A theoretical study of the acidification of the rhinovirus capsid, FEBS Lett. 257 (1989) 403–407.

[342] J. Warwicker, Model for the differential stabilities of rhinovirus and poliovirus to mild acidic pH, based on electrostatics calculations., J. Mol. Biol. 223 (1992) 247–57.

[343] S. Nakowitsch, M. Wolschek, A. Morokutti, T. Ruthsatz, B.M. Krenn, B. Ferko, et al., Mutations affecting the stability of the haemagglutinin molecule impair the immunogenicity of live attenuated H3N2 intranasal influenza vaccine candidates lacking NS1., Vaccine. 29 (2011) 3517–24.

[344] B.M. Krenn, A. Egorov, E. Romanovskaya-Romanko, M. Wolschek, S. Nakowitsch, T. Ruthsatz, et al., Single HA2 mutation increases the infectivity and immunogenicity of a live attenuated H5N1 intranasal influenza vaccine candidate lacking NS1., PLoS One. 6 (2011) e18577.

[345] S. Murakami, T. Horimoto, M. Ito, R. Takano, H. Katsura, M. Shimojima, et al., Enhanced growth of influenza vaccine seed viruses in vero cells mediated by broadening the optimal pH range for virus membrane fusion., J. Virol. 86 (2012) 1405–10.

[346] P. Massin, S. Van der Werf, N. Naffakh, Residue 627 of PB2 is a determinant of cold sensitivity in RNA replication of avian influenza viruses, J. Virol. 75 (2001) 5398–5404.

[347] E.K. Subbarao, W. London, B.R. Murphy, A single amino acid in the PB2 gene of influenza A virus is a determinant of host range., J. Virol. 67 (1993) 1761–4.

[348] J. Steel, A.C. Lowen, S. Mubareka, P. Palese, Transmission of influenza virus in a mammalian host is increased by PB2 amino acids 627K or 627E/701N., PLoS Pathog. 5 (2009) e1000252.

[349] Z. Li, H. Chen, P. Jiao, G. Deng, G. Tian, Y. Li, et al., Molecular basis of replication of duck H5N1 influenza viruses in a mammalian mouse model., J. Virol. 79 (2005) 12058–64.

[350] G. Gabriel, A. Herwig, H.-D. Klenk, Interaction of polymerase subunit PB2 and NP with importin alpha1 is a determinant of host range of influenza A virus., PLoS Pathog. 4 (2008) e11.

[351] H. Wan, D.R. Perez, Amino acid 226 in the hemagglutinin of H9N2 influenza viruses determines cell tropism and replication in human airway epithelial cells., J. Virol. 81 (2007) 5181–91.

[352] X. Xiong, S.R. Martin, L.F. Haire, S. a Wharton, R.S. Daniels, M.S. Bennett, et al., Receptor binding by an H7N9 influenza virus from humans., Nature. 499 (2013) 496–9.

[353] Y. Chen, W. Liang, S. Yang, N. Wu, H. Gao, J. Sheng, et al., Human infections with the emerging avian influenza A H7N9 virus from wet market poultry: Clinical analysis and characterisation of viral genome, Lancet. 381 (2013) 1916–1925.

[354] H. Zhu, D. Wang, D.J. Kelvin, L. Li, Z. Zheng, S.-W. Yoon, et al., Infectivity, transmission, and pathology of human-isolated H7N9 influenza virus in ferrets and pigs., Science. 341 (2013) 183–6.

[355] J. a Belser, K.M. Gustin, M.B. Pearce, T.R. Maines, H. Zeng, C. Pappas, et al., Pathogenesis and transmission of avian influenza A (H7N9) virus in ferrets and mice., Nature. (2013) 1–5.

[356] Q. Zhang, J. Shi, G. Deng, J. Guo, X. Zeng, X. He, et al., H7N9 influenza viruses are transmissible in ferrets by respiratory droplet., Science. 341 (2013) 410–4.

[357] T. Watanabe, M. Kiso, S. Fukuyama, N. Nakajima, M. Imai, S. Yamada, et al., Characterization of H7N9 influenza A viruses isolated from humans., Nature. 501 (2013) 551–5.

[358] J. Knepper, K. Schierhorn, A. Becher, M. Budt, M. Tönnies, T.T. Bauer, et al., The novel human influenza A (H7N9) virus is naturally adapted to efficient growth in human lung tissue, MBio. 4 (2013) 9–13.

[359] J. Zhou, D. Wang, R. Gao, B. Zhao, J. Song, X. Qi, et al., Biological features of novel avian influenza A (H7N9) virus., Nature. 499 (2013) 500–3.

[360] J.B. Kimble, E. Sorrell, H. Shao, P.L. Martin, D.R. Perez, Compatibility of H9N2 avian influenza surface genes and 2009 pandemic H1N1 internal genes for transmission in the ferret model., Proc. Natl. Acad. Sci. U. S. A. 108 (2011) 12084–8.

[361] E.M. Sorrell, H. Wan, Y. Araya, H. Song, D.R. Perez, Minimal molecular constraints for respiratory droplet transmission of an avian-human H9N2 influenza A virus., Proc. Natl. Acad. Sci. U. S. A. 106 (2009) 7565–70.

[362] K.B. Ku, E.H. Park, J. Yum, H.M. Kim, Y.M. Kang, J.C. Kim, et al., Transmissibility of novel H7N9 and H9N2 avian influenza viruses between chickens and ferrets., Virology. 450-451 (2014) 316–23.

[363] L.-M. Chen, O. Blixt, J. Stevens, A.S. Lipatov, C.T. Davis, B.E. Collins, et al., In vitro evolution of H5N1 avian influenza virus toward human-type receptor specificity., Virology. 422 (2012) 105–13.

[364] I. Koerner, M.N. Matrosovich, O. Haller, P. Staeheli, G. Kochs, Altered receptor specificity and fusion activity of the haemagglutinin contribute to high virulence of a mouse-adapted influenza A virus., J. Gen. Virol. 93 (2012) 970–9.

[365] M. Hatta, Y. Hatta, J.H. Kim, S. Watanabe, K. Shinya, T. Nguyen, et al., Growth of H5N1 influenza A viruses in the upper respiratory tracts of mice., PLoS Pathog. 3 (2007)1374–9

[366] T. Narasaraju, M.K. Sim, H.H. Ng, M.C. Phoon, N. Shanker, S.K. Lal, et al., Adaptation of human influenza H3N2 virus in a mouse pneumonitis model: Insights into viral virulence, tissue tropism and host pathogenesis., Microbes Infect. 11 (2009) 2–11.

[367] M. Lakadamyali, M. Rust, X. Zhuang, Ligands for clathrin-mediated endocytosis are differentially sorted into distinct populations of early endosomes, Cell. 124 (2006) 997–1009.

[368] S. Ludwig, S. Pleschka, O. Planz, T. Wolff, Ringing the alarm bells: signalling and apoptosis in influenza virus infected cells., Cell. Microbiol. 8 (2006) 375–86.

[369] E. Król, M. Rychłowska, B. Szewczyk, Antivirals-current trends in fighting influenza., Acta Biochim. Pol. 61 (2014).

[370] J. Yang, M. Li, X. Shen, S. Liu, Influenza A virus entry inhibitors targeting the hemagglutinin., Viruses. 5 (2013) 352–73.

[371] E. Vanderlinden, F. Göktas, Z. Cesur, M. Froeyen, M.L. Reed, C.J. Russell, et al., Novel inhibitors of influenza virus fusion: structure-activity relationship and interaction with the viral hemagglutinin., J. Virol. 84 (2010) 4277–88.

[372] K.K. Lee, Architecture of a nascent viral fusion pore., EMBO J. 29 (2010) 1299–311.

[373] S. V Avilov, D. Moisy, S. Munier, O. Schraidt, N. Naffakh, S. Cusack, Replication-competent influenza A virus that encodes a split-green fluorescent protein-tagged PB2 polymerase subunit allows live-cell imaging of the virus life cycle., J. Virol. 86 (2012) 1433–48.

Appendix

Sequence alignment of H5 LP of A/teal/Germany/Wv632/2005 (H5N1) and of H5 HP of A/chicken/Vietnam/P41/2005 (H5N1)

```
                                                                  110
H5 LP    DQICIGYHANNSTEQVDTIMEKNVTVTHAQDILEKAHNGKLCSLNGVKPLILRDCSVAGW    60
H5 HP    DQICIGYHANNSTEQVDTIMEKNVTVTHAQDILEKTHNGKLCDLDGVKPLILRDCSVAGW    60
         ************************************:*******.*:***************

                                                                  110
H5 LP    LLGNPMCDEFLNVPEWSYIVEKDNPVNGLCYPGDFNDYEELKHLLSSTNHFEKIRIIPRS   120
H5 HP    LLGNPMCDEFINVPEWSYIVEKANPVNDLCYPGDFNDYEELKHLLSRINHFEKIQIIPKS   120
         **********:*********** ****.******************  ******:***:*

                                                                  184
H5 LP    SWSNHDASSGVSSACPYNGNSSFFRNVVWLIKKNNAYPTIKRSYNNTNQEDLLVLWGIHH   180
H5 HP    SWPSHEASLGVSSACPYQGKSSFFRNVVWLIKKNSTYPTIKRSYNNTNQEDLLVLWGIHH   180
         **..*:** ********:*:**************.:************************

                                      212 216   221
H5 LP    PNDAAEQTKLYQNPTTYVSVGTSTLNQRSVPEIATRPRVNGQSGRMEFFWTILKPNDAIN   240
H5 HP    PNDAAEQTKLYQNPTTYISVGTSTLNQRLVPRIATRSKVNGQSGRMEFFWTILKPNDAIN   240
         ******************:********** **.****.:************************

H5 LP    FESNGNFIAPEYAYKIVKKGDSAIMKSGLEYGNCNTKCQTPMGAINSSMPFHNIHPLTIG   300
H5 HP    FESNGNFIAPEYAYKIVKKGDSTIMKSELEYGNCNTKCQTPMGAINSSMPFHNIHPLTIG   300
         **********************:**** ********************************

                                              Fusion peptide
H5 LP    ECPKYVKSDRLVLATGPRNVPQKE---TRGLFGAIAGFIEGGWQGMVDGWYGYHHSNEQG   357
H5 HP    ECPKYVKSNRLVLATGLRNSPQRERRKKRGLFGAIAGFIEGGWQGMVDGWYGYHHSNEQG   360
         ********:******* ** **:*   .**********************************

H5 LP    SGYAADKESTQKAIDGITNKVNSIIDKMNTQFEAVGKEFNNLEGRIENLNKKMEDGFLDV   417
H5 HP    SGYAADKESTQKAIDGVTNKVNSIIDKMNTQFEAVGREFNNLERRIENLNKKMEDGFLDI   420
         ****************:******************:****** ***************:

H5 LP    WTYNAELLVLMENERTLDFHDSNVKNLYDKVRLQLRDNAKELGNGCFEFYHKCDNECMES   477
H5 HP    WTYNAELLVLMENERTLDFHDSNVKNLYDKVRLQLRDNAKELGNGCFEFYHKCDNECMES   480
         ************************************************************

H5 LP    VRNGTYDYPQYSEEARLNREEISGVKLESMGTYQILSIYSTVASSLALAIMVAGLSFWMC   537
H5 HP    VRNGTYDYPQYSEEAKLKREEISGVKLESIGIYQILSIYSTVASSLALAIMVAGLSLWMC   540
         ***************:*:***********:* ***********************:***

H5 LP    SNGSLQCRICI   548
H5 HP    SNGSLQCRICI   551
         ***********
```

Abbreviations

4HB	four-helix-bundle
6HB	six-helix-bundle
BCA	bicinchoninic acid
BGH	bovine growth hormone
BHA	bromelain cleaved hemagglutinin
BSA	bovine serum albumin
CDC	center disease control
CHO	Chinese hamster ovary
CME	clathrin mediated endocytosis
CMV	human cytomegalovirus
CPE	cytopathic effect
Cryo-EM	cryogenic electron microscopy
DAPI	4',6-diamidino-2-phenylindole
DAG	diacylglycerol
DiI	1,1'-dioctadecyl-3,3,3'3'-tetramethylindocarbocyanine perchlorate
DiO	3,3′ -dioctadecyloxacarbocyanine perchlorate
DMEM	Dulbecco's modified Eagle medium
DMSO	Dimethylsulfoxid
dNTP	deoxynucleotide
DSP	3, 3-dithiobissuccinymidylpropionate
EDTA	Ethylenediaminetetraacetic acid
EE	early endosomes
EGF	epidermal growth factor
Env	envelope protein
ER	endoplasmic reticulum
FAST protein	fusion-associated small transmembrane protein
FBS	fetal bovine serum
FD	fusion domain
FF	fusion failure
FP	fusion peptide
FRET	Foerster resonance energy transfer
Gal	Galactose
GFP	green fluorescent protein
Glc	Glucose

GPI	glycophosphatidylinositol
HA	hemagglutinin
HA0	hemagglutinin precursor protein
HAT	human airway
HCl	hydrochloride
HD	hemifusion diaphragm
HEPES	4-(2-hydroxyethyl)-1-piperazineethanesulfonic acid
HIV	human immunodeficiency virus
HP	highly pathogenic
HPAIV	highly pathogenic avian influenza virus
HRA/B	heptad repeat region A/B
IFN	interferon
LB medium	Luria-Bertani medium
LB-Amp	Luria-Bertani medium containing ampicillin
LB-Kan	Luria-Bertani medium containing kanamycin
LE	late endosomes
LP	low pathogenic
LPAIV	low pathogenic avian influenza virus
LPC	lysophosphatidylcholine
MDCK	Madin Darby canine kidney
MES	2-(N-morpholino)ethanesulfonic acid
MFI	mean fluorescent intensity
MOI	multiplicity of infection
MTOC	microtubuli organization center
MSPL	massive surface protein
NA	neuraminidase
NaCl	sodium chloride
NAG	N-acetylglucosamine
NaOH	sodium hydroxide
NCR	non-coding region
NEB	New England Biolabs
NEP	nuclear export protein
NF-kB	nuclear factor kB
NLS	nuclear localization signal
NP	nucleoprotein
NSF	N-ethylmaleimide-sensitive factor
CMV	human cytomegalovirus
PBS-	phosphate buffered saline without CaCl and MgCl

PBS+	phosphate buffered saline with CaCl and MgCl
PC	phosphatidylcholine
PCR	polymerase chain reaction
PE	phophatidylethanolamine
PEG	polyethylenglycerol
PFA	paraformaldehyde
Pfu	Plaque forming units
PHD	Pleckstrin homology domain
R18	ocadecyl rhodamine B chloride
RBC	red blood cell
RBS	receptor binding site
RE	recycling endosome
RIG-I	retinoic acid inducible gene I
RNP	ribonucleoprotein
RT	room temperature
-S-S-	disulfide bond
SA	sialic acid
SARS	severe acute respiratory syndrome
SDS	sodium dodecyl sulfate
SDS PAGE	sodium dodecyl sulfate polyacrylamide gelelectrophoresis
SFV	semliki forest virus
SNAP	soluble NSF attachment protein
SNARE	SNAP receptor
SP	signal peptide
TBEV	tick borne encephalitis virus
TBHA2	thermolysin treated and bromelain cleaved hemagglutinin
$TCID_{50}$	Tissue culture infectious dose
TEM	transmission electron microscopy
TLR	Toll like receptor
TMD	transmembrane domain
TMPRSS	type II transmembrane serine protease
vRNP	viral ribonuleoprotein
VSV	vesicular stomatitis virus
WHO	World Health Organization
YFP	yellow fluorescent protein

List of Figures

List of Tables

Acknowledgements

First of all I want to thank **Prof. Dr. Andreas Herrmann** for the opportunity to work on an exciting project in a fantastic lab. *Thank your for your constant support, your endless time correcting oral presentations and manuscripts, for your positive motivation, your trust and your ease which creates a special motivating lab atmosphere*.

I owe special thanks to **Tim Meyer** for a very good collaboration, his support of my experimental data and his wonderful images of protein structures. *Thank you for all the hours sitting together over a crystal structure and the good discussions.*

Many thanks also go to **Christian** for always having an ear for my technical problems, the great experimental support and the many fruitful discussions that helped me to get a direction for my work. *Thank you for providing structure into my sometimes confused mind and for your motivating enthusiasm.*

Roland, *I do not only want to thank you for introducing me to biophysical methods and your enormous help in cell culture, image and data analysis but also for being the best desk neighbor I could ever imagine. Thank you for your humor, your sensitiveness and for drinking thousands of coffees with me!*

I also thank my second supervisor **PD Dr. Michael Veit** and his group for sharing his expertise in influenza virus research, for providing plasmids and cells and for critical feedback on manuscripts.

Thanks to **Dr. Kai Ludwig** for helping out with electron microscopy images, **Dr. Qiang Huang** for his programming skills and **Max Schelker** for his help in fitting the data.

Special thanks also go to **Chris** for sharing her expertise in virology and Western blotting and for sharing the room with me in the last months of thesis writing. *Thank you for your empathy. I hope I did not distract you too often from work ;)*
For technical support I want to thank **Katjana Schneider** who was willing to do not only her bachelors project but also her study project under my supervision. Without her I would probably not have handled all the experiments *Thanks a lot!*

Andrea, Joanna *and* ***Aouefa****, how can I thank you?! You were the greatest support in the every-day lab-life and the besides-lab life; you shared with me the darkest moments and the best. Thank you so much for your friendship!* ***Andrea****, thank you for your generosity and for always being there when I needed some advice, no matter what!* ***Joanna****, I love you for your serenity and your humor. Thanks for sharing so many exciting adventures with me on the bike, on the surfboard, at the fusion festival and at the "Schwedter Nordwand".* ***Aouefa****, I will miss you so much when we will not share the room anymore! Merci beaucoup pour ton soin, pour ta sensibilité et pour m'emmener dans ton monde spécial avec de l'art, de la musique et la cuisine expérimentale. Merci aussi pour toujours me supporter et m'aider à considérer des choses sous un autre angle. Prends soin de toi!*

I also want to thank all the other members of the **Molecular Biophysics Lab** for the good atmosphere and cooperation of everybody, especially **Gabi** for her support with FACS and molecular biology and for some wonderful *Zwiebelkuchen* on the balcony, **Matthias** for his mindfulness and for always correcting my *deutsches* English, **Lotte** for her open-mindedness and **Luisa** for her organizing talent.

Many thanks go to **Dr. Thomas Korte, Gudrun, Sabine** and **Silvia** for the technical support in the every-day-lab's life, **Dr. Peter Müller** for some interesting conversations about Österreich and the world, and **Uta** and **Frau Piater** for handling all the financial issues.

This work was supported by the 7th Framework Program of the Marie Curie Actions of the **European Commission**.

Ganz besonders möchte ich mich auch bei **meinen Eltern** und **Geschwistern** bedanken, für ihre Liebe, ihre Unterstützung und ihren Rat.

Thomas, Evi, Regina *und* ***Sebastian****, vielen Dank für eure Unterstützung und Freundschaft trotz der räumlichen Distanz.*
Nadine *und* ***Erika****, danke für eure herzliche Aufnahme in Berlin und eure Freundschaft vom ersten Tag an.*

Peter*, ich danke dir für alles, ganz besonders für deine enorme Unterstützung und Geduld während meiner Doktorarbeit und dafür, mich manchmal auch davon abgelenkt zu haben.*

Publications

Articles and Manuscripts

Mair, C. **M.**, Ludwig K., Herrmann A., Sieben C. (2014) Receptor binding and pH stability – How influenza A virus hemagglutinin affects host-specific virus infection, *Biochimica et Biophysica Acta, 1838*(4), 1153-1168. doi:10.1016/j.bbamem.2013.10.004

Mair C. M., Meyer T., Schneider K., Huang Q., Veit M., Herrmann A. (2014) A histidine residue of the influenza virus hemagglutinin controls the pH dependence of membrane fusion at low pH, *Journal of Virology,* doi:10.1128/JVI.01704-14

Schelker M.#, **Mair C. M.#**, Jolmes F., Herrmann A., Klipp E., Flöttmann M., Sieben C. (2014) RNA degradation and diffusion act as a bottleneck for the influenza A infection efficiency. *In preparation*

 # equal contribution

Oral presentations

2nd Year and Midterm Meeting Virus Entry
Stockholm, Sweden, June 2011
Influence of salt bridges in the influenza virus HA for host adaptation and pathogenicity

56th Biophysical Society Meeting
San Diego, USA, February 2012
Tracking influenza virus fusion – Effect of salt bridges on fusion activity of the influenza virus hemagglutinin

3rd Year Meeting - Virus Entry
Menorca, Spain, May 2012
Tracking influenza virus fusion – Relation between stability and fusion pH of influenza virus hemagglutinin

4th Year Meeting - Virus Entry
Greifensee, Switzerland, February 2013

Influenza virus hemagglutinin regulates membrane fusion by fine-tuning of its histidines

International Meeting of Virus Entry

Tel Aviv, Israel, August 2013

Influenza virus membrane fusion – Role of histidines for HA conformational change

26th Annual Meeting of the Society of General Virology

Alpbach, Austria, March 2014

His184 at the HA1-HA1 interface of the influenza virus hemagglutinin is an essential regulator of membrane fusion at low pH

Poster presentations

2nd International Influenza Meeting

Muenster, Germany, September, 2010

Stability of Influenza virus hemagglutinin is a crucial factor of virus pathogenicity in humans

7th Virus Assembly Symposium

Menorca, Spain, May 2012

Tracking influenza virus fusion – Relation between endosomal pH and pathogenicity

3rd International Influenza Meeting

Muenster, Germany, September 2012

Tracking influenza virus fusion – Relation between endosomal pH and pathogenicity

57th Biophysical Society Meeting

Philadelphia, USA, February 2013

Influenza virus hemagglutinin regulates membrane fusion by fine-tuning of its histidines

Selbstständigkeitserklärung

Hiermit erkläre ich, dass ich die vorliegende Arbeit selbständig und nur unter Verwendung der angegebenen Literatur und Hilfsmittel angefertigt habe. Alle Stellen, die dem Wortlaut oder dem Sinn nach anderen Werken entnommen sind, sind nach bestem Wissen und Gewissen durch Angabe der Quellen als Entlehnung kenntlich gemacht worden. Wurden Ergebnisse in Kooperation produziert, ist dies entsprechend angegeben.
Ich besitze keinen entsprechenden Doktorgrad und habe mich anderwärts nicht um einen Doktorgrad beworben.
Die dem Promotionsverfahren zugrunde liegende Promotionsordnung ist mir bekannt.

Berlin, den 10.12.2014
Caroline Mair